KU LEUVEN

FACULTEIT INGENIEURSWETENSCHAPPEN

Modeling, predicting and controlling epileptic seizures

Roel Henckaerts

Thesis voorgedragen tot het behalen van de graad van Master of Science in de ingenieurswetenschappen: wiskundige ingenieurstechnieken

Promotor:
Prof. dr. ir. B. De Moor

Assessoren:
Prof. dr. ir. K. Meerbergen
Prof. dr. ir. D. Nuyens

Begeleider:
Dr. ir. O. M. Agudelo

Academiejaar 2013 – 2014

Preface

I really have enjoyed working on this thesis for the past year. It has been a very interesting and educational experience for me. I would like to thank some people, without whom this would have not been possible. First of all, I would like to thank my promotor, prof. dr. ir. Bart De Moor, for giving me the opportunity to work on this subject. Healthcare engineering is namely a research topic that I find very interesting.

Secondly, I would like to thank dr. ir. Oscar Mauricio Agudelo for his guidance throughout the year. He was always available for a meeting when I contacted him and during a meeting he took his time to discuss everything in detail with me. The feedback that I got from Mauricio was always very helpful.

Thirdly, I would also like to thank my assessors, prof. dr. ir. Karl Meerbergen and prof. dr. ir. Dirk Nuyens, for reading my thesis and giving comments on my work.

Last but not least, I would like to thank my family and friends for their support throughout the year. Special thanks go to my parents for giving me the opportunity to study and eventually produce this thesis. Without their support, none of this would have been possible.

Roel Henckaerts

Contents

Preface i

Abstract iii

Samenvatting iv

List of Figures vi

List of Tables vii

List of Abbreviations and Symbols ix

1 Introduction 1
- 1.1 Epilepsy . . . 1
- 1.2 Modeling framework for epilepsy . . . 5
- 1.3 Treatments for epilepsy . . . 7
- 1.4 Prediction framework for epilepsy . . . 9

2 Modeling epileptic seizures 11
- 2.1 Model for absence seizures . . . 11
- 2.2 Model for temporal lobe epilepsy . . . 18

3 Controlling epileptic seizures 25
- 3.1 Introduction . . . 25
- 3.2 Methods . . . 26
- 3.3 Results . . . 29
- 3.4 Conclusion . . . 36

4 Predicting epileptic seizures 37
- 4.1 Introduction . . . 37
- 4.2 Methods . . . 38
- 4.3 Results . . . 45
- 4.4 Conclusion . . . 60

5 Conclusion and discussion 63
- 5.1 Modeling epileptic seizures . . . 63
- 5.2 Controlling epileptic seizures . . . 64
- 5.3 Predicting epileptic seizures . . . 65

A Introduction to neuroscience 69

B Mathematical details of the model for absence seizures 73

B.1 The model 73
B.2 From presynaptic firing rate to membrane potential 74
B.3 From membrane potential to postsynaptic firing rate 75

C Mathematical details of the model for TLE **77**
C.1 The model 77
C.2 From presynaptic firing rate to membrane potential 78
C.3 From membrane potential to postsynaptic firing rate 79

D Paper **81**

E Poster **89**

Bibliography **91**

Abstract

Epilepsy is a very diverse neurological disorder, characterized by recurrent seizures. Two specific types are considered in this study, namely absence seizures and mesial temporal lobe epilepsy (MTLE). The most common treatments for epilepsy are medication and surgery. Since these are not effective for all the patients, there is a lot of current research aimed towards the development of alternative treatments. Computational modeling can play a major role in this development. Two computational models from the literature are therefore implemented in this study.

The first model is a thalamocortical model for absence seizures. This model can simulate normal and epileptic activity. It very well mimics the dynamics that are in play during transitions from one type of activity to the other. This allows some interaction with the model. A control system is designed for this model, with the goal of disrupting a started seizure. Absence seizures have a sudden onset and can therefore not be predicted. The control system consists of a detection and a stimulation part. The detection happens purely based on the amplitude of the electroencephalography (EEG). This allows for a fast detection, but unfortunately lacks the possibility for generalization towards real life signals. The stimulation part will send pulses into the model, to interrupt the seizures. This fits perfectly in the framework of brain stimulation techniques as an alternative treatment for epilepsy. The obtained results show that the seizures can be controlled very well, if a fast detection is possible. However, this is only the case for some well tuned, patient-specific, parameters of the control system.

The second model is a hippocampal model for MTLE. This model can simulate six different types of behavior. It is used to generate artificial data to build a prediction framework for MTLE. Interictal (between seizures), preictal (right before a seizure) and ictal (during a seizure) periods of the EEG are simulated. The EEG of MTLE, unlike for absence seizures, shows some dynamical changes prior to seizure onset. These changes can be used to find the preictal periods of the EEG. Predicting a seizure thus boils down to a classification problem. There is a lot of neuronal synchrony during the preictal and ictal periods. Therefore, measures that characterize synchrony are computed from the EEG channels. These measures are used to classify the EEG. Classification is first done by thresholding the synchrony measures, with a resulting classification accuracy of 95%. This method is however very likely to fail on real life signals. Classification is therefore also performed with support vector machines (SVMs) after including some filtered versions of the synchrony measures. An accuracy of 98% is obtained on independent test signals.

Samenvatting

Epilepsie is een zeer diverse neurologische ziekte, gekarakteriseerd door terugkerende aanvallen. Twee specifieke types worden beschouwd in deze studie, namelijk absences en mesiale temporale kwab epilepsie (MTLE). De meest gebruikte behandelingen tegen epilepsie zijn medicatie en chirurgie. Aangezien deze niet doeltreffend zijn voor alle patiënten, is er tegenwoordig veel onderzoek naar de ontwikkeling van alternatieve behandelingen. Computationele modellen kunnen hier een belangrijke rol in spelen. Daarom zijn twee computationele modellen uit de literatuur geïmplementeerd in deze studie.

Het eerste model is een thalamocorticaal model voor absences. Dit model kan normale en epileptische activiteit simuleren. Het model imiteert de dynamische aspecten die in het spel zijn tijdens de overgang van één type van activiteit naar de andere zeer goed. Dit laat enige interactie met het model toe. Een controlesysteem is ontwikkeld voor dit model, met als doel het verstoren van begonnen aanvallen. Absences hebben een plotselinge aanvang en kunnen daarom niet voorspeld worden. Het controlesysteem bestaat uit een detectie- en een stimulatiegedeelte De detectie gebeurt volledig gebaseerd op de amplitude van de elektro-encefalografie (EEG). Dit laat een zeer snelle detectie toe, maar is jammer genoeg niet uitbreidbaar naar signalen uit het echte leven. Het stimulatiegedeelte zal pulsen in het model sturen en proberen om de aanvallen te controleren. Dit past perfect in de denkwijze van hersenstimulatie technieken als een alternatieve behandeling voor epilepsie. De behaalde resultaten tonen dat de aanvallen goed gecontroleerd kunnen worden, indien een snelle detectie mogelijk is. Dit is echter enkel het geval voor goed afgestelde, patiënt specifieke, parameters van het controlesysteem.

Het tweede model is een hippocampaal model voor MTLE. Dit model kan zes verschillende types van gedrag simuleren. Het wordt gebruikt om artificiële data te genereren en zo een voorspellingsmethode voor MTLE op te bouwen. Interictale (tussen aanvallen), pre-ictale (net voor een aanval) en ictale (tijdens een aanval) periodes van de EEG worden gesimuleerd. De EEG van MTLE toont, in tegenstelling tot die van absences, enkele dynamische veranderingen voor de aanvang van een aanval. Deze veranderingen kunnen worden benut om de pre-ictale periodes in de EEG te vinden. Een aanval voorspellen komt dus neer op een classificatieprobleem. Er is heel wat synchronie tijdens de pre-ictale periode en sommige ictale periodes. Daarom worden maten die synchronie karakteriseren berekend uit de EEG. Deze maten worden gebruikt om de EEG te classificeren. Classificatie gebeurt eerst door een drempelwaarde te kiezen voor elke maat. De nauwkeurigheid van deze methode

is 95%, maar deze zal waarschijnlijk falen op signalen uit het echte leven. Daarom wordt classificatie ook gedaan aan de hand van *support vector machines* (SVMs) nadat sommige gefilterde versies van de maten zijn inbegrepen. Een nauwkeurigheid van 98% wordt bekomen op onafhankelijke test signalen.

List of Figures

2.1 The thalamocortical model of Suffczynski et al. [76]. The cortical module consists of an excitatory population of PY cells and an inhibitory population of IN cells. The thalamic module is built from an excitatory population of TC cells and an inhibitory population of RE cells. A mathematical description of this model can be found in Appendix B. . . 13

2.2 The simulated signals of the thalamocortical model of absence seizures. a) The time evolution of the mean membrane potential of the PY cells in the cortex. This output represents the dynamics of an EEG and shows both interictal and ictal activity with spontaneous transitions between them. The parts with a high amplitude are the ictal parts. b) A close-up of an ictal part of the EEG, where the quasi-sinusoidal activity is clearly visible. c) The PSD for the ictal activity shows a clear peak at 9 Hz. d) A close-up of an interictal part of the EEG, which clearly shows the waxing-and-waning progress of the interictal signals. e) The PSD of the interictal activity is centered around 11 Hz. This shows that the interictal activity has a slightly higher frequency than the ictal activity. 14

2.3 The phase portrait for the model of absence seizures. The state space trajectories were obtained by using the method of delays with $\tau = 20\,ms$ and $m = 2$. The mean membrane potential of the PY cells in the cortex (V_{PY}) is plotted against a delayed version of itself. a) The state space trajectories when there is no noise on the external inputs. There will be no transitions from interictal to ictal (or vice versa) in this case. The red dot represents the interictal activity and clearly forms an equilibrium point. The blue curve represents the ictal activity and forms a limit cycle. b) After introducing a low level of noise on the external input to the TC cells, the equilibrium point and limit cycle can be seen to deviate a little bit from their previous path. This low level of noise is however not high enough to cause transitions from the equilibrium point to the limit cycle (or vice versa). c) Transitions from one attractor to the other start to happen when the noise level is increased. This implies that transitions from interictal to ictal activity (and vice versa) are possible for these noise levels. 16

2.4 The model of the hippocampus of Wendling et al. [42]. There are two excitatory populations: the main cells and the distant PY cells. There are also two inhibitory populations: the slow dendritic and the fast somatic inhibitory neurons. A mathematical description of this model can be found in Appendix C. 19
2.5 The impulse responses for the three different types of synaptic interaction. Fast somatic inhibition (blue) has the fastest dynamics, followed by excitatory synaptic transmission (green). The slow dendritic inhibition (red) has the slowest dynamics. 20
2.6 The six different types of EEG behavior generated by the model of Wendling et al. [42]. a) Type 1: normal background activity (interictal). b) Type 2: slow rhythmic activity (interictal). c) Type 3: sporadic spikes (interictal). d) Type 4: sustained spikes (preictal). e) Type 5: low voltage rapid activity (ictal). f) Type 6: quasi-sinusoidal activity (ictal). 21
2.7 A 6-channel EEG recording that contains the six qualitatively different types of signals that can be produced by the model. The channels are labeled Ch1 up to Ch6. Every type of possible activity is simulated for five seconds (type 1 up to type 6). 22

3.1 The detection system to detect a seizure in the model for absence seizures. 27
3.2 The control system together with the model. The model is included in the light blue subsystem. Both the detection systems are shown in green. The stimulation part is indicated in yellow. The red addition element combines the two control signals into one signal. The switch element determines whether the control signal is sent into the model or not. . . 28
3.3 The results when the control system is not connected to the model. a) The average membrane potential of the PY population in the cortex (which represents an EEG recording) clearly shows interictal and ictal activity. The ictal activity has a noticeable higher amplitude compared to the interictal activity. The thresholds of the detection system are shown as red horizontal lines. Below this threshold is classified as interictal, above as ictal activity. b) The amount of $GABA_B$ activation. This activation represents the postsynaptic current generated by the $GABA_B$ receptor and therefore corresponds to ictal activity. c) The amplitude of the control signal over time. These pulses are generated when ictal activity is detected but they are not sent into the model yet. 30
3.4 The results when the control system is connected to the model. a) The EEG recording does not show any noticeable ictal activity anymore, but only spindle oscillations. The only type of signal that is present is the waxing-and-waning interictal activity. This means that the control system has succeeded in annihilating the seizures. b) There is almost no more $GABA_B$ activation. This also points towards the absence op epileptic activity. c) Only a small part of the control pulses from Figure 3.3c are needed to control the seizures. This implies that a single pulse at the start of a seizure can annihilate the entire seizure. 31

3.5 The results when the control system is connected to the model, but with a too low threshold parameter. a) The recorded EEG shows some very strange behavior. Neither ictal nor interictal activity are visible in this case. Too much electrical stimulation has made the output of the model physically meaningless. b) There is no $GABA_B$ activation, but this has no biological meaning anymore. c) There are way too much detections because of the too low threshold parameter. The brain will therefore be overstimulated. 33

3.6 The results when the control system is connected to the model, but with a too high threshold parameter. a) The EEG still shows both interictal and ictal activity. b) The $GABA_B$ activation points towards ictal activity. The seizures are not well controlled in this case. c) The detection of ictal activity happens too late, which allows the seizure to develop and become noticeable. Counter stimuli will be sent too late by the control system. . 33

3.7 The results when the control system is connected to the model, but with a too low amplitude parameter. a) The EEG still shows some ictal activity. b) The $GABA_B$ activation also still shows some peaks with a high amplitude. These both results point towards a poor performance of the control system with these parameters. c) A lot of control signals are sent into the model, but the amplitude of the signals is too small to interrupt every seizure. 34

3.8 The results when the control system is connected to the model, but with a too high amplitude parameter. a) Some strange high frequency signals are present in the EEG recording. This is the result of a too large amplitude of the control signal. The dynamics of the brain are tangled up. b) The $GABA_B$ activation has small values, but the physical meaning of these is gone since the dynamics of the model are not respected anymore. c) The control pulses with a large amplitude that cause the model to generate strange EEG measurements. 34

3.9 The results when the control system is connected to the model, but with a too low duration parameter. a) The measured EEG still shows some ictal activity. The control pulse did not last long enough to control these seizures. b) There are still some uncontrolled seizures that lead to large peaks of $GABA_B$ activation. c) The control pulses with a too short duration. 35

3.10 The results when the control system is connected to the model, but with a too high duration parameter. a) Some high frequency oscillations can be seen in the EEG recording. The long duration of the control pulses has caused this unwanted behavior. b) There is still some clear $GABA_B$ activation in this case. c) The different pulses follow each other too fast which does not leave any 'quiet time' between them. 35

4.1 The 2-channel EEG recording that was used to calculate the synchrony measures and the corresponding class labels of every type of activity. a) The first EEG channel. Every type of activity (type 1 up to type 6) is simulated for 200 seconds. b) The second EEG channel. Also here every type of activity is simulated for 200 seconds. c) The class labels that belong to the different types of EEG activity. The labels 1, -1 and 0 respectively correspond to interictal, preictal and ictal activity. 46

4.2 The evolution over time of the four synchrony measures for the 2-channel EEG of Figure 4.1. High values indicate synchrony and can be found during preictal activity ($600 - 800\,s$) and one type of ictal activity ($1000 - 1200\,s$). a) The time evolution of the maximal cross-correlation. b) The time evolution of the coherence. c) The time evolution of the nonlinear interdependence (blue for N(X|Y), red for N(Y|X)). d) The time evolution of the PLV. 47

4.3 The evolution over time of the synchrony measures for the 2-channel EEG of Figure 4.1 after LP filtering (cut-off frequency 9 Hz). High values are now only found during the preictal segment of the signal ($600 - 800\,s$). a) The time evolution of the maximal cross-correlation after LP filtering. b) The time evolution of the coherence after LP filtering. c) The time evolution of the nonlinear interdependence after LP filtering (blue for N(X|Y), red for N(Y|X)). d) The time evolution of the PLV after LP filtering. 48

4.4 The evolution over time of the synchrony measures for the 2-channel EEG of Figure 4.1 after LP filtering and aggregating the measures over multiple windows. These measures now show a much more smooth progress, without outliers. a) The time evolution of the maximal cross-correlation after LP filtering and aggregation. b) The time evolution of the coherence after LP filtering and aggregation. c) The time evolution of the nonlinear interdependence after LP filtering and aggregation (blue for N(X|Y), red for N(Y|X)). d) The time evolution of the PLV after LP filtering and aggregation. 49

4.5 The classification results by using a threshold and the PLV as an example (other measures can also be used). a) The time evolution of the PLV after LP filtering and aggregation (blue) together with the chosen threshold of 0.42 (black). This threshold was chosen after some tuning. Values of the PLV above the threshold are classified as preictal, while values of the PLV below the threshold are classified as 'not preictal'. b) The predicted labels (red) together with the true labels (blue). The labels were chosen to be 1 and -1 for respectively 'not preictal' and 'preictal'. 50

4.6 PCA on the input features when the filtered versions of the PLV are not included. Green, blue and red circles respectively represent features from interictal, preictal and ictal stages from the EEG. The red cluster close to the green one represents the ictal low voltage rapid activity, while the red cluster close to the blue one represent the ictal synchronous activity. a) The distribution of the features according to principal component one and two. b) The distribution of the features according to principal component one and three. c) The distribution of the features according to principal component two and three. d) The distribution of the features according to principal component one, two and three. From these figures it is clear that the preictal and ictal synchronous activity can not be separated from each other. 53

4.7 PCA on the input features when the filtered versions of the PLV are included. Green, blue and red circles respectively represent features from interictal, preictal and ictal stages from the EEG. The red cluster close to the green one represents the ictal low voltage rapid activity, while the red cluster close to the blue one represent the ictal synchronous activity. a) The distribution of the features according to principal component one and two. b) The distribution of the features according to principal component one and three. c) The distribution of the features according to principal component two and three. d) The distribution of the features according to principal component one, two and three. From these figures it is clear that including the band-pass filtered versions of the PLV leads to the possibility of separating the preictal and ictal synchronous clusters. These two clusters are no longer mixed with each other, but separated by a gap. 54

4.8 The prediction accuracy (in %) for the different types of SVMs and different subsets of features. Linear OVO, RBF OVO, linear OVA and RBF OVA SVMs are respectively represented by dark blue, light blue, yellow and bordeaux bars. The different feature subsets are denoted on the x-axis. 'Corr', 'Coh' and 'PLV' respectively imply that only the maximal cross-correlation, coherence or PLV is used as measure. The label 'Filt' means that the seven filtered versions of the PLV are used and 'All' implies that all the measures are used. The number that completes the label indicates how much channel combinations are used in the feature vector. The accuracy results for linear/RBF OVO/OVA SVMs are very comparable for a specific feature subset. The linear OVO SVM sometimes obtains a substantially smaller accuracy compared to the three others. This figure clearly shows that it is very important to include the filtered versions of the PLV in the feature vector to obtain high accuracy results. The numerical values can be found in Table 4.3. . 57

4.9 The classification results for the ten different test datasets when using the RBF OVO SVM with the 'All 4' feature subset. The true class labels are represented by blue circles and the predicted ones by red stars. The accuracy obtained for every dataset is shown to the right of the figure. a) - j) The results for test dataset 1 up to test dataset 10. 61

A.1 A neuron as an input-output device. A neuron consists of three parts: dendrites (for input), the soma and an axon (for output). A neuron gets its input from presynaptic neurons and sends its output to postsynaptic neurons. Excitatory presynaptic neurons (green in the figure) will generate an excitatory postsynaptic potential (EPSP) and will depolarize the neuron. Inhibitory presynaptic neurons (red in the figure) will generate an inhibitory postsynaptic potential (IPSP) and will hyperpolarize the neuron. A summation of all these PSPs happens at the soma. If the neuron is depolarized above a threshold, it will fire an action potential (the black bars in the figure). 71

B.1 The thalamocortical model of Suffczynski et al. [76] 73

C.1 The model of the hippocampus of Wendling et al. [42] 77

List of Tables

4.1 The time needed (in msec) to calculate the different measures for a window of 5 seconds. Timed on a laptop with an Intel Core i5 processor, a clock rate of 2.40 GHz and 4 GB of RAM. 48
4.2 The results for classification with thresholding on the different measures. The optimal threshold range and the obtained accuracy are shown for every measure. 51
4.3 The numerical result of Figure 4.8. The prediction accuracy (in %) for the different types of SVMs and different subsets of features. The subsets of features are denoted by the same labels as in Figure 4.8. 58
4.4 The prediction accuracy (in %) for the different types of SVMs and specific subsets of features. The subset 'Filt 4' contains the seven filtered versions of the PLV for the following channel combinations: Ch1+Ch2, Ch2+Ch3, Ch3+Ch6 and Ch5+Ch6. The subset 'All 4' contains the maximal cross-correlation, coherence, (unfiltered) PLV and the seven filtered versions of the PLV for the following channel combinations: Ch1+Ch2, Ch2+Ch3, Ch3+Ch6 and Ch5+Ch6. 58
4.5 The training (in s) and prediction timings (in ms) for different types of SVMs for the feature subset 'All 4'. Note that the units for both are not the same (s versus ms). The SVMs with linear kernels are trained and predicted a lot faster than those with RBF kernels. The OVO strategy is clearly faster than the OVA strategy for both training and prediction. . 59

List of Abbreviations and Symbols

Abbreviations

AED	Anti-epileptic-drug
PSP	Postsynaptic potential
EPSP	Excitatory postsynaptic potential
IPSP	Inhibitory postsynaptic potential
GABA	γ-aminobutyric acid
AMPA	α-amino-3-hydroxy-5-methyl-4-isoxazolepropionic acid
NMDA	N-methyl-D-aspartate
EEG	Electroencephalography
SW	Spike and wave
TLE	Temporal lobe epilepsy
MTLE	Mesial temporal lobe epilepsy
LTLE	Lateral temporal lobe epilepsy
VNS	Vagus nerve stimulation
FDA	Food and Drug Administration
DBS	Deep brain stimulation
RNS	Responsive neurostimulation system
TMS	Transcranial magnetic stimulation
ChR2	Channelrhodopsin-2
NpHr	Halorhodopsin
AR	Autoregressive
SVM	Support vector machine
NN	Neural network
SOP	Seizure occurrence period
SPH	Seizure prediction horizon
S	Sensitivity
FPR	False prediction rate
$\mathrm{FPR}_{\mathrm{max}}$	Maximal false prediction rate
SPC	Seizure prediction characteristic
ROC	Receiver operating characteristic

WAG/Rij	Wistar albino Glaxo from Rijswijk
GAERS	Generalized absence epilepsy rat from Strasbourg
I_T	Low threshold calcium current
PY	Pyramidal neurons
IN	Interneurons
TC	Thalamocortical relay cells
RE	Reticular thalamic neurons
PSD	Power spectral density
LTS	Low threshold spike
SDI	Slow dendritic inhibition
FSI	Fast somatic inhibition
PPS	Pulses per second
PLV	Phase locking value
LP	Low-pass
RBF	Radial basis function
OVO	One-versus-one
OVA	One-versus-all
PCA	Principal component analysis

Symbols

x_i	One point of a time series
$\{x_i\}$	Time series
$\vec{\boldsymbol{x_i}}$	One point in state space (a vector)
$\{\vec{\boldsymbol{x_i}}\}$	State space trajectory
N	Number of points in a signal
t	Time
$v(t)$	Average membrane potential of a neuronal population
$r(t)$	Average firing rate of a neuronal population
$h(t)$	Impulse response function
m	Embedding dimension (method of delays)
τ	Delay (method of delays)
A	Amplitude for excitatory synaptic interactions
B	Amplitude for SDI synaptic interactions
G	Amplitude for FSI synaptic interactions
$1/a$	Time constant for excitatory synaptic interactions
$1/b$	Time constant for SDI synaptic interactions
$1/g$	Time constant for FSI synaptic interactions
C_{max}	Maximum linear cross-correlation
$C_{xy}(\tau)$	Linear cross-correlation
$\Gamma(f)$	Linear coherence
$G_{xy}(f)$	Cross-spectral density
$X(f)$	Fourier transform of $x(t)$
$*$	Complex conjugation
k	Number of nearest neighbors
$R_i^{(k)}(x)$	Squared mean distance of $\vec{\boldsymbol{x_i}}$ to its k nearest neighbors
$R_i^{(k)}(x\|y)$	Y-conditioned squared mean distance for $\vec{\boldsymbol{x_i}}$
$N^{(k)}(x\|y)$	Nonlinear interdependence
$\phi(t)$	Instantaneous phase of a signal
$\tilde{s}(t)$	Hilbert transform of $s(t)$
C	Regularization constant of a SVM
γ	RBF kernel parameter

Chapter 1

Introduction

1.1 Epilepsy

Epilepsy is a neurological disorder, characterized by recurrent seizures. About 50 million people around the world are affected by epilepsy, that is approximately 0.8% of the total world population [1]. Not only normal living is disrupted by these seizures, they can also cause mental and physical damage and even death. There are many different kinds of epileptic seizures, so epilepsy is a very diverse disease. Something that all kinds of seizures have in common is that they all involve abnormal excessive firing and synchrony of neurons in a part of the brain. The most common way to start the classification is to distinguish between focal (partial) and generalized seizures [2]. The onset of the seizure is localized in one hemisphere of the brain for focal seizures and involves both hemispheres for generalized seizures. Focal seizures can be further divided based on the location of seizure onset and the extent to which consciousness is affected. Awareness is unaffected for a simple partial seizure and affected for a complex partial seizure. A seizure can start local and eventually diverge into the entire brain, this is called a secondary generalized seizure. Generalized seizures can be further divided based on the effect that they have on the body. The different kinds of generalized seizures are absence, tonic, clonic, tonic-clonic, myoclonic and atonic seizures. All these seizures involve a loss of consciousness. This way of classification, based on clinical and electrographic observations, is in accordance with the scheme proposed by the International League Against Epilepsy (ILAE) in 1981 [3]. To sum up, epileptic seizures are classified as follows:

1. Focal seizures
    a) Simple partial seizures: no reduced consciousness
    b) Complex partial seizures: reduced consciousness
        i. Simple partial onset followed by reduction of consciousness
        ii. Reduced consciousness at onset
    c) Secondary generalized seizures
        i. Simple partial onset that evolves to a generalized seizure

   ii. Complex partial onset that evolves to a generalized seirure
   iii. Simple partial onset that evolves to a complex partial seizure and afterwards to a generalized seizure

2. Generalized seizures (convulsive or non-convulsive)

   a) Absence seizures (petit mal): brief loss and return of consciousness
   b) Myoclonic seizures: unintentional twitching of muscles
   c) Clonic seizures: involuntary rhythmic jerking of muscles
   d) Tonic seizures: involuntary stiffening of muscles
   e) Tonic-clonic seizures (grand mal): alternation between a tonic and clonic phase
   f) Atonic seizures: unintentional loss of muscle tone (extreme relaxation)

3. Unclassified epileptic seizures

This list shows that epilepsy is not just one specific disease, but a very diverse disorder. Both focal and generalized seizures will be considered in this thesis. The specific type for focal seizures will be mesial temporal lobe epilepsy (MTLE), because it is the most common type of focal epilepsy. MTLE has its onset in the inner part of the temporal lobe of the brain. It can express itself as a simple or complex partial seizure or as a secondary generalized seizure. The specific type for generalized seizures will be absence seizures, because this seizure can occur up to one hundred times a day.

There are various methods to treat epilepsy nowadays [4]. The most common are medication and surgery. Many epileptic patients have seizures that are well controlled by anti-epileptic-drugs (AEDs). Approximately 30% of the patients suffer from medically refractory epilepsy [5]. For these patients, the seizures can not be controlled by AEDs. This has caused a lot of modern epilepsy research to be focused at the understanding of the underlying mechanisms of these seizures and the development of alternative treatments. Computational modeling has become an important tool in this context. There are a lot of good reasons for this. First of all, a model can be used to check assumptions that follow from experiments. A model can also generate a new hypothesis, that can be checked by experiments. This implies that computational modeling will not replace experiments, but that they will work together to generate new insights into pathogenesis and treatment of epilepsy. Another reason for computational modeling is the fact that experiments that are hard to perform in real life can be simulated on a computer. Also experiments that are ethically not allowed on people can easily be simulated. Computational modeling of epilepsy has been used a lot in the past for different purposes: getting insights into cellular and network mechanisms of epileptic seizures [6], predicting epileptic seizures [7] and developing strategies for therapy [8].

Alternative strategies for treatment are very important for the patients that have seizures that can not be controlled by AEDs. This thesis will hopefully contribute to

this field of research. The motive to do all this is to improve the quality of life for epileptic patients. It will turn out that looking at epilepsy as a dynamical disease is very useful [9]. The basic idea is to look at an evolving brain as going from one attractor to another in a multi-stable phase plane. These transitions can be the result of changes in the parameters of the system (bifurcation) or external disturbances to the system. Since not every reader may have a background in neuroscience, this thesis includes an appendix that introduces the basic concepts. It is highly recommended to read Appendix A before continuing to the next section if the reader does not have any background in neuroscience.

1.1.1 Absence seizures in a thalamocortical circuit

Absence seizures are generalized epileptic seizures of a brief duration (often less than twenty seconds) that start and end abruptly. The number of occurrences can range from a few times a day to one hundred times a day. During the seizure the patient has a loss of consciousness, but he usually does not suffer from convulsions. These types of seizures normally occur during childhood and often disappear with adolescence. This is however not always the case. Absence seizures have a very characteristic EEG-pattern, namely spike and wave (SW) discharges [10]. Intracellular recordings have shown that the 'spike' and 'wave' components are associated with neuronal firing and neuronal silence respectively [11]. This neuronal silence is due to hyperpolarization, which corresponds to a change in the membrane potential of a neuron towards more negative voltages. This already suggested an active role of inhibitory processes and γ-aminobutyric (GABA) receptors. These are the receptors that respond to the neurotransmitter GABA, which is the main inhibitory neurotransmitter in the brain (see Appendix A for more information about hyperpolarization and GABA). Experimental models from the last decades made it possible to identify the brain structures that are involved in absence seizures. A lot of these experiments have pointed out that the thalamus plays a critical role in the generation of absence seizures:

- Lesions or inactivation of the thalamus caused SW seizures to disappear [12–14].
- It is possible to gradually transform spindle oscillations into SW discharges [15, 16]. Spindle oscillations are waxing-and-waning oscillations of 7-14 Hz that are generated in the thalamic circuits [17, 18].
- Thalamic and cortical neurons fired in phase with the 'spike' component and during the 'wave' component all cell types were silent [11, 19, 20].
- Mice that were genetically modified so that they lacked the gene for the T-type calcium current in thalamic relay cells showed a resistance to absence seizures [21]. The T-type current is responsible for the bursting behavior of thalamic cells and is essential to generate absence seizures.

Just like for the thalamus, experimental models showed that the cortex is necessary for the generation of absence seizures:

- There were no SW discharges when high doses of $GABA_A$ antagonists were injected in the thalamus. A cortical injection of the same drug did led to SW patterns [22, 23].
- The threshold for generating absence seizures was much higher in the thalamus compared with the cortex [23].
- During a cortical seizure with SW patterns, a large fraction of the thalamic cells were completely silent [24, 25].

These experimental models show that the thalamus and cortex are both actively involved in the generation of absence seizures. They also have led to more insights into the basic neuronal mechanisms of absence seizures. The thalamocortical (thalamus and cortex) mechanisms of sleep spindle generation are currently believed to lie at the basis of SW discharges [17, 26, 27]. The development of some computational models, namely a couple of thalamic and thalamocortical models, also resulted in more insight into the basic neuronal mechanisms of SW discharges [24, 28–30]. However, these models did not address a very important subject, namely the mechanisms of the spontaneous transitions between normal spindle oscillations and epileptic SW discharges. The model that will be used in this thesis can make the transitions between normal and epileptic activity and will be introduced in Chapter 2 (Section 2.1).

1.1.2 Temporal lobe epilepsy in the hippocampus

Temporal lobe epilepsy (TLE) is the most common type of focal epilepsy. The onset of TLE is located in the temporal lobe of the brain. There are two main types of TLE: mesial temporal lobe epilepsy (MTLE) and lateral temporal lobe epilepsy (LTLE). MTLE has its onset in the inner aspect of the temporal lobe, namely the hippocampus or the amygdala. The onset of LTLE is located in the neocortex, which is the outer surface of the temporal lobe. Because different regions within the brain are strongly interconnected, seizures starting in one part can always diverge into the other parts and also in further regions of the brain. MTLE is the most common form of TLE and will therefore be considered further in this thesis. AEDs are often inefficient for patients with TLE. The surgical removal of the epileptogenic region (the region that causes the seizure) is often the only way to eliminate or reduce the seizures [31]. Unfortunately, such a surgery is only effective in approximately 50% of the cases [32]. The study of mechanisms that trigger these seizures is essential to improve the efficiency of surgery and the development of new therapeutic strategies. For being able to remove the epileptogenic region, the location of this area first has to be determined. For generalized seizures this is often not possible, because the onset for these seizures is not localized. In these cases pathways that consistently contribute to the propagation of seizures can be removed.

MTLE has a characteristic electrophysiological pattern during the onset of a seizure. Typically, there is a development of spikes with a high amplitude and a low frequency. This activity is then succeeded by oscillations of a low amplitude and

a high frequency (low voltage rapid discharges). When EEG signals are recorded with intracerebral (inside the cerebrum) electrodes during a presurgical evaluation, both types of signals are often observed at seizure onset [33, 34]. It is also possible that only the high-frequency oscillations develop at seizure onset [35, 36]. These high-frequency signals contain maximum frequencies belonging to the γ-band (30-100 Hz) and originate from epileptogenic regions. Experimental and computational studies provided new findings in the neuronal mechanisms that are responsible for these low voltage rapid discharges. First of all, inhibitory interneurons in the hippocamus or neocortex were shown to have close relations with these high-frequency oscillations [37, 38]. Secondly, it was stated that two different kinds of $GABA_A$ responses played an important role in the generation of γ-rhythms [39]. Wendling et al. showed that neuronal population models could explain different rhythms of depth-EEG signals [40]. This model consisted of three interacting populations. There was a population of main cells (excitatory pyramidal neurons in the hippocamus), a population of other excitatory pyramidal cells and an inhibitory population of interneurons. The second population of pyramidal cells is included because there are a lot of excitatory connections from pyramidal cells to other pyramidal cells in CA1 (a particular region in the hippocampus) [41]. In this study however, they were not able to generate γ-rhythms. The model that will be used in this thesis is an extended version of that model [42]. This model will be introduced in Chapter 2 (Section 2.2).

1.2 Modeling framework for epilepsy

It is a general trend in the world of engineering to build mathematical models of dynamical systems that need to be analyzed. It is important to bear in mind that every model is a simplification of the real world. This degree of simplification is a very important choice of the designer. In the ideal case, the model is the most simple model possible, while giving good results that are relevant to the questions that are asked. Based on the amount of simplification, two classes of computational models can be distinguished: micro-scale and macro-scale models.

In the framework of micro-scale models, neuronal networks are built from models of individual neurons with a certain degree of biophysical reality. These individual neurons are often based on the Hodgkin-Huxley framework [43]. The dynamics of the entire network then follow from the activity of the individual neurons and their interconnections. These models are used to answer questions that are related to the dynamical behavior of the membrane potential of individual neurons. This approach is usually used for modeling neuronal networks within a given brain region. The focus at single neuron level can be on changes in the kinetic properties of ion-channels or the role of neuronal morphology (by building the individual neuron out of several compartments). At network level the focus is on network topology and synaptic interactions between neurons. This type of modeling can become computationally expensive, especially when a network consists of thousands of neurons. For this reason there are various simplified neuronal models available. These models are designed to reduce the complexity of the system. Some examples are the Morris-Lecar [44],

Hindmarsh-Rose [45] and FitzHugh-Nagumo [46, 47] models.

A macro-scale model does not try to model the dynamics of individual neurons, but the dynamics of neuronal populations. These models are much more suitable to answer questions about interactions between different brain regions. The framework of macro-scale modeling started with Wilson and Cowan in the 1970s [48, 49]. In macro-scale modeling, the degrees of freedom in a dynamical system (a population of neurons) are reduced to a distribution function. This distribution function describes the probabilistic evolution of neuronal states in the population [50]. This approach can be simplified further by only taking into account the first moment of the distribution function. This is equivalent to the center of mass and represents the mean firing rate of the neuronal population. These models are known as neural mass models [51] and have become a very successful tool in the field of computational neuroscience [52–54]. The average presynaptic firing rate $r(t)$ of a subpopulation is transformed into the average postsynaptic firing rate of the same subpopulation in two steps. First, the average postsynaptic membrane potential (PSP) $v(t)$ of this subpopulation is obtained as the convolution of the average presynaptic firing rate with an impulse response function:

$$v(t) = r(t) * h(t) \tag{1.1}$$

where the impulse response function has the next form:

$$h(t) = A \cdot a \cdot t \cdot e^{-at}. \tag{1.2}$$

The constant A determines the amplitude of the average voltage and the constant a determines the rise time of the average voltage. In the second step, this average PSP $v(t)$ is transformed into the average postsynaptic firing rate of the subpopulation. This is done by a nonlinear sigmoidal function that generates $s(v(t))$ from $v(t)$. The most common form for this sigmoid function is given by:

$$s(v(t)) = \frac{e_0}{1 + e^{(p(v_0 - v(t)))}}. \tag{1.3}$$

The parameter e_0 represents the maximal firing rate of the subpopulation, v_0 acts as a threshold for firing and p is the slope of the sigmoid. Maybe a little clarification of terminology is needed here. The average presynaptic firing rate of a population is the firing rate of incoming signals to a population. These signals are coming from neurons which are presynaptic neurons for the considered population. The average postsynaptic firing rate of a population is the firing rate which the considered population sends to its postsynaptic neurons. The average PSP of a population is just the average of all the membrane potentials of the neurons within a population.

A lot of experimental techniques for measuring brain activity involve large populations of neurons. Some examples are Electroencephalography (EEG) and field potential recordings. The results of macro-scale models can be compared directly with these experimental findings. The control and prediction of epileptic seizures will be based on EEG-data. For this reason, the models studied in this thesis will be macro-scale models (neural mass models).

1.3 Treatments for epilepsy

There are few alternative treatments for patients suffering from epileptic seizures which are not controlled by AEDs. A careful analysis is performed to check if a surgery is possible for such a patient. An extensive evaluation is required to ensure that the operation is likely to reduce or eliminate the epileptic seizures without causing any damage to essential functions of the brain. Several tests, including long EEG monitoring, are necessary to locate the damaged region of the brain that is causing the seizures. This location determines if surgery is a possibility and what type of surgery should be used. For focal seizures, the location of onset of a seizure is confined to a small region. This is the reason why surgery is used mostly in the case of focal seizures. This means that surgery is not possible in all types of epilepsy and if it is possible, it is not always effective [32, 55]. Therefore it is important that alternative treatments are found for these patients.

The ketogenic diet is a high-fat, adequate-protein, low-carbohydrate diet which is mainly used to treat refractory epilepsy in children [56]. This diet is effective in about 30% of the patients that remained on the diet, but only 55% of the patients keep on following the diet [57]. Most patients that discontinue the diet do this because it is not effective enough or too restrictive.

The successes of brain stimulation as a treatment for Parkinson's disease have encouraged the search for brain stimulation techniques to treat epilepsy [58]. Two alternative treatments will be discussed here: electrical stimulation and optogenetic techniques.

1.3.1 Electrical stimulation

Two very important parameters for electrical stimulations to the brain are the brain structure to be stimulated and the stimulation protocols (type of pulses, frequency, amplitude,...). Nowadays there are a couple of different types of electrical stimulation techniques [59, 60].

Vagus nerve stimulation (VNS) The vagus nerve is the tenth of twelve cranial nerves. The cranial nerves are nerves that emerge from the brain and not from the spinal cord (spinal nerves). VNS is applied by an electrical device, implanted in the chest, that connects to the left vagus nerve in the neck. It is an indirect electrical stimulation of the brain and is currently the only stimulation therapy for epilepsy approved by the Food and Drug Administration (FDA). VNS is an open-loop stimulation technique, which means that there are automatic intermittent stimulations. The patient can also generate on-demand stimulations by the use of a magnet.

Deep brain stimulation (DBS) DBS is applied by an electrical device, also implanted in the chest, that delivers electrical stimulations to deep brain structures (the anterior nuclei of thalamus). This is done by depth electrodes that are implanted through the skull. DBS stimulates the brain directly and is a promising

technique, but it is not yet approved by the FDA. It is, like VNS, an open-loop stimulation technique.

Responsive neurostimulation system (RNS) The RNS is an electrical device that is implanted in the skull and delivers electrical stimulations to epileptic foci. The implanted electrodes send EEG signals to the RNS and when the RNS detects a seizure, it will stimulate the brain with the goal of disrupting the seizure. This is a closed-loop stimulation technique, so there is only electrical stimulation when the device detects a seizure. RNS is also not yet approved by the FDA.

Transcranial Magnetic Stimulation (TMS) TMS is a noninvasive method that can be used to depolarize or hyperpolarize neurons in the brain through electromagnetic induction. The therapeutic results of this method are however not so encouraging.

The ultimate goal of these methods is to create an implantable device ('a brain pacemaker') that can control the epileptic seizures. A lot of research in epilepsy is directed towards the application of control engineering practices to prevent epileptic seizures. These practices can be integrated perfectly in the framework of computational modeling [61–63]. One of the goals in this thesis is to develop and implement a control system for absence seizures. This will be done in Chapter 3. The model for absence seizures, introduced in Section 2.1, will be used to develop the control system.

1.3.2 Optogenetic techniques

Optogenetics is a new technology that combines optics and genetics and allows to control the behavior of single neurons in the living brain with a high degree of temporal and spatial resolution [64]. Neurons can be genetically modified so that they contain a certain light-sensitive protein. This makes the neurons sensitive to light of a certain frequency. Blue light opens the channelrhodopsin-2 (ChR2) ion-channels and causes a ChR2-expressing neuron to spike. Yellow light activates the chloride pump halorhodopsin (NpHR) and this causes a NpHR-expressing neuron to be silent (no spiking activity). The reader is referred to [65] for details about these mechanisms. Since optogenetics can be used to regulate the network excitability, it can become a very important tool for the treatment of epilepsy. This is especially the case for partial seizures, where the epileptogenic region is confined. A lot of studies proved that the optogenetic approach can be useful to control epileptic activity [66, 67]. In this thesis two macro-scale models are considered. This means that one of the great properties of optogenetics, namely the high spatial resolution, can not be used. For this reason, optogenetic control will not be considered further in this thesis, but it deserved to be described shortly.

1.4 Prediction framework for epilepsy

It is clear that detecting and controlling a seizure is not enough to make patients completely free of seizures. In order to do this, the seizure needs to be predicted well in time so that actions can be taken to avoid the upcoming seizure. If this all is to happen on an implantable device, a low computational cost is very important. There has been a lot of research aimed towards the prediction of epileptic seizures. An extensive overview of this topic can be found in [68]. As stated before, it is not always possible to predict an incoming seizure, because there are two different ways for a seizure to develop [9]. Take for example absence seizures, they show sudden transitions between interictal and ictal stages. In this case the EEG does not contain any dynamical changes that can be used to detect the seizure before it starts. Partial seizures like TLE on the other hand, show gradual changes in EEG dynamics that can be detected and used to predict the seizure.

The first work on seizure prediction was carried out by Viglione and Walsh in the 1970s [69]. Quickly, different groups of researchers followed their example. During these early stages, linear measures were used to find seizure precursors. These measures are derived from the signal in the time-domain or the frequency-domain. An example in the time-domain is autoregressive (AR) modeling. An AR model is defined by

$$x_i = \sum_{n=1}^{p} a_n x_{i-n} + \epsilon_i$$

and states that the current value of a time series is the linear combination of p past values and a random noise term ϵ_i. The parameters $\{a_n\}_1^p$ need to be estimated by fitting the model to the data. Studies have used these parameters to predict seizures either directly [70] or by giving these parameters as features to a support vector machine (SVM) [71]. Some other linear measures that have been used are: statistical moments, spectral band power and accumulated energy [68].

In the 1980s there was an emergence of non-linear system theory. Non-linear approaches are of course much better suited to describe complex behavior than linear approaches. Thanks to this, non-linear measures were introduced in the field of seizure prediction. In contrast with linear ones, non-linear measures are often not calculated directly from the signal in the time-domain or frequency-domain. Non-linear measures are usually derived from state space trajectories of a dynamical system. This means that the time series $\{x_i\}_1^N$ must be transformed into a state space trajectory. A popular way to achieve this, is by using 'the method of delays' [72]. In this method the discrete signal is assumed to be sampled from a continuous signal

$$x_i = x(i\tau_s) \qquad i = 1 \dots N$$

with τ_s the sampling time. The trajectory, $\mathbf{x}(t)$, in m dimensions is given by

$$\mathbf{x}(t) = (x(t), x(t-\tau_d), \dots, x(t-(m-1)\tau_d))$$

where the delay time τ_d is an integer multiple of τ_s. The largest Lyapunov exponent was used to describe the chaotic behavior of an EEG and it was shown that there

was a decrease before seizure onset [73]. Another non-linear measure, the correlation density, was shown to decrease during the pre-ictal stage [74]. Some other non-linear measures are the correlation dimension, correlation entropy and the dynamical similarity index [68]. All the measures (linear and non-linear) defined thus far are univariate measures. There also exist bivariate measures that can be used for seizure prediction. Some linear bivariate measures are the maximum linear cross-correlation and the linear coherence [68]. Both of these quantify the amount of synchronization between two signals. Some bivariate non-linear measures are the non-linear interdependence (quantify generalized synchronization), dynamical entrainment (entrainment between two brain regions based on the difference between the largest Lyapunov exponents) and phase synchronization [68]. All these measures can be used directly by defining thresholds or they can be used as input features for a classifier, for example an SVM or a neural network (NN).

In a perfect world, a method for predicting an epileptic seizure would give the exact moment in time when the seizure will occur. This is however not possible with the current prediction methods. This uncertainty will be incorporated by talking about the seizure occurrence period (SOP). The SOP is the period in which the seizure is expected to occur. In order to be able to avoid the seizure (by electrical stimulation for example) or to warn the patient, there has to be some time between the alarm signal of the prediction method and the moment that the SOP starts. This time interval will be defined as the seizure prediction horizon (SPH). When evaluating a seizure prediction method, one always has to consider sensitivity and specificity together. Sensitivity (S) is the proportion of correctly predicted seizures with respect to all the seizures. An appropriate measure for the specificity in this case is the number of false predictions in a given time interval. This is also called the false prediction rate (FPR). When lowering some threshold value, the method will predict more seizures in the pre-ictal stages, but will also generate more false predictions in the interictal stages. Too much false predictions could lead to side-effects resulting from the unneeded interventions or the patient's ignorance towards the alarm. Therefore the false prediction rate should be kept below a maximum allowed value (FPR_{max}). A seizure prediction method should not only have good results in terms of sensitivity and specificity, but should also be statistically valid: it should at least perform better than a random or periodic predictor. All these important characteristics led to the development of the seizure prediction characteristic (SPC) for comparing different prediction methods. The SPC shows the dependence of the sensitivity with respect to the maximum allowed false prediction rate, the seizure occurence period and the seizure prediction horizon: $S = f(FPR_{max}, SOP, SPH)$ [75]. This can actually be seen as a type of receiver operating characteristic (ROC), but then specifically designed for seizure prediction purposes.

One of the goals in this thesis is to develop a prediction method for MTLE. Artificial data is generated with the model for MTLE, which is introduced in Section 2.2. This data will then be used in Chapter 4 to develop the prediction method.

Chapter 2

Modeling epileptic seizures

This chapter is about building computational models for epileptic seizures. Both models that will be used throughout this thesis will be introduced here. In Section 2.1, the model for absence seizures is presented. The general outline of the model as well as the possible types of activity will discussed in that section. Mathematical details about this model can be found in Appendix B. It turns out that this model mimics the dynamics of absence seizures very well. This allows the user to interact with the model and see what the effect on the seizures is. In Chapter 3, a control system for this model will be designed and implemented. In Section 2.2, the model for MTLE will be introduced. The general outline of the model is presented together with the types of signals that this model can produce. Mathematical details about this model can be found in Appendix C. This model will be used to develop a prediction framework for MTLE in Chapter 4.

2.1 Model for absence seizures

2.1.1 Introduction

As already mentioned in Section 1.1.1, there were no computational models that addressed the mechanisms of the spontaneous transitions between normal spindle oscillations and epileptic SW discharges. Suffczynski et al. presented a computational model that made a novel contribution to the research field for this aspect of absence seizures [76].

2.1.2 Methods

Suffczynski et al. built a computational model for SW discharges that were recorded from the Wistar albino Glaxo from Rijswijk (WAG/Rij) rat [77]. A WAG/Rij rat is a genetic animal model of absence epilepsy and has similar characteristics as the generalized absence epilepsy rat from Strasbourg (GAERS) [78]. Both are inbred strain of rats that suffer from spontaneous absence seizures with SW discharges. The model of Suffczynski et al. is an extended model of that one proposed by Lopes

da Silva et al. [79]. In the new model there are three very important extensions incorporated with respect to absence seizures:

- The model is built out of two interconnected populations, a cortical and a thalamic one. As already explained by the experimental models in Section 1.1.1, both of these regions are necessary to generate absence seizures with SW discharges.
- The burst firing of thalamic cells is taken into account when transforming the mean membrane potential to the mean firing rate in the thalamic populations. This is done by incorporating the low threshold I_T calcium current in this transformation. Knock-out mice that were lacking the gene for this I_T current did not suffer from absence seizures [21].
- The GABA receptor is subdivided in a fast $GABA_A$ and a slow $GABA_B$ receptor type. The $GABA_B$ receptors have nonlinear activation properties [80].

The cortical module of the model consists of an excitatory population of pyramidal neurons (PY) and an inhibitory population of interneurons (IN). These populations are interconnected, so the PY cells excite the IN cells and the IN cells inhibit the PY cells. The thalamic module of the model consists of an excitatory population of thalamocortical relay cells (TC) and an inhibitory population of reticular thalamic neurons (RE). These two populations are also interconnected. So the TC cells excite the RE cells and the RE cells inhibit the TC cells. The cortical and thalamic module are further also connected to each other. The PY cells excite the TC and RE cells, while the TC cells excite the PY and IN cells. There are three external inputs to the model. The RE population receives an inhibitory external input, which represents neighboring RE cells. The TC population receives an external excitatory input, which represents sensory inputs. The PY population also receives an external excitatory input, which represents the input from other PY cells. All the excitatory synaptic connections are regulated by glutamate α-amino-3-hydroxy-5-methyl-4-isoxazolepropionic acid (AMPA) receptors. All the inhibitory synaptic interactions are regulated by the γ-aminobutyric acid (GABA) receptor. As already mentioned, the $GABA_A$ receptor mediates a fast response to GABA, while the $GABA_B$ receptor mediates slow responses to GABA. Note that for the inhibitory case the neurotransmitter and the receptor are both named GABA. In the excitatory case the neurotransmitter is glutamate and the receptor is named AMPA. The model of Suffczynski et al. is shown in Figure 2.1. The four populations are framed (green for the excitatory and red for the inhibitory populations). The input and the output of these colored boxes are respectively the average presynaptic firing rate and the average postsynaptic firing rate of the populations. The blocks AMPA, GABAa and GABAb transform the average presynaptic firing rate into the average postsynaptic current. The integrator turns this into the mean membrane potential (average postsynaptic potential) and the saturation block transforms this into the average postsynaptic firing rate. All these quantities are defined as an average over the entire population, not for individual neurons inside a population. The mathematical details of this model can be found in Appendix B.

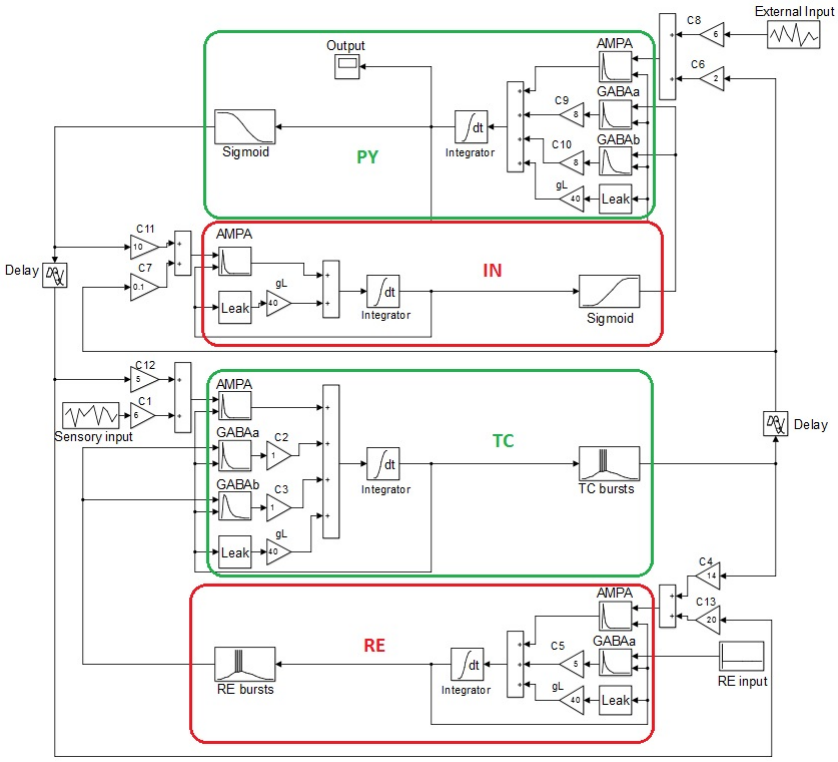

Figure 2.1: The thalamocortical model of Suffczynski et al. [76]. The cortical module consists of an excitatory population of PY cells and an inhibitory population of IN cells. The thalamic module is built from an excitatory population of TC cells and an inhibitory population of RE cells. A mathematical description of this model can be found in Appendix B.

2.1.3 Results

The model can generate two qualitatively different types of signals. These are in accordance with what is seen in animal models (WAG/Rij and GAERS). On the one hand there is the waxing-and-waning spindle oscillations with a frequency around 11 Hz. On the other hand there is the seizure activity with high amplitudes and a frequency around 9 Hz. The first one is the normal activity and the second one is the epileptic activity. A terminology that is often used when talking about signals that contain seizures is 'interictal' and 'ictal'. The ictal part of the signal is the part that contains the seizures while the interictal part refers to the intervals between seizures. It is important to note that the goal of this model was not to simulate realistic waveforms, but to be able to investigate the transitions from normal spindle activity to SW discharges. The waxing-and-waning form of the spindle oscillations however looks realistic. The typical SW pattern is not visible in the simulated epileptic activity, instead it is a quasi-sinusoidal wave of the right frequency (9 Hz). These two different types of signals are shown in Figure 2.2. Figure 2.2a shows both types of signals with spontaneous transitions. It can be seen that, just like in real life, the

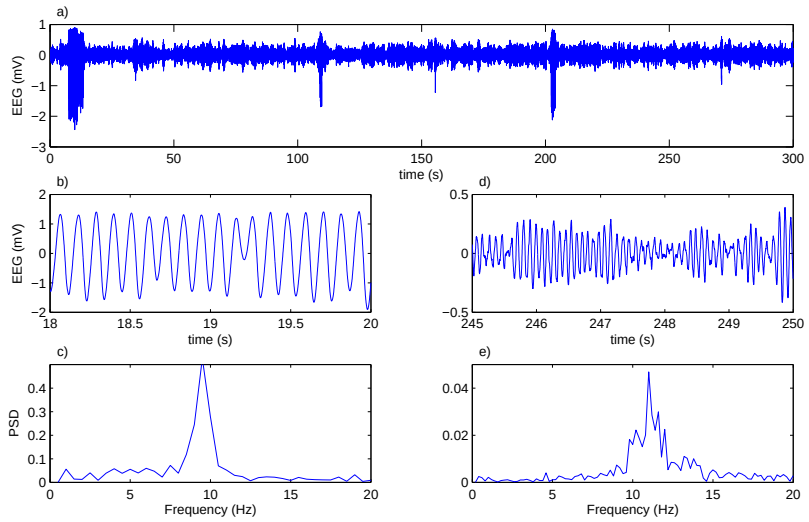

Figure 2.2: The simulated signals of the thalamocortical model of absence seizures. a) The time evolution of the mean membrane potential of the PY cells in the cortex. This output represents the dynamics of an EEG and shows both interictal and ictal activity with spontaneous transitions between them. The parts with a high amplitude are the ictal parts. b) A close-up of an ictal part of the EEG, where the quasi-sinusoidal activity is clearly visible. c) The PSD for the ictal activity shows a clear peak at 9 Hz. d) A close-up of an interictal part of the EEG, which clearly shows the waxing-and-waning progress of the interictal signals. e) The PSD of the interictal activity is centered around 11 Hz. This shows that the interictal activity has a slightly higher frequency than the ictal activity.

signal shows long periods of normal EEG activity with epileptic activity intermingled only occasionally. Figure 2.2b shows a close-up of the epileptic activity. This is a quasi-sinusoidal signal with a frequency around 9 Hz (see Figure 2.2c). Figure 2.2d shows a close-up of the normal activity. The waxing-and-waning pattern is clearly visible and the frequency of this signal is 11 Hz (see Figure 2.2e). The fact that only these two types of behavior are simulated is justified by the observations that SW discharges predominantly occur during sleep spindle oscillations [81, 82]. This type of oscillations usually occur when a person is somewhat drowsy or sleepy.

The model can operate in bistable mode: it can generate both types of activity and spontaneous transitions between them. The bistability is a result of specific properties of $GABA_B$ receptors and I_T current in TC neurons. A lot of studies on animal models of absence epilepsy have confirmed the necessity of $GABA_B$ activation to generate seizures [83, 84]. $GABA_B$ receptors have non-linear activation properties, so they need a strong stimulus to be activated. This strong stimulus is not the case during normal activity. The seizure starts when $GABA_B$ receptors in TC cells are activated. The long lasting inhibition caused by these receptors results in a prolonged hyperpolarization. Because of this long hyperpolarization, the inactivation of I_T

current in TC cells is removed. This causes burst firing in TC cells and these bursts activate the RE cells strongly. These RE cells can then again activate the $GABA_B$ receptors and the cycle can start again. The seizure stops when this cycle fails to reinitiate. This mechanism was also found to be responsible for absence seizures in other studies [85, 86]. A bifurcation analysis shows that an equilibrium point (normal activity) and a limit cycle (seizure activity) are present simultaneously in the phase plane. It also points out that random fluctuations in the external inputs are responsible for transitions between these two types of behavior. The phase portrait of the system is illustrated in Figures 2.3a-c for respectively the case without noise, a very low level of noise and a high level of noise on the external input to the TC cells. The value of the external input to the PY cells was, in the case of Figures 2.3a-b, kept constant to a certain value so that the system was in the state of normal behavior (red) or seizure activity (blue). To be able to switch from one attractor to the other, there are noise terms needed in both the external inputs. Since these transitions are produced by a random process, they are inherently unpredictable. The goal in this thesis for this model is to detect a seizure and to control it. The detection of a seizure can be based on two criteria: the activation level of $GABA_B$ receptors in TC cells and the amplitude of the mean membrane potential of the PY cells. In this model, both can be measured, but in real life the activation level of $GABA_B$ receptors can not be used to detect seizures. Only the mean membrane potential of the PY cells will be used for this reason and the activation level of $GABA_B$ receptors can be used afterwards to check the results. An EEG is a recording of the electrical activity of a large neuronal population in the cortex. The mean membrane potential of the PY cells is assumed to have the same dynamics as the EEG recordings. This is an important reason to base the detection of a seizure on the mean membrane potential of the PY cells, because the detection in real life can then be done by using recorded EEG signals. Once detected, the seizure has to be controlled. This will be done by giving stimuli to the brain (brain stimulation therapy).

An important thing to do when starting to work with a model is to check if the model is valid with respect to what researchers found out by carrying out experiments. This was done by changing parameters in the model and checking if the seizure activity behaved as in real experiments. The most important ones are given in the list below. The model with the reference set of parameters was used as the control for the comparisons:

- Increasing the AMPA conductances in the PY neurons led to more SW discharges, for the simple reason that this causes cortex hyperexcitability. During an epileptic seizure there is an increased neuronal excitability. This causes more feedback in the thalamocortical system and is a possible mechanism for absence seizures [87].

- Increasing the $GABA_A$ conductances in the PY cells led to less SW discharges. There will only be sleep spindles if the cortex stays under strict control of $GABA_A$ [88]. The cortical hyperexcitability can be due to the decrease of $GABA_A$ inhibition [89].

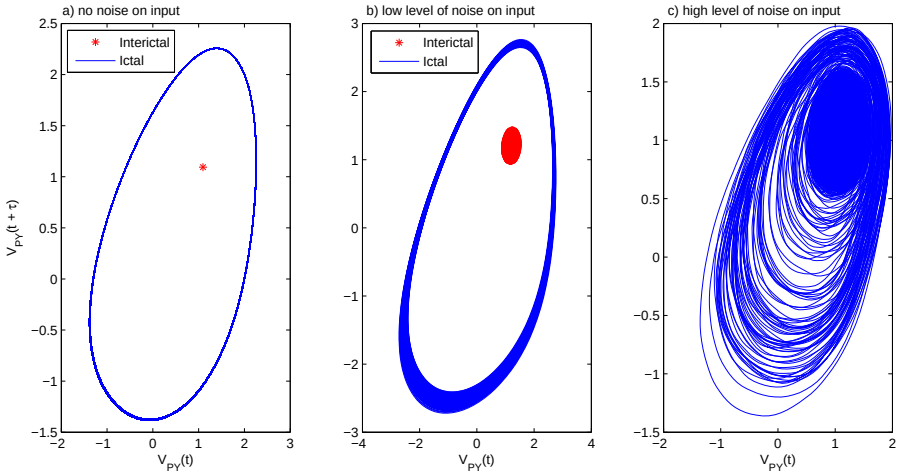

Figure 2.3: The phase portrait for the model of absence seizures. The state space trajectories were obtained by using the method of delays with $\tau = 20\,ms$ and $m = 2$. The mean membrane potential of the PY cells in the cortex (V_{PY}) is plotted against a delayed version of itself. a) The state space trajectories when there is no noise on the external inputs. There will be no transitions from interictal to ictal (or vice versa) in this case. The red dot represents the interictal activity and clearly forms an equilibrium point. The blue curve represents the ictal activity and forms a limit cycle. b) After introducing a low level of noise on the external input to the TC cells, the equilibrium point and limit cycle can be seen to deviate a little bit from their previous path. This low level of noise is however not high enough to cause transitions from the equilibrium point to the limit cycle (or vice versa). c) Transitions from one attractor to the other start to happen when the noise level is increased. This implies that transitions from interictal to ictal activity (and vice versa) are possible for these noise levels.

- The blocking of $GABA_B$ receptors in the PY and TC cells resulted in an activity free of seizures. This is because the $GABA_B$ receptors are necessary for seizure generation as stated before.

- The increase of AMPA conductances in the RE cells led to more SW discharges. This is because a stronger activation of RE cells results in a bigger possibility that the $GABA_B$ receptors in the TC cells are activated.

- An increase of the $GABA_A$ conductance in RE cells led to less SW discharges. This decreased the pacemaking property of these cells as stated in [85]. It can also be seen as the opposite of the previous point.

- An increase of $GABA_A$ in TC cells led to the opposite effect as in the RE cells, namely more SW discharges. This is consistent with the findings of other studies [90].

- The parameters of the sigmoids also have a big effect on SW discharges. The sigmoids are used to convert the mean membrane potential into the average postsynaptic firing rate in the cortical populations (see Appendix B). The maximum firing rate parameter and the parameter for the threshold of firing are easy to understand. Increasing the maximum firing rate will increase the number of SW discharges, because of cortical hyperexcitability. Increasing the threshold parameter for firing will decrease the number of SW discharges. The effect of changing the slope of the sigmoid is not so obvious. Increasing the slope will narrow the distribution of firing thresholds in a neuronal population. This will cause more neuronal synchrony and this is a typical characteristic of epileptic activity in the brain [11, 19, 20].

- An increase of calcium currents in the thalamic modules led to more SW discharges. There will be more bursts because of this increase. This is in accordance with experimental findings [91].

- The importance of the coupling between thalamus and cortex was also confirmed by this model. The coupling could be changed by changing the coupling constants or by playing with the time-delay between these modules. In every case, a reduced coupling between the two resulted in less SW discharges.

2.1.4 Conclusion

This model generates two qualitatively different types of behavior (ictal and interictal) with spontaneous transitions between them. It is not a problem that the generated waveforms for the ictal part do not look like the typical SW pattern that is seen in real life. The most important job for this model is to mimic the dynamics that are in play for absence seizures. The above list shows that the model captures the important aspects of absence seizures. This means that the model is a good starting point for trying to detect and control the seizures. The fact that the model can operate in bistable mode suggests that it should be possible to switch from one attractor to another by sending external stimuli to the model (brain).

2.2 Model for temporal lobe epilepsy

2.2.1 Introduction

As stated in Section 1.1.2, the problem with the first model of Wendling et al. was the fact that γ-rhythms could not be simulated by their model [40]. To cope with this problem, Wendling et al. extended their original model [42]. In their original model there were three populations: two excitatory and one inhibitory. In the new model, a fourth subset was added that represented another population of inhibitory interneurons. This new inhibitory population had faster dynamics than the one already included in the previous model. These two inhibitory populations represented two different types of $GABA_A$ responses. There is a fast response for the neurons that form synapses close to the soma ($GABA_{A,fast}$) and a slow response for neurons forming synapses on the dendrites ($GABA_{A,slow}$). By making this distinction, γ-rhythms could be simulated by their model.

2.2.2 Methods

The entire model of the hippocampus is built out of four populations: the main cells (excitatory pyramidal neurons), distant excitatory pyramidal cells, slow inhibitory interneurons and fast inhibitory interneurons. The slow inhibitory interneurons are projecting on the dendrites of the main cells, while the fast inhibitory interneurons are projecting on the soma of the main cells. All these populations are interconnected with each other. The main cells excite the three other populations. The distant pyramidal cells excite the main cells and both inhibitory populations inhibit the main cells. The inhibitory populations also interact with each other: the fast interneurons are inhibited by the slow interneurons. There is also an external noise input included in the model that represents excitatory input from neighboring and more distant areas. The excitatory synaptic connections are mediated by AMPA receptors and the inhibitory connections are mediated by GABA receptors. The model is shown in Figure 2.4. The four different populations are framed, the two excitatory populations in green and the two inhibitory ones in red. The mean membrane potential of the main cells is interpreted as an EEG signal. The transformation of presyaptic firing rate to postsynaptic firing rate happens like explained in Section 1.2 by Formulas 1.2 and 1.3. The mathematical details about the model can be found in Appendix C.

There are three different impulse responses for the three different types of interaction:

- $h_{EXC}(t) = A \cdot a \cdot t \cdot e^{-at}$ for the excitatory synaptic interactions,
- $h_{SDI}(t) = B \cdot b \cdot t \cdot e^{-bt}$ for the slow dendritic inhibition (SDI) and
- $h_{FSI}(t) = G \cdot g \cdot t \cdot e^{-gt}$ for the fast somatic inhibition (FSI).

The somatic time constant $(1/g)$ is smaller than the dendritic time constant $(1/b)$, giving the interneurons projecting on the soma faster kinetics than the ones projecting on the dendrites. The three different impulse responses are shown in Figure 2.5 for

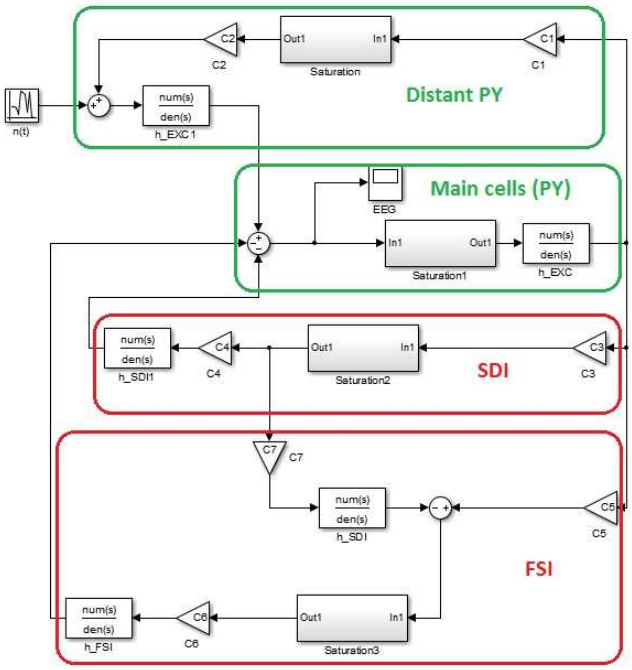

Figure 2.4: The model of the hippocampus of Wendling et al. [42]. There are two excitatory populations: the main cells and the distant PY cells. There are also two inhibitory populations: the slow dendritic and the fast somatic inhibitory neurons. A mathematical description of this model can be found in Appendix C.

$A = B = G = 10$ and a, b and g equal to their reference values. It can be seen that h_{FSI} has the fastest dynamics and h_{SDI} the slowest. The amplitudes for the impulse responses were randomly chosen equal to each other, just to show the influence of the time constants.

The model as described so far, built from four populations, represents a certain region of the hippocampus. The output (namely the mean membrane potential of the main cells) represents the EEG signal that can be measured at this region. In this thesis, a small extension is made to this model. The eventual goal is to use this model for deriving a predicting framework for temporal lobe epilepsy. As will become clear further on in Chapter 4, bivariate measures are well suited to do this. For that reason, the model is extended to be able to generate a multi-channel EEG signal as output. This is done by taking six different models as they have been described so far and interconnecting them with each other. The output of each of the six models serves as an extra input for each of the other models. Every population incorporates a time delay on its efferent connections, because the signals have to propagate from one region to another and this takes time. The parameters for each model now consist of a fixed term in combination with a random term. This random term can not be too large because the different models still need to produce the same type of activity. In this way a large model that consists of six modules is created. The output of every single module of the extended model can now be seen as the

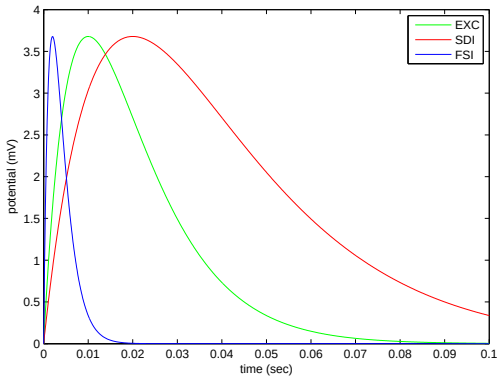

Figure 2.5: The impulse responses for the three different types of synaptic interaction. Fast somatic inhibition (blue) has the fastest dynamics, followed by excitatory synaptic transmission (green). The slow dendritic inhibition (red) has the slowest dynamics.

EEG signal that is measured in a certain region of the hippocampus. These are six different regions, one for each module. The output of this extended model can thus be interpreted as a 6-channel EEG.

2.2.3 Results

The model can generate six qualitatively different kinds of EEG signals by adjusting the parameters A, B and G. These parameters are the synaptic gains in the impulse response functions for the specific synaptic interactions. The six types of signals are: normal background activity (type 1), slow rhythmic activity (type 2), sporadic spikes (type 3), sustained spikes (type 4), low voltage rapid discharge (type 5) and slow quasi-sinusoidal activity (type 6). Type 1, 2 and 3 are signals typically seen during interictal periods. Type 4 can often be seen right before the beginning of a seizure (preictal). Type 5 usually appears at seizure onset and type 6 normally follows the rapid activity and represents ictal activity. These different types of signals are illustrated in Figure 2.6. The frequency of the low voltage rapid activity signal lies in the range 30-40 Hz, which is indeed in the γ band.

Wendling et al. used their model to explain the neuronal mechanisms responsible for low voltage rapid discharges [42] and the transition from interictal to ictal stages in human MTLE [92]. An increase of excitation and a decrease of inhibition was not sufficient to explain the high-frequency EEG activity. It turned out that the division of inhibitory interneurons in fast and slow populations was crucial for generating γ-rhythms. While the dendritic inhibition went down, the somatic inhibition had to stay above a certain level to be able to generate the high-frequency behavior [93]. This means that the GABAergic inhibition decreased, but not uniformly in the dendrites and the soma. Right before the onset of the seizure, the dendritic inhibition increased to compensate the increasing excitation. At seizure onset this dendritic

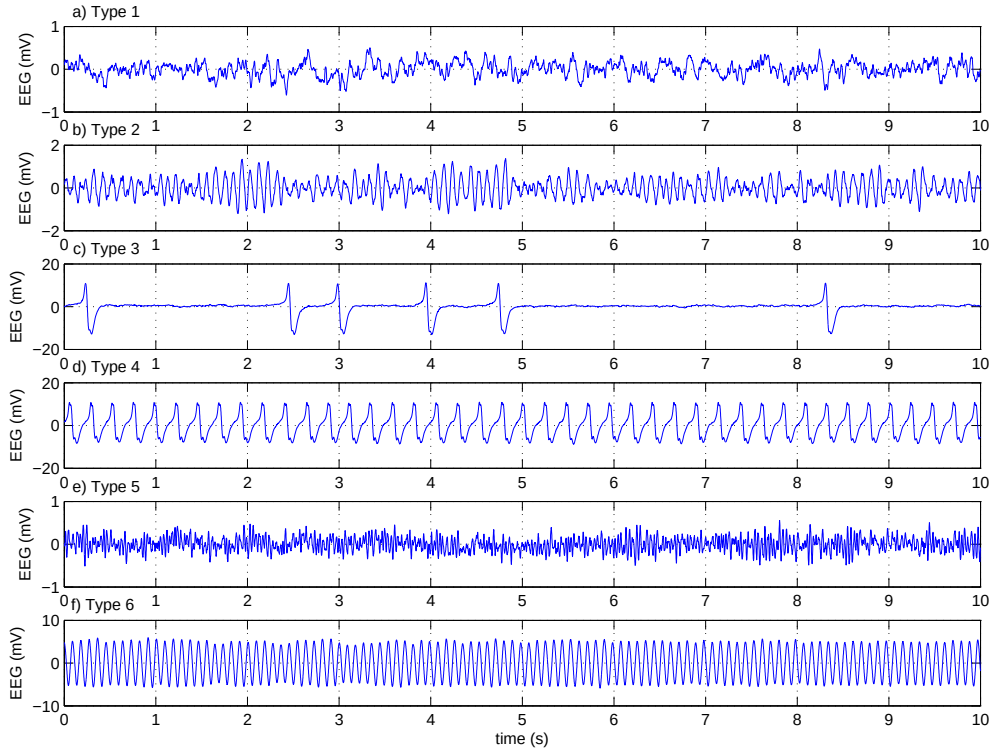

Figure 2.6: The six different types of EEG behavior generated by the model of Wendling et al. [42]. a) Type 1: normal background activity (interictal). b) Type 2: slow rhythmic activity (interictal). c) Type 3: sporadic spikes (interictal). d) Type 4: sustained spikes (preictal). e) Type 5: low voltage rapid activity (ictal). f) Type 6: quasi-sinusoidal activity (ictal).

inhibition made a huge drop due to a 'fatigue process', while the somatic inhibition remained constant or increased. The high-frequency ictal oscillations are generated by the feedback loop consisting of the pyramidal cells and the inhibitory interneurons that project on the soma of these cells. For details the readers are referred to the papers of Wendling et al. [42, 92].

Figure 2.7 shows an example of a 6-channel EEG recording, generated by the extended model proposed in this thesis. Five seconds of each type were simulated and afterwards concatenated. The order or the signals is first type 1, then type 2 and so on until type 6. There is clearly a large difference in the amplitude of the different types of signals. Because of this the types 1, 2 and 5 are not clearly visible on the figure. Close-ups on the different kind of signals can already be seen on Figure 2.6.

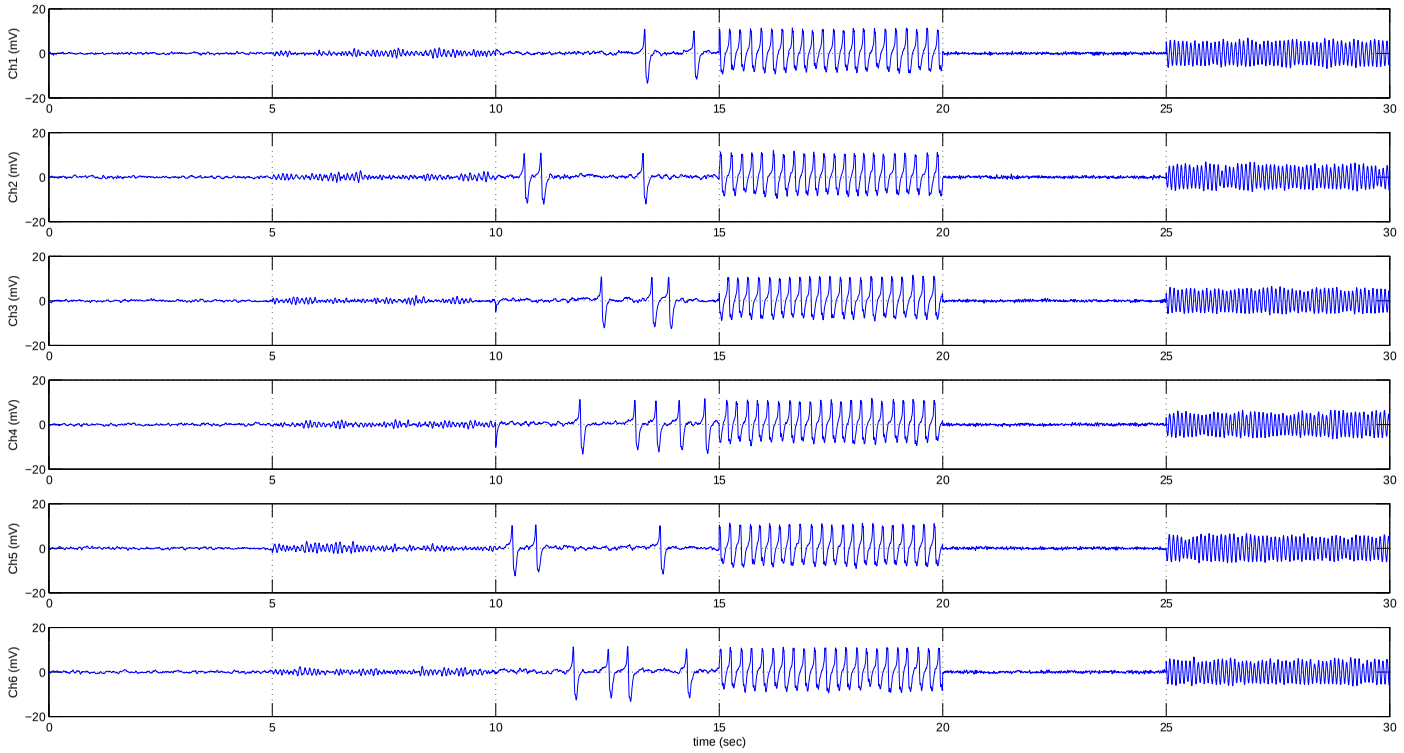

Figure 2.7: A 6-channel EEG recording that contains the six qualitatively different types of signals that can be produced by the model. The channels are labeled Ch1 up to Ch6. Every type of possible activity is simulated for five seconds (type 1 up to type 6).

2.2.4 Conclusion

The model for TLE can generate six qualitatively different kinds of EEG signals. These different types of signals correspond to different stages in the development of the seizure. Next to an ictal and interictal stage there also exists a pre-ictal stage for TLE. This stage comes between the interictal and ictal stage and can be used to predict seizures before they are actually happening. This was not the case for the spontaneous transitions in absence seizures. The goal of this model in this thesis is to generate artificial (but realistic) EEG data that can be used to work out a prediction framework for MTLE.

Chapter 3

Controlling epileptic seizures

This chapter deals with the control of epileptic seizures via brain stimulation techniques. More specifically, a control system for the model of absence seizures (introduced in Section 2.1) will be designed and implemented. The control system consists of a detection part and a stimulation part. In Section 3.1, a short introduction is presented on the subject. The detection and the stimulation part of the control system are explained in Section 3.2. The overall picture of the control system is presented and the important parameters are emphasized. The results of the control system are presented in Section 3.3. The influence of parameter changes are also shown in this section. It turns out that the control system works very good, but only for well tuned parameters. The performance drops when the parameters are not chosen optimally. To end this chapter, a conclusion and some remarks are given in Section 3.4.

3.1 Introduction

The most common treatments for epilepsy that are used nowadays are medication and surgery. These are unfortunately, as stated in Chapter 1, not effective for all the patients. For this reason, there is a lot of research aimed at developing alternative treatments. In this chapter a brain stimulation therapy will be developed and implemented for the thalamocortical model of absence seizures. This model very well mimics the dynamics that are in play during absence seizures. This allows the user to interact with the model: it makes it possible to send pulses into the model with the goal of controlling the seizures. The objective in this case is to hinder a seizure after its onset. There is no possibility for prediction, because absence seizures are generalized seizures. The best that can be done is an early detection. Pulses will only be sent into the model when a seizure is detected. This makes the developed control system a closed-loop system. In an open-loop system, intermittent pulses would be sent into the model without making use of any kind of detection system. A closed-loop system is chosen because it disturbs the brain of the patient less than an open-loop system.

3.2 Methods

Both the detection system and the stimulation protocol will be described in this section. The overall outline of the detection system and its parameters are presented in Section 3.2.1. The regions to stimulate and also the type of pulses that are used are presented in Section 3.2.2.

3.2.1 Detection

The model for absence seizures generates two different types of EEG behavior. On the one hand there are the interictal spindle oscillations with a low amplitude. On the other hand there are the ictal quasi-sinusoidal oscillations with a larger amplitude. Detecting a seizure in the model implies being able to make the distinction between these types of activity. The interictal and ictal activity clearly have a different order of amplitude. This is because during the ictal activity there is a lot of synchrony in the brain and this causes the EEG to have larger amplitudes. A simple detection system is therefore based on the amplitude of the EEG output signal. When the amplitude gets larger than a certain threshold value, a seizure is detected. This method for detection can of course only be used in this model. Other types of EEG behavior with a large amplitude that do not represent ictal activity will wrongly cause a seizure detection. Because the model only generates two types of activity, this simple method can be used. The big advantage of this method is a very fast detection. The seizure is detected right after it starts. This would not be the case if some type of sliding window had to be used. The delay between the start of a seizure and the actual detection would then probably be larger. This simple method therefore allows to check if a patient can be made free of seizures if a very fast detection is possible.

The Simulink diagram of the detection system is shown in Figure 3.1. There are three conditions that have to be satisfied so that the system will output a seizure detection. First of all, the incoming EEG signal has to be decreasing. Why this condition has to be satisfied will become clear in the next section. Secondly, the absolute value of the difference between the incoming EEG signal and the average of the EEG signal has to be larger than a couple of times the standard deviation of the EEG signal. This causes a detection when the EEG signal deviates a lot from its mean value, which indicates that the amplitude of the EEG signal has passed some threshold. The average and the standard deviation of the EEG signal are computed during a pre-processing step. The average is measured from a signal that contains interictal and ictal activity while the standard deviation is measured from a signal that contains only interictal activity. This is done in this way because the ictal activity is not completely symmetric. The average will therefore be a little bit smaller if ictal activity is included with respect to only interictal activity. The third condition that has to be satisfied is that the previous point in the signal would not cause a seizure detection according to condition two. This will cause the output of the detection system to be 1 at the time of seizure detection and 0 afterwards. If this third condition was not included, a series of ones would be generated after a

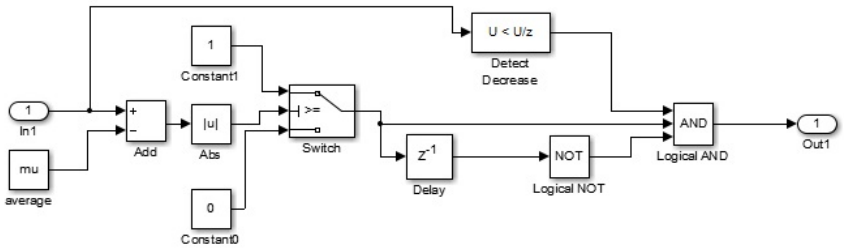

Figure 3.1: The detection system to detect a seizure in the model for absence seizures.

seizure detection.

Once the average and standard deviation of the EEG signal are measured, this system contains one important parameter. The deviation of the incoming EEG signal from its average is compared with a couple of times the standard deviation. This 'couple of times' is an important parameter. If this is chosen too low, the system will generate a lot of false detections. If on the other hand this value is too high, the system will not detect a seizure or detect it too late. Careful tuning of this parameter is therefore required.

3.2.2 Stimulation

Once a seizure is detected, it has to be controlled. External stimuli are sent into the model to do this. The stimuli can be sent into the cortical or into the thalamic module of the model. The thalamus lies deep inside the brain. Sending stimuli to the thalamus therefore requires depth electrodes which penetrate into this deep brain structure. The cortex is the outer surface of the brain, which makes cortical stimulation a much less invasive method. For this reason, the external control stimuli are sent into the cortical module of the model. The type of signal that is used is a block pulse of a certain amplitude and duration. These are two important parameters that also have to be tuned very carefully. When the amplitude of the pulse is chosen too small, it will not have any disrupting effect on the starting seizure. When on the other hand the amplitude is chosen too large, the entire system will be disorganized. In real life it is also not advisable to send pulses of a too large amplitude inside a patient's brain. The amplitude can also take a positive or a negative value. This is because a seizure can be detected during an increasing or during a decreasing progress of the EEG signal. When the detection happens on a rising EEG signal, the pulse will have a negative amplitude. If the detection happens on a decaying EEG signal, the pulse will have a positive amplitude. This means that there are two detection systems like in Figure 3.1. The one in this figure had as first condition that the EEG signal had to be decreasing. In the second detection system, this condition is replaced with the condition that the EEG signal has to be increasing. The two different detection systems will each generate their pulses when needed. Afterwards these signals are combined and sent into the model as one control signal. An important note about the units of the amplitude has to be made here. Since the

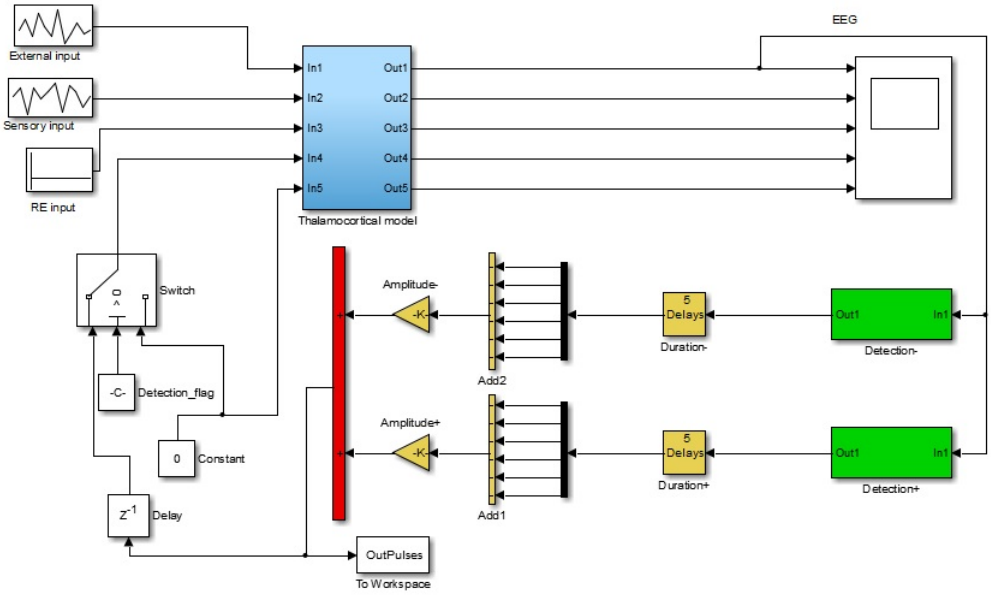

Figure 3.2: The control system together with the model. The model is included in the light blue subsystem. Both the detection systems are shown in green. The stimulation part is indicated in yellow. The red addition element combines the two control signals into one signal. The switch element determines whether the control signal is sent into the model or not.

model that is being used is a macro-scale model, the units of the amplitude of the control signal will be pulses per second (pps). This is in accordance with the units of the incoming signals of other populations in the model, which represent firing rates. A negative amount of pps might seem strange at first sight. A positive amplitude is therefore interpreted as sending an amount of depolarizing pulses (per second), while a negative amplitude is interpreted as sending an amount of hyperpolarizing pulses (per second). The duration of the control pulse is also important to tune. The pulse can not be too short or too long. The generation of the pulse happens by sending the output of the detection system through a delay bank. In this way the duration of the pulse can take on a discrete multiple of the used sample time with which the model is simulated. In real life the calculations will of course also be done in a discrete way.

Tuning of all the parameters was done by trial and error. The entire control system together with the model is shown in Figure 3.2. The model itself is included in the light blue subsystem. Both the detection systems are shown in green. They are driven by the average membrane potential of the PY population (EEG). The stimulation part for each detection system is indicated in yellow. The red addition element combines the two control signals into one signal. The switch element determines if the control signal is sent into the model or not, based on an external parameter.

3.3 Results

As already mentioned, careful tuning is needed for some parameters in the control system. In real life, this tuning will be done for every patient individually and not just one tuning for all the patients. The reason therefore is that every patient has slightly different EEG recordings. Considering this control system, the average and standard deviation of the EEG signal are of importance. To incorporate this into the model, the tuning is done for a certain fixed seed for the random inputs to the model and for fixed parameters in the model of absence seizures. When one of all these parameters changes, the tuning has to be done again, because this represents the EEG recordings of a different patient.

There won't be a lot of ictal activity when the reference set of parameters is used in the model of absence seizures. This means that the simulation would have to be done on a large interval to very well see the effect of the control system. When the results are shown for large intervals, the visibility will of course not be very good. So, for the sake of better visibility, a certain parameter in the model (the gain for AMPA receptors in the PY population) will be enlarged a little bit. This will cause a lot more ictal activity and allows to see the effect of the control system on smaller simulation intervals. Note however that no patient in the world will have this much of ictal activity on short intervals. This is purely to be able to show the results of the control system in a clear fashion.

In Figure 3.3 the results are shown when the control system is not connected to the model. The average membrane potential of the PY population in the cortex is shown in Figure 3.3a, together with the thresholds of the detection system (in red). This represents the activity which would be measured during an EEG. Both the ictal and interical activity can be seen in this signal. The ictal part of the signal clearly has a larger amplitude than the interictal part. Also the asymmetry of the ictal part can be seen in this figure. In Figure 3.3b one can see the activation of the $GABA_B$ receptor in the PY population. Remember that activation of this receptor was necessary to generate seizures in the model. In this figure one can clearly see that activation of the $GABA_B$ receptor corresponds to ictal activity in the EEG signal. This activation represents the current that is generated by these receptors. That explains why it has a negative value, since these receptors will cause hyperpolarization. In Figure 3.3c, the pulses that are generated by the control system are shown. It can be seen that a pulse is fired every time the amplitude of the EEG signal crosses the threshold that separates ictal and interictal amplitudes. Whether the pulse is negative or positive depends on the fact whether the signal is rising or decaying at that moment. Note however that these pulses are not sent into the model since the control system is not connected to the model yet.

Now the control system is connected to the model. The results are shown in Figure 3.4. It can be seen that the EEG signal does not contain any (noticeable) ictal activity anymore. Only the interictal spindle-oscillations are present in this signal. The conclusion that can be drawn here is that the control system is doing its job very well. The same conclusion can also be drawn by looking at the $GABA_B$ activation. There is still one well defined peak present in the beginning of the signal,

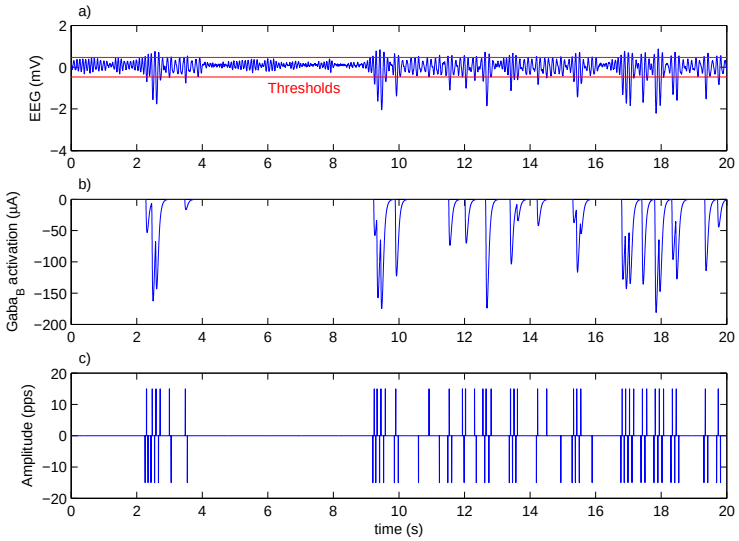

Figure 3.3: The results when the control system is not connected to the model. a) The average membrane potential of the PY population in the cortex (which represents an EEG recording) clearly shows interictal and ictal activity. The ictal activity has a noticeable higher amplitude compared to the interictal activity. The thresholds of the detection system are shown as red horizontal lines. Below this threshold is classified as interictal, above as ictal activity. b) The amount of $GABA_B$ activation. This activation represents the postsynaptic current generated by the $GABA_B$ receptor and therefore corresponds to ictal activity. c) The amplitude of the control signal over time. These pulses are generated when ictal activity is detected but they are not sent into the model yet.

but its magnitude is of the order of 10^{-3}. This is very small when compared with the magnitude of the order of 10^2 without the control system. There are also some peaks of the order of 10^{-6} present, but they are not very visible in the figure. It is normal that there is still a little bit of $GABA_B$ activation. The system will control a seizure when it is detected (after the onset of the seizure). A started seizure will involve a little bit of $GABA_B$ activation. In Figure 3.4c one can also see that from all the pulses shown in Figure 3.3c, only a small part is actually sent into the model. This means that a single pulse at the beginning of the seizure is often successful in annihilating the entire seizure. These results are obtained with some well tuned parameters. The threshold in the detection system is $2.4 \cdot \sigma$, with σ the standard deviation of the EEG. The amplitude of the pulses is 15 *pps* and the duration of the pulses is 6 *ms*. The sensitivity of the detection system with respect to these parameters will now be investigated. One parameter will be adapted while the others are kept to their reference values.

First, the sensitivity of the performance with respect to the threshold is checked. If the parameter for the threshold is chosen too small, there will be a lot of false

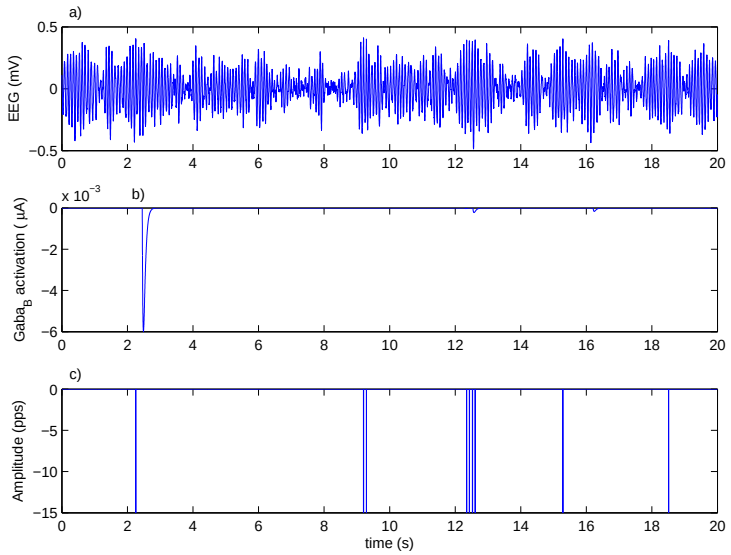

Figure 3.4: The results when the control system is connected to the model. a) The EEG recording does not show any noticeable ictal activity anymore, but only spindle oscillations. The only type of signal that is present is the waxing-and-waning interictal activity. This means that the control system has succeeded in annihilating the seizures. b) There is almost no more $GABA_B$ activation. This also points towards the absence op epileptic activity. c) Only a small part of the control pulses from Figure 3.3c are needed to control the seizures. This implies that a single pulse at the start of a seizure can annihilate the entire seizure.

detections. This will cause a lot of unwanted interference with the brain of the patient. Results for a threshold of $1.2 \cdot \sigma$ are shown in Figure 3.5 for a connected control system. When looking at Figure 3.5c, one can see that there are detections throughout the entire signal, even in clearly interictal parts. It can also be seen that a lot of these false detections are actually sent into the model by the control system. This causes the EEG signal in Figure 3.5a to lose its waxing-and-waning character, which is typical for the interictal signals of absence seizures. This waxing-and-waning pattern was still clearly visible in Figure 3.4a. The $GABA_B$ activation in Figure 3.5b may well be extremely small, the fact that the EEG signal is deformed does not give this $GABA_B$ activation any physical meaning anymore. This implies that giving too much unneeded stimuli to the brain is definitely not a good idea. Experimental studies could examine what the effect of this would be on behavior. When on the other hand the threshold is chosen too large, the detection system will not detect a lot of seizures or it will detect them not as fast as with a well tuned threshold. Results for a threshold of $3.6 \cdot \sigma$ are shown in Figure 3.6 for a connected control system. In Figure 3.6c, one can see that there are a lot less detections in this case. It however seems that there is still at least one detection for each seizure. The problem is that this detection happens too late. The seizure will already have developed for a

long enough time to be noticable in the EEG recordings. This can be seen in Figure 3.6a. The seizure activity is certainly less prominent as without the control system, but the high amplitudes of ictal activity are clearly visible. Also the $GABA_B$ receptor activation takes on values of the order of 10^2, which points towards ictal activity. This experimentation shows that it is very important to tune the parameter for the threshold carefully. The performance of the control system will decrease firmly is this parameter is not chosen optimally. The seizures will either not be blocked completely or the patient's brain goes crazy because of too much electrical interference of the stimuli.

Next, the sensitivity of the performance of the system will be investigated with respect to changes in the amplitude of the control pulse. The results for a connected control system are shown in Figure 3.7 for an amplitude parameter of 3 *pps*. The control system will in this case generate its signals on time to control the seizures, because the parameter for the threshold is again well tuned. The problem in this case is the fact that the control pulse his amplitude is not high enough to interrupt the started seizure. As can be seen in Figure 3.7a, there is still some ictal activity going on. This can also be confirmed by looking at the $GABA_B$ receptor activation. Control pulses with a too small amplitude will not have enough impact on the brain to control the seizures completely. When on the other hand the amplitude of the control pulses is chosen too high, the brain of the patient will produce strange EEG measurements. The results are shown in Figure 3.8 for a connected control system and an amplitude parameter of 60 *pps*. Note that in this figure, the signals are only shown on an interval of five seconds. This is to be able to clearly illustrate the strange EEG activity. Every time a control pulse is sent into the model, the produced EEG signal will show some high frequency behavior. This can be seen in Figure 3.8a. This clearly is not the desired interictal activity. Again, to know what the implication of this is on behavior, some experimental studies are necessary. It can however be stated that it is not a good idea to use too high amplitudes. It is very important to ensure the safety of the patient. The amplitude is therefore important to tune. When this is not done carefully there won't be enough interference with the brain or there will be way too much interference with the patient's brain.

Finally, the effect of changing the duration of the control pulses will be investigated. The results that are obtained with a duration of 2 *ms* are shown in Figure 3.9 for a connected control system. From this figure it can be seen that having a smaller duration will have a negative effect on the performance. Almost all the upcoming seizures can be stopped, except two. This means that a shorter pulse will usually be sufficient, but not always. It is of course better to choose the parameter settings such that every seizure can be controlled. In Figure 3.10 the results are shown for a duration of 30 *ms*. Only five seconds are simulated to be able to clearly see the effect on the control pulses. In Figure 3.10c, one can see that the positive and negative control pulses follow each other very fast. There is no 'quiet time' between subsequent pulses. This can have the negative effect of rather sustaining the seizure instead of controlling it, as can be seen in Figure 3.10a. This will probably be caused by the fact that there is too much interference with the brain. Therefore, it is important to tune this parameter optimally.

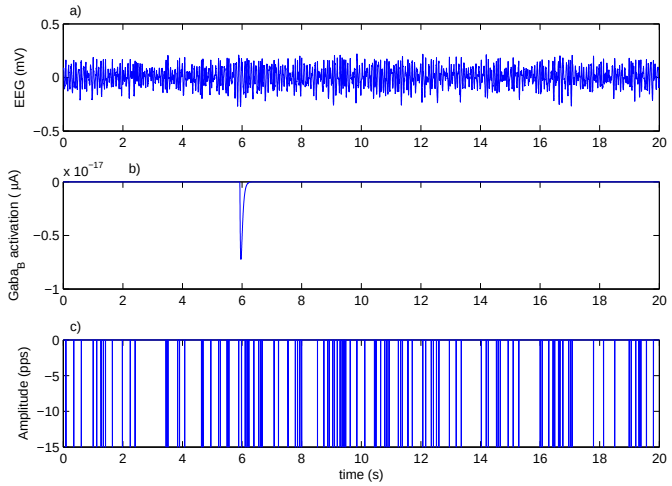

Figure 3.5: The results when the control system is connected to the model, but with a too low threshold parameter. a) The recorded EEG shows some very strange behavior. Neither ictal nor interictal activity are visible in this case. Too much electrical stimulation has made the output of the model physically meaningless. b) There is no $GABA_B$ activation, but this has no biological meaning anymore. c) There are way too much detections because of the too low threshold parameter. The brain will therefore be overstimulated.

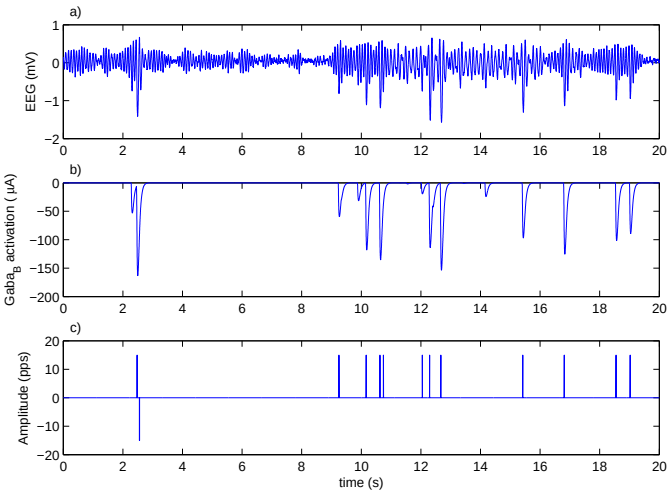

Figure 3.6: The results when the control system is connected to the model, but with a too high threshold parameter. a) The EEG still shows both interictal and ictal activity. b) The $GABA_B$ activation points towards ictal activity. The seizures are not well controlled in this case. c) The detection of ictal activity happens too late, which allows the seizure to develop and become noticeable. Counter stimuli will be sent too late by the control system.

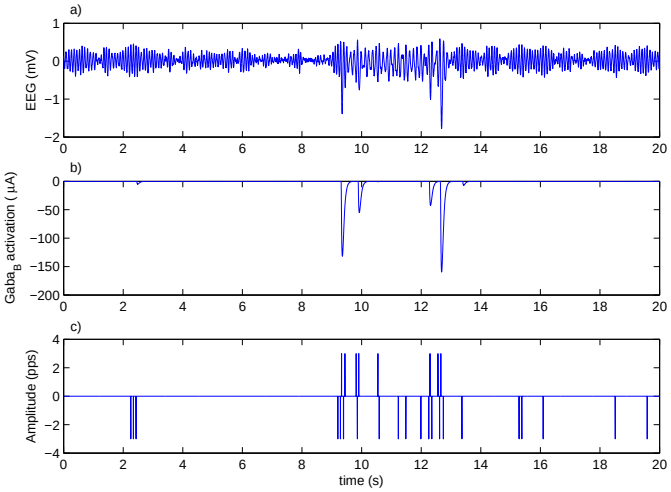

Figure 3.7: The results when the control system is connected to the model, but with a too low amplitude parameter. a) The EEG still shows some ictal activity. b) The $GABA_B$ activation also still shows some peaks with a high amplitude. These both results point towards a poor performance of the control system with these parameters. c) A lot of control signals are sent into the model, but the amplitude of the signals is too small to interrupt every seizure.

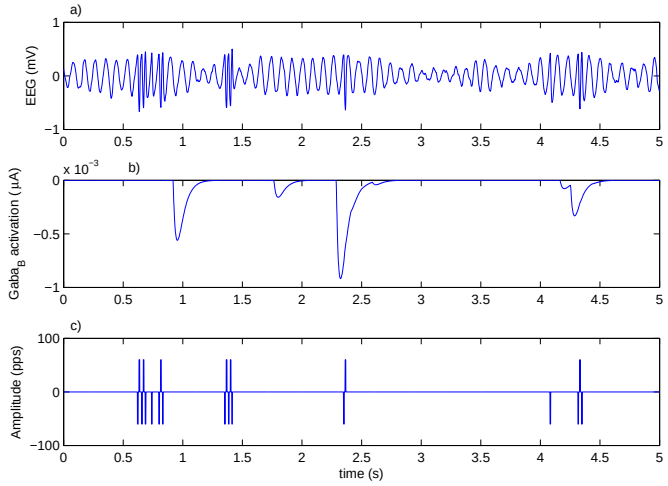

Figure 3.8: The results when the control system is connected to the model, but with a too high amplitude parameter. a) Some strange high frequency signals are present in the EEG recording. This is the result of a too large amplitude of the control signal. The dynamics of the brain are tangled up. b) The $GABA_B$ activation has small values, but the physical meaning of these is gone since the dynamics of the model are not respected anymore. c) The control pulses with a large amplitude that cause the model to generate strange EEG measurements.

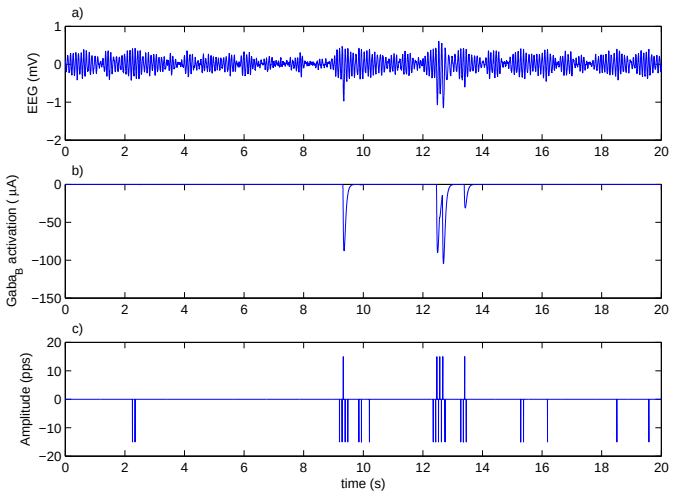

Figure 3.9: The results when the control system is connected to the model, but with a too low duration parameter. a) The measured EEG still shows some ictal activity. The control pulse did not last long enough to control these seizures. b) There are still some uncontrolled seizures that lead to large peaks of $GABA_B$ activation. c) The control pulses with a too short duration.

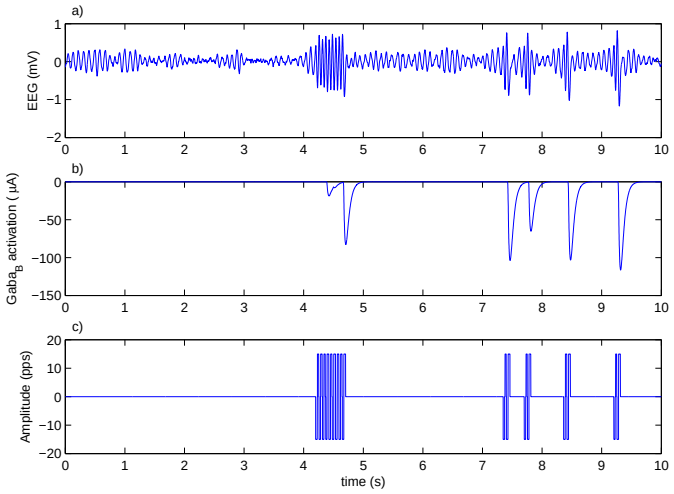

Figure 3.10: The results when the control system is connected to the model, but with a too high duration parameter. a) Some high frequency oscillations can be seen in the EEG recording. The long duration of the control pulses has caused this unwanted behavior. b) There is still some clear $GABA_B$ activation in this case. c) The different pulses follow each other too fast which does not leave any 'quiet time' between them.

All these experiments suggest that a careful tuning of the parameters of the control system is crucial for its performance. The values that were chosen during these experiments were a little bit exaggerated so that the effect could be clearly illustrated. Every parameter has a small range wherein it has to be chosen to obtain a good performance of the control system. This tuning of parameters is patient-specific and will require long EEG monitoring during a pre-surgical evaluation.

Manually tuning the parameters for every patient can become a time-consuming job. Letting an automated process take care of this tuning would save physicians a lot of time. Automating this step will not be very easy in case of the thresholding technique that is used in this chapter. The tuning system has to know when a seizure is happening and when not to determine the optimal threshold of the detection system. For applications in real life, this thresholding technique will not be used for detection. Some more advanced methods, for example from the field of machine learning, will be used to detect a seizure. These models can be learned from a set of training data. For supervised methods, a physician would still need to generate a set of training data with the appropriate class labels. From that point on however, the model can be learned automatically. Automatic tuning of the parameters for the stimulation part can be done by starting with low values and increasing them until the seizures can be interrupted. It is very important that an upper boundary is chosen for these values, because otherwise there can be too much interference with the brain of the patient.

3.4 Conclusion

The suggested control system is able to do its job and interrupt all the started seizures. To do this however, the parameters need to be tuned optimally. This is very crucial for the overall performance of the system. If this is not done correctly, then not all the seizures will be controlled. It was also shown that badly tuned parameters can have even more severe consequences. If there was too much interference with the brain, some strange EEG activities were recorded. Some experimental studies could point out what the behavioral effects of these are. It is important to note that the proposed detection system is limited in its application. The results obtained can not just be generalized to every other model. The control system makes use of the assumption that only two types of signals are encountered, namely some high amplitude ictal activity and some low amplitude interictal activity. In real life this will of course not be the case. The detection system will then need to be extended to classify more types of EEG signals. The goal here however, was to see if computational modeling can be useful for the development of alternative treatments for epilepsy. By making use of computer models, one can see which treatments could be useful and then evaluate them further based on real experiments. The control system was successful in this respect and suggests that responsive neurostimulation could become a very important treatment for epilepsy in the near future.

Chapter 4

Predicting epileptic seizures

This chapter deals with the prediction of epileptic seizures based on EEG signals. More specifically, a prediction framework for MTLE is developed, based on signals generated from the hippocampal model (introduced in Section 2.2). In Section 4.1, a short introduction on the subject is presented. The methods used to do the prediction are explained in Section 4.2. The different measures that are extracted from the EEG are defined in this section. All these measures are bivariate measures that characterize synchrony between two signals. The different methods for doing classification are also introduced in this section. Both thresholding and support vector machines (SVMs) are used for doing classification. The results are presented in Section 4.3. It turns out that the bivariate measures for synchrony are well suited to find preictal periods in EEG signals. Classification by thresholding these measures shows accuracies up to 95%, but is limited in its generalization towards real life signals. To solve this problem, SVMs are used to do the classification in a more general way. By using the right type of SVMs and the right input features, accuracies up to 98% are obtained. To finish this chapter, a general conclusion and some remarks are given in Section 4.4.

4.1 Introduction

In the previous chapter a control system was developed which interrupted a seizure as soon as possible after its onset. Doing the control in this way allows to annul the started seizure, but it can not make the patient completely free of seizures. This could be seen in Figure 3.4, where there was still a very small amount of $GABA_B$ receptor activation. In order to make a patient completely free of seizures, a seizure needs to be detected before its onset and not as soon as possible after its onset. This means that the seizure needs to be predicted before it has actually started. It has to be noted that this is not possible for all type of seizures. Only partial seizures show gradual changes in EEG activity before the actual onset of the seizure. This implies that for this type of epileptic seizures, one can try to analyze EEG signals of a patient and hopefully see the seizure arising before it has actually started. The hippocampal model for MTLE will be used to generate artificial EEG data. This data will then

be used to develop a prediction framework for MTLE. After a seizure is predicted, the next step would be to try to prevent the seizure from happening. This could also be done by some brain stimulation techniques like in the previous chapter. The model which is used for generating the data however, does not mimic the dynamics that are in play during transitions from one type of EEG activity to another. For this reason, it is not possible to interact with the model as it was the case in the previous chapter. The goal here will be to build a reliable prediction system for patients suffering from MTLE. The EEG signals recorded from the brain of patients with MTLE can be divided in interictal, preictal and ictal segments. Predicting a seizure then boils down to finding the preictal periods in the EEG recordings.

4.2 Methods

This section elaborates on the different steps that were followed to develop the prediction framework. First of all, the data generation is described in Section 4.2.1. From this data, a couple of features are extracted. How this is done and which features are chosen will be explained in Section 4.2.2. Finally, these features will be used to classify between interictal, preictal and ictal stages of the EEG signal. The way this is done is presented in Section 4.2.3.

4.2.1 Data generation

The hippocampal model for MTLE is used to generate artificial EEG data. The choice to let the data be generated artificially by a computational model has two reasons. The first one is that it is not easy to get data for free nowadays. Most of the datasets that were available for free in the past are now collected into bigger datasets which are only available after purchase. An example is the former free dataset of the Seizure Prediction Project Freiburg, which is now part of the bigger European EPILEPSIAE database. Unfortunately, one has to pay a lot of money to gain access to this database. The second reason to use a computational model is to show that computational modeling can be a very convenient tool to solve real life problems regarding epilepsy.

The model for TLE can generate six qualitatively different types of EEG activity. Three of these six types represent interictal activity, one type represents preictal activity and the other two represent ictal activity. Which of these is simulated depends on the parameter settings of the model. There are three parameters that determine the type of the output. By adjusting these, one can generate a segment of each type. These segments are afterwards concatenated into one long signal. This means that the signals are generated off-line. Afterwards, they are used to extract features for the classification in an on-line fashion. Remember that the signals represent a 6-channel EEG recording. The sampling rate was chosen to be 256 Hz, which is in accordance with the dataset from the Seizure Prediction Project Freiburg.

4.2.2 Feature extraction

Features are extracted from the generated EEG data and will serve as an input for the classification algorithm. When choosing which features one is going to extract, it is important to think about what one wants to do with them. In this case, the features will serve as the input for a classification algorithm that needs to distinguish between interictal, preictal and ictal stages of an EEG signal. It therefore is important to choose features which will have a discriminative property regarding these three stages. It is known that when a seizure starts to develop, a lot of regions in the brain will organize in a synchronous manner. This means that there is a lot of synchrony during preictal and ictal stages. This also implies that features which characterize synchrony may be the key to a good classification. This is the reason why the model of Wendling et al. was extended to generate a 6-channel EEG signal as output. This allows one to extract bivariate features that characterize synchrony between different channels. The detection of synchrony between two channels has the physical meaning of detecting synchrony between different regions in the hippocampus. This is an indication that a seizure is developing and that the signal has entered its preictal stage. Linear as well as nonlinear measures for synchrony will be used. The different measures that are used will be presented now. The maximum linear cross-correlation and the linear coherence are both linear bivariate measures. The nonlinear interdependence and the phase locking value (PLV) are both nonlinear bivariate measures [68].

Maximum linear cross-correlation

The similarity of two signals $\{x_i\}$ and $\{y_i\}$ can be evaluated by computing the maximum of the normalized cross-correlation function. It is defined by:

$$C_{max} = \max_{\tau} \left\{ \left| \frac{C_{xy}(\tau)}{\sqrt{C_{xx}(0) \cdot C_{yy}(0)}} \right| \right\} \tag{4.1}$$

and can be considered as a measure for lag synchronization. In Formula 4.1, the linear cross-correlation is given by:

$$C_{xy}(\tau) = \begin{cases} \frac{1}{N-\tau} \sum_{i=1}^{N-\tau} x_{i+\tau} y_i & \tau \geq 0 \\ C_{yx}(-\tau) & \tau < 0 \end{cases} \tag{4.2}$$

with N the length of the signals. C_{max} is bound to the interval $[0, 1]$. Values close to zero indicate that the signals are not similar. Values close to one on the other hand, indicate that both signals have approximately the same progress in time. The maximum is taken over a small range of τ to allow some time lag between the signals.

Linear coherence

The amount of linear synchronization between two signals $\{x_i\}$ and $\{y_i\}$ can be assessed by the linear coherence function. This function is defined as:

$$\Gamma(f) = \left| \frac{G_{xy}(f)}{\sqrt{G_{xx}(f) \cdot G_{yy}(f)}} \right| \tag{4.3}$$

where $G_{xy}(f)$ is the cross-spectral density. This is given by:

$$G_{xy}(f) = X(f) \cdot Y(f)^* \tag{4.4}$$

where $X(f)$ and $Y(f)$ denote the Fourier transform of $\{x_i\}$ and $\{y_i\}$ respectively and the asterisk denotes a complex conjugation. The linear coherence function is also bound to the interval $[0, 1]$ and can be applied for specific frequencies. Again, values close to zero correspond to very little synchronization and values close to one denote a lot of synchronization between the signals.

Nonlinear interdependence

The amount of generalized synchronization between two signals $\{x_i\}$ and $\{y_i\}$ for $i = 1, \ldots, N$ can be evaluated by the nonlinear interdependence function. To calculate this measure, one has to reconstruct state space trajectories $\{\vec{\boldsymbol{x}}_i\}$ and $\{\vec{\boldsymbol{y}}_i\}$ for both time series. This can be done by the method of delays. A point in state space is computed as: $\vec{\boldsymbol{x}}_i = (x_i, x_{i-\tau}, \ldots, x_{i-(m-1)\cdot\tau})$ and similar for $\vec{\boldsymbol{y}}_i$. The parameter m is the embedding dimension and the parameter τ represents the time delay. The nonlinear interdependence actually measures how neighborhoods in one attractor project into the other attractor. The time indices of the k nearest neighbors of $\vec{\boldsymbol{x}}_i$ and $\vec{\boldsymbol{y}}_i$ are denoted respectively by r_{ij} and s_{ij} for $j = 1, \ldots, k$. The squared mean Euclidian distance for every $\vec{\boldsymbol{x}}_i$ to its k nearest neighbors is defined as:

$$R_i^{(k)}(x) = \frac{1}{k} \sum_{j=1}^{k} \left\| \vec{\boldsymbol{x}}_i - \vec{\boldsymbol{x}}_{r_{ij}} \right\|_2^2 . \tag{4.5}$$

The y-conditioned squared mean Euclidian distance for every $\vec{\boldsymbol{x}}_i$ is calculated by substituting r_{ij} with s_{ij} in Formula 4.5. This implies that the nearest neighbors of $\vec{\boldsymbol{x}}_i$ are replaced by the corresponding time partners of the nearest neighbors of $\vec{\boldsymbol{y}}_i$:

$$R_i^{(k)}(x|y) = \frac{1}{k} \sum_{j=1}^{k} \left\| \vec{\boldsymbol{x}}_i - \vec{\boldsymbol{x}}_{s_{ij}} \right\|_2^2 . \tag{4.6}$$

Both $R_i^{(k)}(y)$ and $R_i^{(k)}(y|x)$ are defined in an analogous way.

All the $\vec{\boldsymbol{x}}_i$ vectors together for a point cloud in state space with an average squared radius $R(x) = (1/N) \sum_{i=1}^{N} R_i^{N-1}(x)$. When the signals are strongly correlated with each other, one has that $R_i^{(k)}(x) \approx R_i^{(k)}(x|y) \ll R(x)$. When the signals are independent one has that $R_i^{(k)}(x|y) \approx R(x) \gg R_i^{(k)}(x)$. This suggest that a measure for the interdependence can be defined as:

$$S^{(k)}(x|y) = \frac{1}{N} \sum_{i=1}^{N} \frac{R_i^{(k)}(x)}{R_i^{(k)}(x|y)} . \tag{4.7}$$

Starting from the above reasoning, it is easily verified that this measure will be close to zero for independent signals and close to one for signals that are highly synchronized. This means that $S^{(k)}(x|y)$ is a normalized measure for the interdependence.

Another measure for the nonlinear interdependence is defined as:

$$H^{(k)}(x|y) = \frac{1}{N}\sum_{i=1}^{N} \log \frac{R_i^{(N-1)}(x)}{R_i^{(k)}(x|y)}. \tag{4.8}$$

This measure produces small values for independent signals and high values for synchronized time series. It is not normalized as the previous one however.

A third measure for nonlinear interdependence is given by:

$$N^{(k)}(x|y) = \frac{1}{N}\sum_{i=1}^{N} \frac{R_i^{(N-1)}(x) - R_i^{(k)}(x|y)}{R_i^{(N-1)}(x)}. \tag{4.9}$$

This measure is normalized in a certain way: it has an upper bound of 1. It is not confined to the interval $[0, 1]$ however, since it can take small negative values. Low values (including the negative ones) indicate independence and values close to one imply synchrony. The measures $S^{(k)}(y|x)$, $H^{(k)}(y|x)$ and $N^{(k)}(y|x)$ are defined in an analogous way.

The measures $N^{(k)}(x|y)$ and $N^{(k)}(y|x)$ will be used because they are normalized in some way, unlike the H measures, and they are more robust than the S measures [94].

Phase Locking Value (PLV)

The PLV is a measure that is often used to quantify the amount of phase synchronization between two signals. The PLV separates the effects of amplitude and phase when determining the correlation between two signals. This is useful when the two signals have synchronized phases while their amplitudes are zero correlated. The phase locking property has to be satisfied to be able to say that the phases of two signals are synchronized:

$$|n \cdot \phi_x(t) - m \cdot \phi_y(t)| = const. \tag{4.10}$$

In this equation, $\phi_x(t)$ and $\phi_y(t)$ denote the instantaneous phases of two signals $x(t)$ and $y(t)$ respectively. Both n and m are integers in this equation and they define the frequency equality ($n\phi'_x = m\phi'_y$). The ratio of these two is fixed to $n : m = 1 : 1$. This is because both phases are computed for signals that emerge out of the same physiological system (i. e. the brain).

The PLV for two signals $x(t)$ and $y(t)$ with instantaneous phases $\phi_x(t)$ and $\phi_y(t)$ respectively, is defined as:

$$PLV = \left| \frac{1}{N}\sum_{j=0}^{N-1} e^{i(\phi_x(j\cdot\Delta t) - \phi_y(j\cdot\Delta t))} \right| \tag{4.11}$$

where N is the number of samples in both signals and Δt is the sampling period. The PLV is bounded in the interval $[0, 1]$, which makes it a normalized measure. Low

values indicate that the signals are unsynchronized and high values point to a lot of synchronization between the signals. The PLV can be applied directly to measure synchrony over the entire frequency band, or after band-pass filtering the signal to measure synchrony in a certain frequency band.

The instantaneous phases of both signals are needed to compute the PLV. There are two different approaches that are often used for measuring the instantaneous phase of a signal. The first one uses the Hilbert transform and the second one makes use of the Wavelet transform. Both approaches are equivalent for the analysis of EEG signals [95]. In this case, the Hilbert transform is used. The instantaneous phase is defined as:

$$\phi(t) = \arctan \frac{\tilde{s}(t)}{s(t)} \tag{4.12}$$

for any signal $s(t)$. In this equation, $\tilde{s}(t)$ represents the Hilbert transform of $s(t)$ and is defined by:

$$\tilde{s}(t) = \frac{1}{\pi} p.v. \int_{-\infty}^{+\infty} \frac{s(\tau)}{t-\tau} d\tau \tag{4.13}$$

where $p.v.$ stands for the Cauchy principal value [68]. This is a method to assign a value to an integral which would otherwise take an undefined value.

Moving window

As already mentioned, the EEG signals are generated off-line. The different features mentioned above are extracted in an on-line fashion by making use of a moving window. A window of a certain length is placed on top of the EEG signal and the features are then extracted for this segment of the signal. Hereafter, the window is shifted to the next part of the EEG signal in a non-overlapping way and the features are extracted for the next segment. This is repeated until the entire EEG signal is treated. The length of the window is an important parameter that has to be chosen carefully. The window can not be too short, because the signal needs to be long enough to yield reliable values for the features. Another reason to avoid too short windows is more computational. Remember that the ultimate goal in the research community is to build an implantable device. One would like this device to be small and this usually means limited computing power. If the lengths of the windows are too short, the features will need to be calculated very often. This could pose a problem when not enough computing power is available on the small device. The length of the window can also not be too long. This would imply that the features are only calculated once on a large interval. The values of the extracted features will not have a very fluent progress in time in this case. The extracted value at the end of this window might also not be very representative for the type of activity at the end of the window in this case. It could be mainly determined by the type of activity that was happening a while ago at the beginning of the window. Choosing the right size of window is therefore very important.

4.2.3 Classification

Once the features are extracted from the EEG, they serve as input to the classification method. The classification is done by using two different approaches. The first one is based on some simple thresholding. This allows the distinction between two different classes. The second approach makes use of support vector machines (SVMs). Such SVMs can be used to make the distinction between more than two classes (multiclass classification).

Thresholding

By using a threshold, one can solve binary classification problems; the feature is either below or above the threshold. There seems to be a problem here at first sight. It was stated that the EEG signal consists of interictal, preictal and ictal periods. This implies that one has to be able to make the distinction between three different classes. This is not possible by performing a binary classification. Two of the three classes are therefore merged into one 'superclass'. Classifying between the other class and the new superclass is hereby transformed into a binary classification problem, which can be solved by thresholding. The question now is which two classes to merge. Since the goal is to predict a seizure, the most important class to find is the preictal one. Therefore the interictal and ictal classes are merged together. This allows one to make the binary classification between 'preictal' versus 'not preictal'.

All the defined measures for synchrony produce a high value for synchronized signals and a low value for unsynchronized signals. When the measure is above a certain threshold, one can conclude that there is synchrony present. The problem is that preictal as well as ictal signals both exhibit synchrony. One could think of an easy way to solve this by combining the preictal and ictal class in one superclass and classifying this superclass against the interictal class. This would however cause that one can no longer distinguish between the cases where a seizure is about to happen and when a seizure is already taking place. A better solution is to keep the preictal class alone and the two other classes in a superclass. The synchronous activity during the preictal stage in the model is of a lower frequency than the synchronous activity produced in the ictal stage. This is exploited by sending the output of the model through a low-pass (LP) filter. Most of the synchronous activity that originated from the ictal stage is therefore filtered out of the EEG signal. When this LP filtered signal is then used to compute the features, one should see a clear distinction between the preictal and ictal stages. This will help to distinguish between 'preictal' versus 'not preictal'.

Support vector machine

SVMs originate from the field of machine learning. An SVM is a supervised learning model that can analyze data and learn certain patterns that are present in this data. Features together with their class labels are given to the SVM during the training phase. Afterwards, a trained SVM can be used to detect these patterns in new,

unseen data during the testing phase. The SVM will then predict the class labels for new features.

Originally, SVMs were designed to accomplish binary linear classification. Such an SVM constructs a hyperplane in the input space that can be used for classification in the same way a threshold can be used. The hyperplane divides the input space in two regions, so this is a higher dimensional equivalent of a threshold. This hyperplane can be found by solving a quadratic programming problem. The objective function and constraint of this optimization problem are defined as follows:

$$\begin{aligned} \min \quad & \frac{1}{2}\|\boldsymbol{w}\|^2 + C\sum_{i=1}^{n}\xi_i \\ s.t. \quad & y_i(\boldsymbol{w}\cdot\boldsymbol{x_i} - b) \geq 1 - \xi_i, \quad 1 \leq i \leq n \end{aligned} \tag{4.14}$$

where $\boldsymbol{x_i}$ and y_i respectively denote the points to be classified and the corresponding class labels, $\boldsymbol{w}$ is the normal vector to the hyperplane, b is the bias of the hyperplane and ξ_i denotes non-negative slack variables. The first term in the objective function in Equation 4.14 is the factor that tries to maximize the margin of the classifier. The margin is a term often used in SVM terminology and refers to the generalization possibilities of the classifier. One does not want a classifier that only fits the training data, but that generalizes well to other data as well. The second factor in this objective function is a regularization term. This term is included to allow some misclassification of data points, because the data will almost never be perfectly classifiable. This is called the soft margin method [96]. A regularization constant C will then make the trade-off between the size of the margin and the amount of misclassification. If not much misclassification is allowed (large C), the margin can probably not become very large. If on the other hand a lot of misclassification is allowed (small C), most of the effort can be directed to maximizing the margin. This regularization constant is therefore an important parameter to tune.

SVMs are also able to make nonlinear classifications by making use of the kernel trick. The kernel trick implicitly maps the inputs into a high-dimensional feature space. A linear classification in the feature space represents a nonlinear classification in the original input space. Linear as well as Gaussian radial basis function (RBF) kernels will be used. RBF kernels introduce a new parameter to tune. An RBF kernel has the following form:

$$k(\boldsymbol{x}_i, \boldsymbol{x}_j) = \exp(-\gamma\|\boldsymbol{x}_i - \boldsymbol{x}_j\|^2) \tag{4.15}$$

where $\gamma > 0$ is an important parameter. This parameter will determine the width of the Gaussian.

From this it follows that for an RBF kernel, there are two important parameters to tune: C and γ, whereas a linear kernel only needs C. It is very important to tune these parameters carefully for obtaining a good classifier. Just choosing these values at random will very likely give poor classification results. Because of the importance of these parameters, they will be determined by N-fold cross-validation. The training data will first be divided in N subsets. The classifier is then trained

(for certain parameter settings) on N-1 of these subsets and the remaining subset is used for validation. This is done for every of the N subsets as validation set and the performance is averaged over these N runs. This averaging over N runs is done to make sure that the results are not dependent on the chosen subset for validation. This will be done for different parameter settings and the parameters that yield the best results are chosen for the eventual classifier. A linear classifier only needs a value for C and the best one is found by performing a line search over a certain range. An RBF SVM uses both C and γ as parameters and the values for these are found by performing a grid search.

As already stated, SVMs were originally developed for binary classification problems. One could use the same technique as with the thresholding method to obtain a classification between 'preictal' versus 'not preictal'. In the case of SVMs one can do better however, because it is possible to do multiclass classification. The most common approach is to transform the original classification problem into the combination of multiple binary classification problems. Two very often used methods are one-versus-one (OVO) and one-versus-all (OVA) classification. In the OVO case, one designs binary classifiers that distinguish between every pair of classes. In the OVA case, one designs binary classifiers that make the distinction between one class and all the other classes. For classification in the OVO case, one uses a voting strategy. Every trained SVM chooses a class and the class with the most votes is chosen as the class to which the input belongs. Classification in the OVA case is done by choosing the SVM with the highest output function. The input is then assigned to the class that is represented by this SVM. Both OVO and OVA will be explored.

The implementations for SVM classification are done by making use of LIBSVM [97]. LIBSVM is a library for support vector machines and can be used for classification purposes. The extracted features from the EEG are used on their own as well as combined together in large feature vectors as input to the SVMs. The effect of using only a single channel combination or all the channel combinations from the 6-channel EEG is also investigated.

4.3 Results

The results for data generation were actually already shown in Section 2.2.3. Here the focus will be on the results of feature extraction and classification.

Feature extraction

A 2-channel EEG recording is generated to illustrate the results of feature extraction. The signals from channel one and two are respectively shown in Figure 4.1a and Figure 4.1b. In both channels, every type of activity that the model for MTLE can produce is present. Type 1 up to type 6 are all simulated for 200 seconds (in increasing order of type). These signals are actually a long variant of the ones shown in Figure 2.7. So for having a more clear view on the signals, one can again take a look at that figure. The simulation time was increased to be able to clearly show the evolution of the features over time. The class labels for every point of the EEG

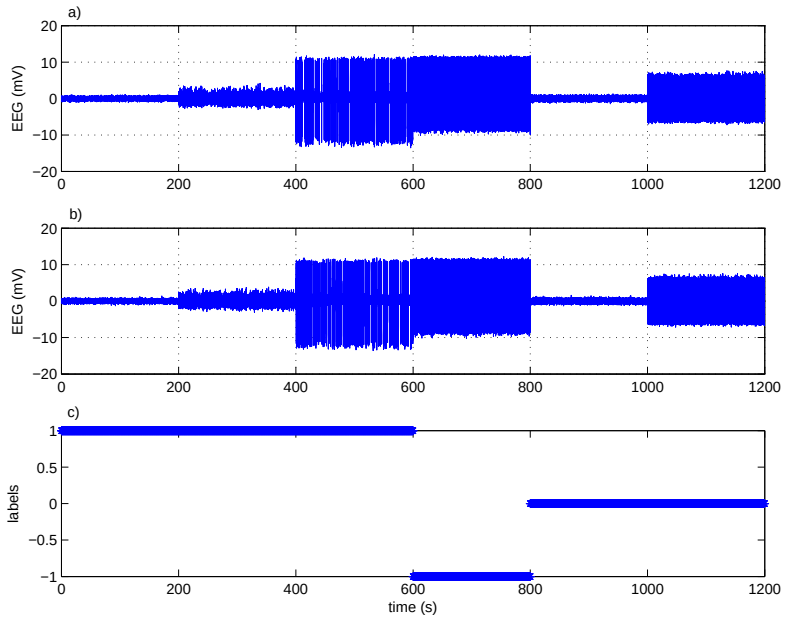

Figure 4.1: The 2-channel EEG recording that was used to calculate the synchrony measures and the corresponding class labels of every type of activity. a) The first EEG channel. Every type of activity (type 1 up to type 6) is simulated for 200 seconds. b) The second EEG channel. Also here every type of activity is simulated for 200 seconds. c) The class labels that belong to the different types of EEG activity. The labels 1, -1 and 0 respectively correspond to interictal, preictal and ictal activity.

are shown in Figure 4.1c. Label 1 is chosen for interictal, label -1 for preictal and label 0 for ictal activity. After extracting the measures one hopes that they have a distinctive property to separate the preictal, interictal and ictal part of the signal.

The time evolution of the four previously described measures for synchrony are shown in Figure 4.2. All the measures are computed for non-overlapping time windows of five seconds. For the nonlinear interdependence, the following parameters are used: $m = 10$, $\tau = 2$ and $k = 10$. When computing the nonlinear interdependence, one searches for vector pairs that are close together in state space. The vector pairs that are simply close together because they are close together in time have to be excluded in this search. In order to do this, a Theiler correction term of 50 is used. The time evolution of the maximal cross-correlation, coherence, nonlinear interdependence and PLV are respectively shown in Figures 4.2a-d. All these measures clearly show that there is a lot of synchrony during the preictal part (from 600 to 800 seconds) and during one type of ictal activity (from 1000 to 1200 seconds). One can also see that all the measures have their values in the interval $[0, 1]$, except the nonlinear interdependence, which also contains small negative values.

The aforementioned problem of synchrony during both the preictal and interictal stage is clearly illustrated in Figure 4.2. This problem can be overcome by first

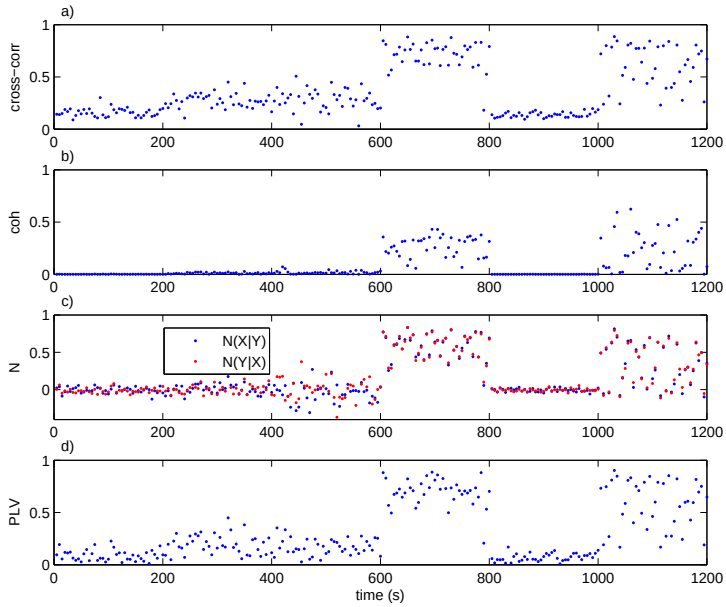

Figure 4.2: The evolution over time of the four synchrony measures for the 2-channel EEG of Figure 4.1. High values indicate synchrony and can be found during preictal activity ($600 - 800\ s$) and one type of ictal activity ($1000 - 1200\ s$). a) The time evolution of the maximal cross-correlation. b) The time evolution of the coherence. c) The time evolution of the nonlinear interdependence (blue for N(X|Y), red for N(Y|X)). d) The time evolution of the PLV.

LP filtering the EEG signals before computing the synchrony measures. The cutoff frequency of the LP filter is set to 9 Hz. Using this approach, the preictal synchronous activity is passed while the ictal one is filtered out. The time evolution of the measures after LP filtering the EEG channels is shown in Figure 4.3. The problem is solved for all the measures. These measures can now be directly used to search the preictal stages by choosing a well tuned threshold. A very big assumption is made here however, namely the assumption that all ictal synchronous activity will be filtered out by this LP filter. This is the case for the signals that are generated by the used model, but this might not always be the case for real life signals. This is a first big shortcoming for doing the classification with a threshold. The second big shortcoming will be described shortly.

Since the entire prediction system has to run in real time, a fast extraction of features is very important. The time needed to calculate the specified measures for an EEG recording of 5 seconds is shown in Table 4.1. All these times are in the order of tens of milliseconds except for the nonlinear interdependence. Computing the nonlinear interdependence for a signal of 5 seconds takes more than one second. This seems far from optimal for usage in an application that has to run in real time. The classification possibilities for this measure will be examined when classifying with a

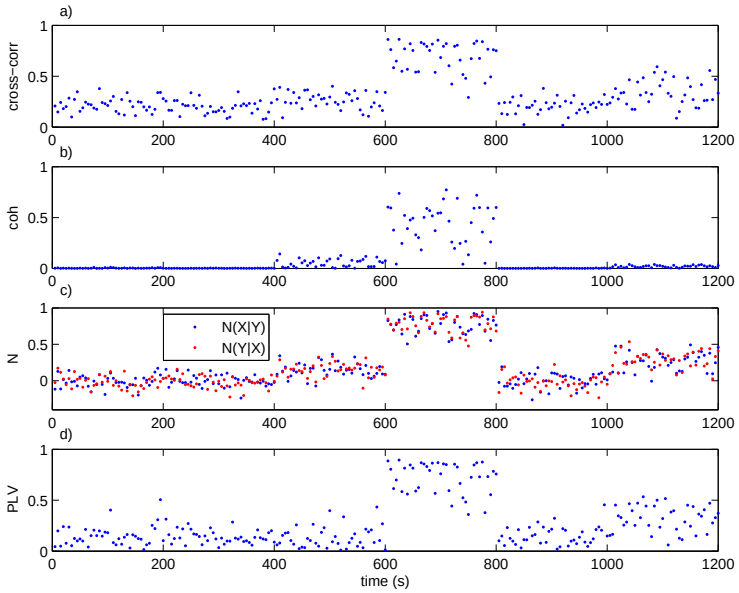

Figure 4.3: The evolution over time of the synchrony measures for the 2-channel EEG of Figure 4.1 after LP filtering (cut-off frequency 9 Hz). High values are now only found during the preictal segment of the signal ($600 - 800\ s$). a) The time evolution of the maximal cross-correlation after LP filtering. b) The time evolution of the coherence after LP filtering. c) The time evolution of the nonlinear interdependence after LP filtering (blue for N(X|Y), red for N(Y|X)). d) The time evolution of the PLV after LP filtering.

	Time (msec)
Maximal cross-correlation	42.1
Coherence	13.2
Nonlinear interdependence	1143.7
PLV	28.7

Table 4.1: The time needed (in msec) to calculate the different measures for a window of 5 seconds. Timed on a laptop with an Intel Core i5 processor, a clock rate of 2.40 GHz and 4 GB of RAM.

threshold, but because of the expensive computation it will no longer be considered when doing the classification with SVMs.

Classification with a threshold

Simply putting a threshold on one of the measures in Figure 4.3 is probably not a good idea. It can be seen that the measures can be quite noisy, which results in the presence of outliers. These points can easily fall on the wrong side of the

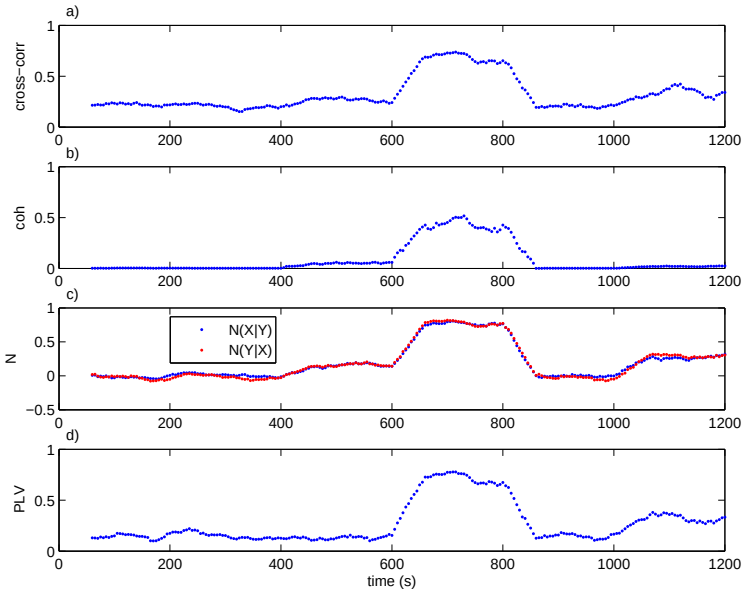

Figure 4.4: The evolution over time of the synchrony measures for the 2-channel EEG of Figure 4.1 after LP filtering and aggregating the measures over multiple windows. These measures now show a much more smooth progress, without outliers. a) The time evolution of the maximal cross-correlation after LP filtering and aggregation. b) The time evolution of the coherence after LP filtering and aggregation. c) The time evolution of the nonlinear interdependence after LP filtering and aggregation (blue for N(X|Y), red for N(Y|X)). d) The time evolution of the PLV after LP filtering and aggregation.

threshold. This is something that needs to be avoided at all times, because it will result in wrongly classified points. A solution for this problem is to smooth the time evolution of the measures. Measures that are calculated from different time windows are aggregated by making use of an overlapping moving window. The aggregated value is the average of the measures that fall into this new window. An example where the aggregation happened over 12 measures is show in Figure 4.4. A point in this figure is calculated from the passed minute of EEG activity, since 12 measures are used which each were calculated from time windows of 5 seconds. The time evolution now shows a much smoother behavior and there are no outliers anymore. The price that has to be paid is that the preictal stage will be detected a little bit later. This does not have to be a problem in general, because preictal stages typically last from a couple of minutes up to an hour.

The results for doing classification with a threshold are shown in Figure 4.5. The PLV is used as an example, but the other measures can also be used. The obtained results will not vary much between the different measures. The time evolution of the PLV together with the chosen threshold can be seen in Figure 4.5a. The threshold

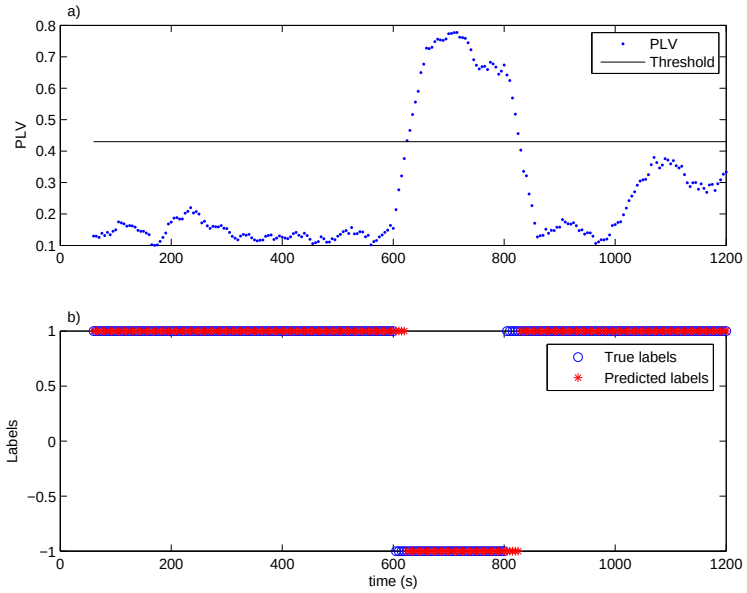

Figure 4.5: The classification results by using a threshold and the PLV as an example (other measures can also be used). a) The time evolution of the PLV after LP filtering and aggregation (blue) together with the chosen threshold of 0.42 (black). This threshold was chosen after some tuning. Values of the PLV above the threshold are classified as preictal, while values of the PLV below the threshold are classified as 'not preictal'. b) The predicted labels (red) together with the true labels (blue). The labels were chosen to be 1 and -1 for respectively 'not preictal' and 'preictal'.

is chosen to be equal to 0.42 after some experimentation with this parameter. The predicted labels together with the true labels are shown in Figure 4.5b. A label of 1 is chosen for the 'not preictal' superclass and a label of -1 represents the 'preictal' class. One can clearly see that the predicted label is -1 whenever the PLV is above the threshold and 1 when the PLV is below this threshold. The obtained prediction accuracy is 95.63%. The only errors that are made are situated in the transition areas from one class to the other. This is because the measure at each moment is calculated from the passed EEG activity and some time is needed for the new type of activity to become dominant in this window. The results for longer signals are also calculated and an accuracy of at least 95% could be obtained consistently. A comparison for the different measures can be found in Table 4.2. The optimal range of the threshold as well as the obtained accuracy on a long test simulation are shown in this table. These optimal ranges are found by changing the thresholds manually and stopping when the accuracy decreased. These results are very positive, but unfortunately, this method has another big shortcoming.

The second big shortcoming of using this thresholding method is that one can only make the distinction between 'preictal' versus 'not preictal'. When a prediction

	Optimal threshold range	Accuracy
Maximal cross-correlation	[0.44,0.47]	96.19%
Coherence	[0.14,0.16]	96.33%
Nonlinear interdependence	[0.36,0.42]	95.49%
PLV	[0.40,0.43]	95.91%

Table 4.2: The results for classification with thresholding on the different measures. The optimal threshold range and the obtained accuracy are shown for every measure.

system is implemented in an implantable device, it can also be useful to be able to make the distinction between interictal and ictal. During interictal periods such a device has to do nothing. But if for some reason, the prediction system failed to prevent the seizure and the patient has entered the ictal stage, then some type of control would come in very handy. By using such a thresholding technique, this will not be possible. At least not by using only one threshold.

Because of the two big shortcomings of using a thresholding technique, the switch is now made to a more sophisticated way of doing classification, namely with SVMs.

Classification with SVMs

Both problems that limit the applicability of thresholding can be solved by using SVMs with the right inputs. It is very important to choose good inputs, since the classifier will be trained on this data. A well known saying states this perfectly: 'garbage in is garbage out'. By combining multiple binary SVMs, one can obtain multiclass classification models. This will allow the classifier to make a distinction between interictal, preictal and ictal instead of just 'preictal' versus 'not preictal'. The problem associated with distinguishing between preictal and ictal synchronous activity can be solved by replacing the LP filter with a filter bank. Often used frequency bands for EEG analysis are:

- Delta: 0.1-4 Hz,
- Theta: 4-7 Hz,
- Alpha: 7-13 Hz,
- Low Beta: 13-15 Hz,
- High Beta: 14-30 Hz,
- Low Gamma: 30-45 Hz and
- High Gamma: 45-100 Hz.

These will be used as passband for the different band-pass filters in the filter bank. The PLV will then be computed for the unfiltered EEG signal and for the seven filtered signals. This results in ten different measures: maximal cross-correlation,

coherence and eight variants of the PLV. Filtered versions are only computed for the PLV, because the time evolution of the two other measures is very similar to that of the PLV. It therefore is assumed that only using the filtered versions of one measure will be sufficient. These measures are computed for all the different channel combinations. There are fifteen possible combinations, since the model generates six channels. All these different measures are combined into a feature vector for input to the SVM. The dimension of such a feature vector is 150 (10 measures for 15 channel combinations).

It is impossible to show the effect of the filter bank on the distinctiveness of the features in 150 dimensions. Therefore, principal component analysis (PCA) was performed on the features to extract the three principal components. This was done for the features without the filtered versions of the PLV and for the features including the seven filtered versions of the PLV. The results without and with the filtered versions can be seen in Figure 4.6 and 4.7 respectively. The green circles represent features extracted from interictal stages, blue ones from preictal stages and red ones from ictal stages. The first thing that one notices, is the fact that there are two clusters for the ictal activity in both cases. That is because during ictal activity two very different types of EEG signals are produced. On the one hand there is the low voltage rapid activity and on the other hand there is the quasi sinusoidal synchronous activity. The first of these two is represented by the red cluster that lies close to the green one, while the second type is represented by the red cluster close to the blue one. In Figure 4.6 it is clearly visible that the preictal synchronous activity and the ictal synchronous activity can not be separated from each other. Figure 4.7 shows that using band-pass filtered version of the PLV can solve this problem. The blue and red cluster that were intermingled first are now separated by a gap. This way of band-pass filtering the signals is a much more general approach than LP filtering and will normally generalize better towards real life signals. Another effect of including the filtered versions is that the three types of interictal activity now form three smaller clusters instead of one big cluster. That is because slightly different frequencies are in play during the three types of interictal activity. This does not form a problem however. As one can see in Figure 4.7, the clusters are still situated close to each other.

From the previous figures it is clear which inputs to the SVMs are suited for the classification task. The training and testing of the SVMs can start now. A dataset for training is generated that contains three periods of successive interictal, preictal and ictal activity. Every of the six possible types is simulated 400 seconds in each period. This implies that there are respectively 1200, 400 and 800 seconds of interictal, preictal and ictal activity in one period. Since there are three periods, this boils down to 3600, 1200 and 2400 seconds for the interictal, preictal and ictal parts. In total this dataset has a duration of two hours, with one hour of interictal data, twenty minutes of preictal data and forty minutes of ictal data. Half of the data points in the training set belong to the interictal class. This might not seem a good idea at first, because it may cause a slight bias of the trained SVM towards the interictal class. The trained SVM however, will be applied to real life signals and will encounter mostly interictal signals. This slight bias towards the interictal class

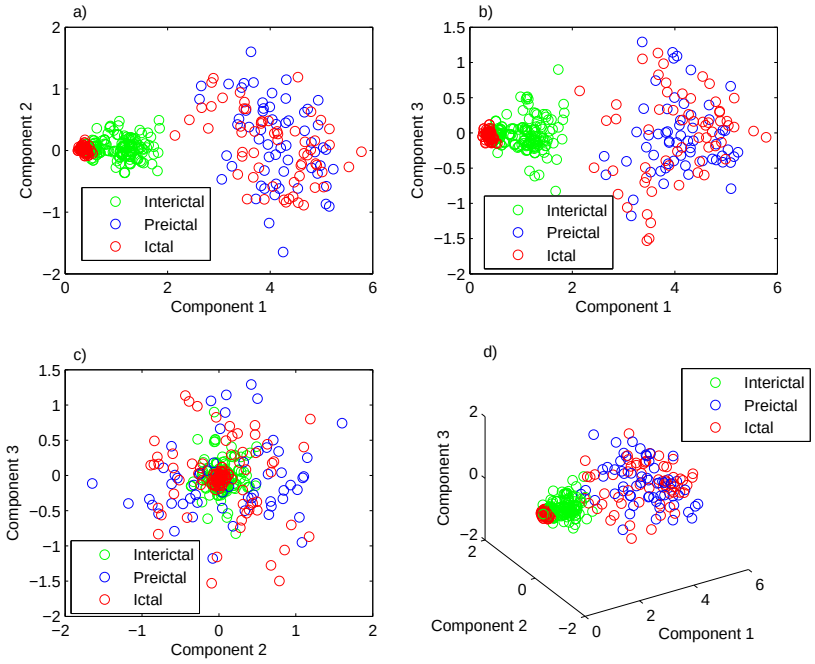

Figure 4.6: PCA on the input features when the filtered versions of the PLV are not included. Green, blue and red circles respectively represent features from interictal, preictal and ictal stages from the EEG. The red cluster close to the green one represents the ictal low voltage rapid activity, while the red cluster close to the blue one represent the ictal synchronous activity. a) The distribution of the features according to principal component one and two. b) The distribution of the features according to principal component one and three. c) The distribution of the features according to principal component two and three. d) The distribution of the features according to principal component one, two and three. From these figures it is clear that the preictal and ictal synchronous activity can not be separated from each other.

can therefore be interpreted as a larger prior probability of this class with respect to the other ones.

SVMs with both linear and RBF kernels will be used. The training phase will start with the estimation of the parameters of the SVM via 5-fold cross validation. For the linear kernel, only the regularization constant C needs to be determined. In addition to this parameter, another one has to be estimated for the RBF kernel, namely γ. In the linear case, the best value for C is found by performing a line search over the interval $[2^{-5}, 2^{-4}, \ldots, 2^{15}]$. For the parameters of the RBF kernel, a grid search is performed over the grid $C = [2^{-5}, 2^{-4}, \ldots, 2^{15}] \times \gamma = [2^{-15}, 2^{-14}, \ldots, 2^{3}]$. Once these parameters are estimated, the entire training dataset is used to train the SVM.

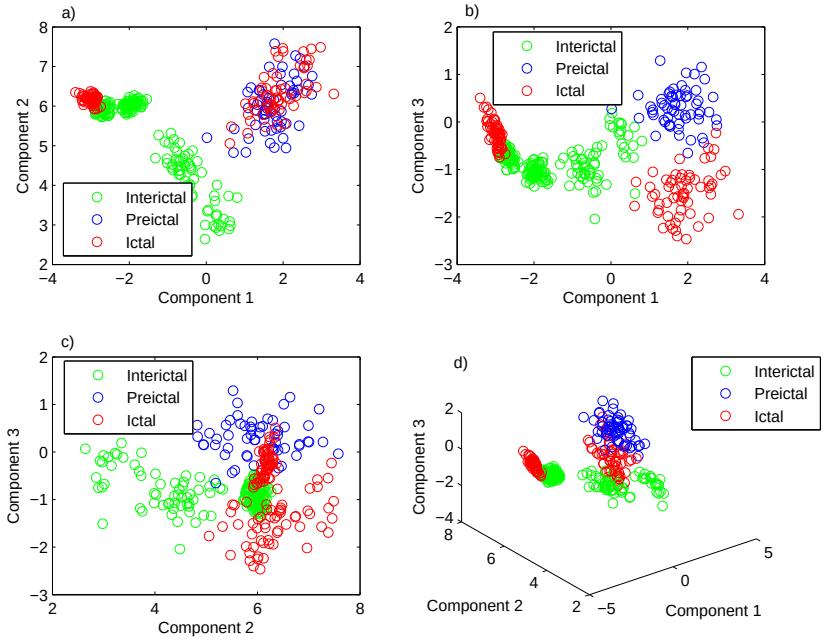

Figure 4.7: PCA on the input features when the filtered versions of the PLV are included. Green, blue and red circles respectively represent features from interictal, preictal and ictal stages from the EEG. The red cluster close to the green one represents the ictal low voltage rapid activity, while the red cluster close to the blue one represent the ictal synchronous activity. a) The distribution of the features according to principal component one and two. b) The distribution of the features according to principal component one and three. c) The distribution of the features according to principal component two and three. d) The distribution of the features according to principal component one, two and three. From these figures it is clear that including the band-pass filtered versions of the PLV leads to the possibility of separating the preictal and ictal synchronous clusters. These two clusters are no longer mixed with each other, but separated by a gap.

Once the SVM is trained on the training data, it will be tested on some unseen test data. Ten different datasets are generated to evaluate the performance of the SVM. By using ten different sets, it is possible to average the performance over these sets. In this way the obtained result is not specific for one dataset. Every dataset for testing is generated in a similar, but slightly different way as the training dataset. Every dataset again consists of three periods. Within these periods, every of the six possible types is simulated once for 100 seconds. This boils down to respectively 300, 100 and 200 seconds of interictal, preictal and ictal activity in each period. The order of these different types within each period is now however chosen randomly. In the training dataset every period consisted of first the three interictal types, followed by the preictal type and finally the two ictal types. In the test dataset this order within each period is not preserved, but permuted randomly. Every single test dataset has a total duration of thirty minutes, from which fifteen minutes are ictal, five minutes are preictal and ten minutes are ictal activity. This random permutation within the test signals is done to make sure that the order of the activities does not matter for classification.

The feature vector that serves as input to the SVM has a dimension of 150 (10 measures for 15 channel combinations). This is a rather high dimension and therefore subsets of this feature vector are taken and compared to the performance of using the entire feature vector. The accuracy results for classification with linear/RBF kernels and OVO/OVA multiclass strategies are shown in Figure 4.8, for different subsets of features. The numerical result can be found in Table 4.3. The results for linear OVO, RBF OVO, linear OVA and RBF OVA SVMs are shown respectively in dark blue, light blue, yellow and bordeaux in the bar graph. The results for a certain subset of features are grouped together for these four possibilities. The used subset of features is denoted on the x-axis. The labels 'Corr', 'Coh' and 'PLV' respectively mean that only the maximal cross-correlation, the coherence or the PLV is used as measure. The number that completes the label indicates how many channel combinations are used in the feature vector. The number '1' implies that only one channel combination is used, while '15' means that all the channel combinations are used. This means that the subsets 'Corr 1', 'Coh 1' and 'PLV 1' are no longer a vector, but just a scalar. The label 'Filt' means that the seven filtered versions of the PLV are used and the label 'All' implies that all the ten measures are used. So the subset 'All 15' is nothing else than the entire 150-dimensional feature vector. From Figure 4.8, one can see that the accuracy results for linear/RBF OVO/OVA SVMs for a certain subset of features are very comparable. Only the linear OVO SVM sometimes shows considerable less accurate classification results when compared to the three other types. Which type of SVM reaches the highest accuracy depends on the particular subset of features. Further it can be noticed that the maximal cross-correlation and coherence give similar accuracy results. The PLV can obtain an accuracy that is a little bit higher compared to these two. It can also be seen that the accuracy starts to reach its highest values only when the filtered versions of the PLV are included in the features. It is, as expected, very important to include these measures in the feature vector. The differences in accuracy between the labels 'Filt' and 'All' are very small. This implies that including the maximal cross-correlation, the coherence

and (the unfiltered version of) the PLV does not yield a lot of profit when the filtered versions of the PLV are already included in the feature vector. Excluding these three measures for fifteen channels immediately reduces the dimension of the feature vector from 150 to 105. In this way, the dimensionality of the feature vector is reduced by 30%, leading to an accuracy reduction of only 1% approximately.

The effect of the number of channels combinations used in the feature vector will be investigated now. The seven filtered versions of the PLV will be used as measures. The maximal cross-correlation, coherence and (unfiltered) PLV are excluded from the feature vector for a moment. So far, only the extreme possibilities are tested. Either one channel combination is used or all of the fifteen combinations are used. The best results in this case are obtained by incorporating all the channel combinations in the feature vector. This can be seen in Figure 4.8 and Table 4.3 when comparing label 'X 1' with 'X 15'. It might be, just like in real life, not be optimal to use all the channel combinations. Whether synchrony is present between different channels of a multi-channel EEG recording depends on the locations of the electrodes in the brain. When two electrodes are both situated in the epileptogenic region, there is a very large chance that there will be some synchrony between their EEG signals. This is not the case when one electrode is situated in the epileptogenic region and the other one in a region that is not involved in the seizure. The EEG signals from these two regions will not show any synchrony, unless occasionally some accidental synchronous activity. Including these uninformative channel combinations in the feature vector will not contribute to a better accuracy result. On the contrary, including uninformative measures in the feature vector will have an unfavorable effect on the accuracy. For this reason, the most informative channel combinations are searched. Several of these are combined in a feature vector and the SVM is trained and tested. The accuracy results for four channel combinations are shown in the column 'Filt 4' of Table 4.4. The combinations that are used are: Ch1+Ch2, Ch2+Ch3, Ch3+Ch6 and Ch5+Ch6. Excluding one of these combinations caused the accuracy to decrease, while including another combination did not cause a notable increase of the accuracy. When comparing the column 'Filt 4' of Table 4.4 with the column 'Filt 15' from Table 4.3, it can be seen that the results obtained with 'Filt 4' are better for three out of the four types of SVMs. The dimension of the feature vector is now 28. This is pretty low when compared to the original dimension of 150. This 28-dimensional feature vector obtains results that are very close to those obtained with the original 150-dimensional feature vector.

Finally, the effect of adding the maximal cross-correlation, coherence and PLV to the feature vector 'Filt 4' for the matching channels is examined. This feature vector will be defined as 'All 4' and the accuracy results are shown in column 'All 4' in Table 4.4. For all the types of SVMs, the accuracy of the subset 'All 4' is better than the subset 'Filt 4'. When 'All 4' is compared with 'All 15' from Table 4.3, one can see that both subsets are most accurate for two out of the four types of SVMs. The differences are very small however. This implies that the 40-dimensional feature vector 'All 4' is equally well suited to do the classification as the 150-dimensional feature vector 'All 15'. Therefore the feature vector 'All 4' is chosen to do the classification.

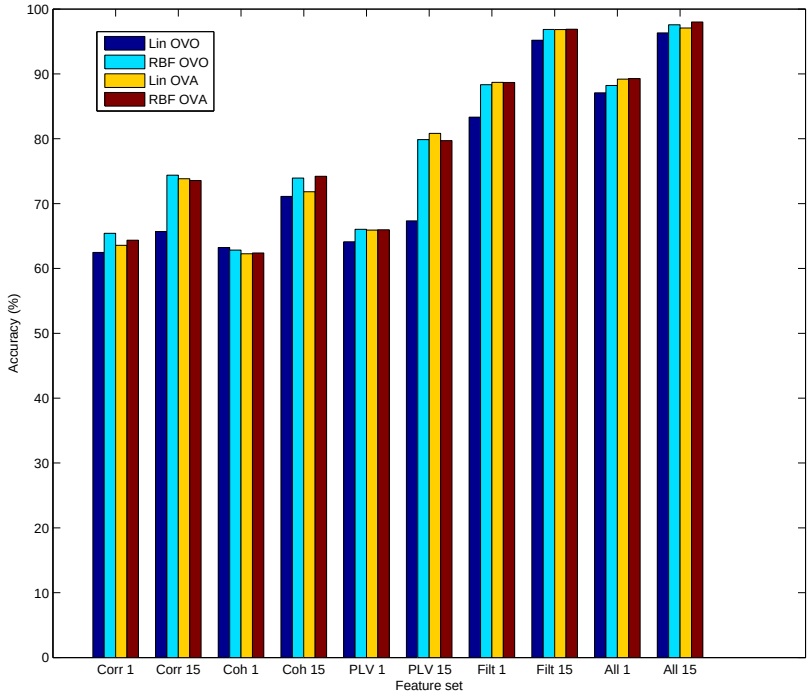

Figure 4.8: The prediction accuracy (in %) for the different types of SVMs and different subsets of features. Linear OVO, RBF OVO, linear OVA and RBF OVA SVMs are respectively represented by dark blue, light blue, yellow and bordeaux bars. The different feature subsets are denoted on the x-axis. 'Corr', 'Coh' and 'PLV' respectively imply that only the maximal cross-correlation, coherence or PLV is used as measure. The label 'Filt' means that the seven filtered versions of the PLV are used and 'All' implies that all the measures are used. The number that completes the label indicates how much channel combinations are used in the feature vector. The accuracy results for linear/RBF OVO/OVA SVMs are very comparable for a specific feature subset. The linear OVO SVM sometimes obtains a substantially smaller accuracy compared to the three others. This figure clearly shows that it is very important to include the filtered versions of the PLV in the feature vector to obtain high accuracy results. The numerical values can be found in Table 4.3.

	Corr 1	Corr 15	Coh 1	Coh 15	PLV 1
Lin OVO	62.47%	65.69%	63.22%	71.11%	64.11%
RBF OVO	65.42%	74.39%	62.83%	73.94%	66.03%
Lin OVA	63.56%	73.83%	62.27%	71.83%	65.92%
RBF OVA	64.36%	73.56%	62.39%	74.22%	65.97%
	PLV 15	Filt 1	Filt 15	All 1	All 15
Lin OVO	67.33%	83.33%	95.19%	87.08%	96.33%
RBF OVO	79.86%	88.33%	96.86%	88.22%	97.58%
Lin OVA	80.83%	88.69%	96.83%	89.19%	97.08%
RBF OVA	79.72%	88.67%	96.89%	89.28%	98%

Table 4.3: The numerical result of Figure 4.8. The prediction accuracy (in %) for the different types of SVMs and different subsets of features. The subsets of features are denoted by the same labels as in Figure 4.8.

	Filt 4	All 4
Lin OVO	95.47%	96.06%
RBF OVO	97.72%	98.06%
Lin OVA	95.97%	96.86%
RBF OVA	97.72%	98.31%

Table 4.4: The prediction accuracy (in %) for the different types of SVMs and specific subsets of features. The subset 'Filt 4' contains the seven filtered versions of the PLV for the following channel combinations: Ch1+Ch2, Ch2+Ch3, Ch3+Ch6 and Ch5+Ch6. The subset 'All 4' contains the maximal cross-correlation, coherence, (unfiltered) PLV and the seven filtered versions of the PLV for the following channel combinations: Ch1+Ch2, Ch2+Ch3, Ch3+Ch6 and Ch5+Ch6.

There still is a choice to be made about the type of SVM that will be used. From Table 4.4, it can be seen that the RBF kernels achieve a higher accuracy of approximately 2%. The accuracy is however not the only criterion that is important to make this choice. The training and prediction timings for the different SVMs on the feature subset 'All 4' are shown in Table 4.5. These timings are recorded from a laptop with an Intel Core i5 processor, a clock rate of 2.40 GHz and 4 GB of RAM. Training happens on a signal with a total duration of two hours and prediction on a signal of half an hour. Note that the units for the training timing is seconds, while the units for prediction timing is milliseconds. These result agree very well with what was to be expected. When the training timings for a linear and an RBF kernel are compared (for the same multiclass strategy), one can see that it takes a lot longer to train an SVM with an RBF kernel. That is because one has to perform a grid search for the parameters during the 5-fold cross validation for an RBF kernel. For linear kernels, only a line search is needed. Forming the eventual decision boundaries is also more complex for the RBF kernel than for the linear one. The prediction timings are, just like the training timings, also higher for RBF kernels than for

	Training time (in s)	Prediction time (in ms)
Lin OVO	2.6	4.2
RBF OVO	154.6	11.6
Lin OVA	15.2	6.9
RBF OVA	334.8	21.9

Table 4.5: The training (in s) and prediction timings (in ms) for different types of SVMs for the feature subset 'All 4'. Note that the units for both are not the same (s versus ms). The SVMs with linear kernels are trained and predicted a lot faster than those with RBF kernels. The OVO strategy is clearly faster than the OVA strategy for both training and prediction.

linear ones. The evaluation is more complex in case of the RBF kernels. The OVO multiclass strategy is faster than the OVA strategy, both for training and prediction. This seems intuitive, because in both cases three binary SVMs are trained. In the OVO case, these SVMs are trained on smaller datasets because only two classes are considered per SVM. In the OVA case, all data points from the three classes are used for every SVM. Training an SVM is a supervised learning method and will therefore happen off-line. The fact that training an RBF SVM is much slower than a linear SVM is therefore not such a big disadvantage, because it does not have to happen on-line. The extra accuracy obtained with the RBF kernel is worth the extra training time. Prediction can be seen to be very fast for every type of SVM. To obtain the optimal mix between accuracy and speed, the RBF OVO SVM is chosen to do the classification. The classifier will eventually be implemented on an implantable device. Computing exponentials might turn out to be a limiting factor if this device has very low computational power. In this case, a linear SVM would be a more suitable choice.

The results of using the RBF OVO SVM with 'All 4' as feature subset are shown in Figure 4.9. Figures 4.9a-j show the result on one of the ten different test datasets. The true class labels are denoted by blue circles, while the predicted class labels are represented by red stars. The obtained accuracy for every dataset is noted to the right of every figure. Remember that label 1, -1 and 0 respectively denoted interictal, preictal and ictal periods of the EEG. From this figure it is clear that the most occurring error is classifying ictal points (0) as interictal (1). The reason for this becomes clear when one looks back at Figure 4.7. The red cluster of ictal points that lies close to the green cluster of interictal points and this green cluster are overlapping a little bit. Because of this, a classification error can be made pretty fast. When the results of the linear kernel were examined, this problem only became larger. That is because the linear decision boundary is a lot less flexible than the RBF decision boundary. This flexibility is very much needed for slightly overlapping classes. A false alarm occurs when an interictal or ictal point is classified as preictal. This only happens twice, both times in Figure 4.9b. Having as few as possible false alarms is very important for a good prediction system.

Taking this altogether, it can be stated that classification with SVMs is a reliable, good method to predict epileptic seizures. High accuracies are obtained on independent test sets. The results can also be generalized much better towards real life signals. This is thanks to the band-pass filtering in specific frequency bands for EEG analysis. This is a lot more general than the LP filtering used in the thresholding method.

4.4 Conclusion

When trying to predict epileptic seizures, one first has to extract useful features from the EEG recording. This chapter has shown that bivariate measures that characterize synchrony between two signals are a good choice. After this feature extraction, the features need to be used to classify the EEG data in interictal, preictal and ictal periods. Two ways to do this were investigated, namely by thresholding and by using SVMs. The method that used thresholds showed high accuracies (around 95%), but there were two very big downsides to using this method. First of all, one could only distinguish between two classes, namely 'not preictal' versus 'preictal'. When the signal was classified as 'not preictal', then it was impossible to know if the EEG was in an interictal or ictal segment. Secondly, this method could probably not generalize very well towards real life signals, because of the LP filtering. The method that uses SVMs solved these two problems and is therefore much more suited for usage on real life signals. Different types of SVMs and different subsets of features were tested. Eventually, the RBF OVO SVM with all the measures for four specific channel combinations (Ch1+Ch2, Ch2+Ch3, Ch3+Ch6 and Ch5+Ch6) yielded accuracy results of 98%. This is of course still on signals generated by the model. The next step would be to use the developed framework on real life signals from patients with MTLE. Predicting epileptic seizures does not stop completely after the classification that was discussed here. This is a very important step, but when the EEG signal is in the preictal stage, one only knows that a seizure is coming. The problem is that the preictal stage can last from a couple of minutes up to an hour. To predict the time of occurrence of a seizure is another problem and is currently under a lot of research. This could unfortunately not be handled in this chapter due to a lack of time and would be a topic for future research.

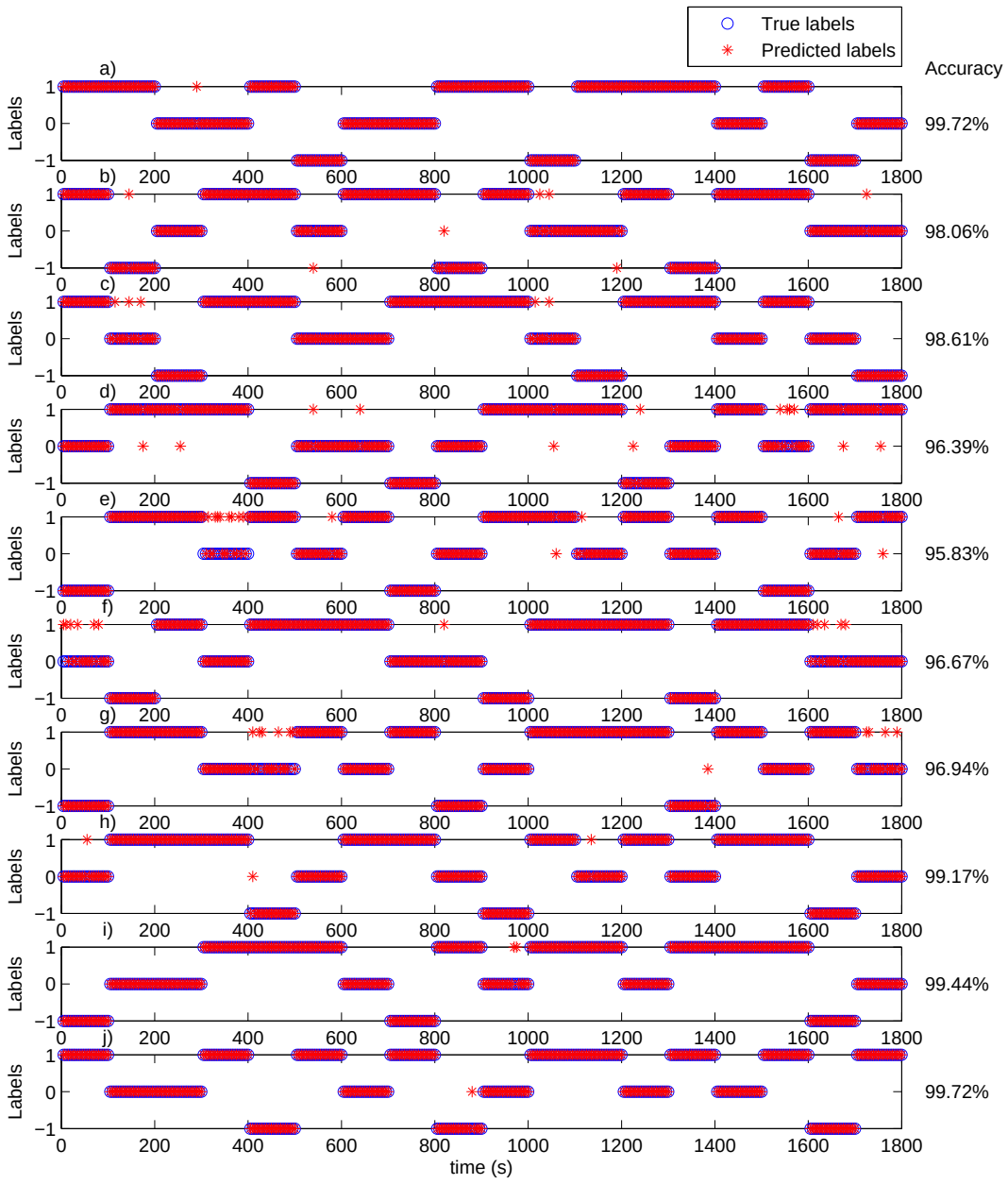

Figure 4.9: The classification results for the ten different test datasets when using the RBF OVO SVM with the 'All 4' feature subset. The true class labels are represented by blue circles and the predicted ones by red stars. The accuracy obtained for every dataset is shown to the right of the figure. a) - j) The results for test dataset 1 up to test dataset 10.

Chapter 5

Conclusion and discussion

5.1 Modeling epileptic seizures

The first computational model that was presented was the thalamocortical model for absence seizures. Two qualitatively different types of EEG signals can be simulated by this model. On the one hand there are the interictal waxing-and-waning spindle oscillations, while on the other hand there is the ictal quasi-sinusoidal activity. The typical SW waveform that is present during epileptic activity in real life signals can not be simulated by this model. Instead, some quasi-sinusoidal activity of the right frequency is produced. The most important aspect about this model is the fact that it operates in a bistable mode. It can therefore exhibit spontaneous transitions from one type of activity to the other. The dynamics that are in play during these transitions were shown to be well described by the model. This is very important given that this model will be used in combination with a control system. Therefore, it should be possible to interact with the model to try and stop a started seizure. A possible extension for this model could be to try to simulate the SW discharges in the ictal parts of the signal instead of the quasi-sinusoidal activity. The model already incorporates a couple of biological important factors, like the subdivision in two GABA receptors and the burst firing character of thalamic neurons (thanks to the I_T calcium current). To account for the SW waveform, the model has to incorporate even more biophysical reality. Other types of receptors (for example NMDA) and currents (for example Mg^{2+} currents) will be needed and one will have to model neurotransmitter concentrations in the synaptic cleft. Another extension to the model could be the simulation of more than two types of behavior. Although absence seizures occur predominantly during spindle oscillations (when a person is sleepy or drowsy), it would make the model more general towards real life signals.

The second computational model that was introduced was the hippocampal model for MTLE. This model can simulate six qualitatively different types of EEG activity by adjusting some parameters of the model. These types are normal background activity, slow rhythmic activity, sporadic spikes, sustained spikes, low voltage rapid discharge and quasi-sinusoidal activity. The first three types are typically seen during interictal periods. The fourth type is typical for preictal periods and the last two

types represent ictal periods. This model was extended to be able to produce a 6-channel EEG recording as output. The output of every module is interpreted as one of the six channels. The model is unfortunately not able to make transitions from one type to another, because these biological relations are not incorporated. Different types of activity are simulated and afterwards concatenated to form long EEG recordings with different types of signals in it. The model is used to generate training and test data for the classification algorithms used for prediction. After making a prediction about an upcoming seizure, the next step would be to try to prevent the seizure from happening. In order to do this, one would need to be able to interact with the model. Thus, a useful extension for this model would be to make the transitions from one type to another possible, according to the biological processes that are in play. However, this will not be so easy, since there are fifteen possible transitions that have to be modeled. If this could be accomplished, it would be possible to use the prediction system on the model and try to prevent any seizure from happening.

5.2 Controlling epileptic seizures

A control system for the thalamocortical model for absence seizures was designed and implemented. It was shown that the system is very successful in controlling the seizures. The EEG did not show any sign of ictal activity, only waxing-and-waning spindle oscillations were present. The activation of the $GABA_B$ receptor was maximally of the order of 10^{-3}, while the order was 10^2 without the control system. This good performance is only obtained when some important parameters are tuned carefully. These are the threshold for detection and the duration and amplitude of the control signal. The threshold in the detection system was set to $2.4 \cdot \sigma$, where σ is the standard deviation of the EEG signal without seizures. The amplitude of the control signal was set to 15 *pps* and the duration to 6 *ms*. This tuning is only optimal for a specific set of model parameters. If the parameters of the model change, the tuning has to be executed again. In real life this tuning will also be patient specific. Setting a too low threshold in the detection system caused too much unneeded interaction with the model and led to strange EEG signals. Choosing the threshold too high on the other hand, caused seizures to be detected too late (or not at al). This allowed the seizures to develop long enough to become noticeable in the EEG recordings. When the amplitude of the control signal was chosen too low, not all the seizures could be controlled. The problem in this case, is the fact that the stimulus is not strong enough to restore the balance. When the amplitude was chosen too high, there was again too much interference with the model. The stimuli were too strong and caused the model to leave its normal working regime. It is of course a bad idea to send pulses with a too high amplitude into a person's brain. Choosing the duration of the control signal too short made it possible for some seizures to develop and become noticeable in the EEG. Choosing the duration too long caused continuous stimulation at some moments. This had the effect of rather sustaining a seizure than annihilating it. These parameters are clearly very important to tune

optimally for obtaining a good performance of the control system. A shortcoming of the used method for detection is a lack of generalization towards real life signals. The detection is based on the amplitude of the EEG signal for the used model. In real life, doing this will often cause false alarms and unneeded stimulations as a result. Better detection methods could make use of machine learning methods. The SVMs used for prediction in this thesis are an example of these type of methods. It is however very important that the detection can happen very fast, since the goal is to control a seizure after its onset. The method used in this thesis shows that this control is possible after an early detection. A topic for future research could now be to develop a more general, but very fast detection algorithm.

5.3 Predicting epileptic seizures

A prediction framework was developed for MTLE, by making use of the hippocampal model for MTLE to generate data. Predicting a seizure boils down to finding preictal periods in the EEG. Several bivariate measures were extracted from the EEG recordings and were used as features for the classification algorithms. The used measures are the maximal cross-correlation, the coherence, the nonlinear interdependence and the PLV. All these measures were shown to produce high values for synchronous signals and low values for independent signals. Since there is a lot of synchrony during preictal periods, these measures are very well suited for the classification task. All these measures can be calculated very quickly, except the nonlinear interdependence. Since the prediction system will have to run in real-time, this measure was excluded from the study. The classification was first done by using a threshold on the smoothed time evolutions of the synchrony measures. A problem here is the fact that there is also synchrony in the EEG during ictal periods. For the used model, this can be solved by first LP filtering the EEG signals. In this way, the preictal synchronous activity is passed, while the ictal synchronous activity is blocked. The obtained classification accuracy between 'preictal' and 'not preictal' is approximately 95%. Unfortunately, this method has a lack of generalization towards real life signals. Simply LP filtering will not suffice for all the possible types of EEG activity. Also the fact that only binary classification is possible with a threshold limits its applicability. To solve these problems, SVMs were used to do the classification between interictal, preictal and ictal periods. In order to be able to make the distinction between preictal and ictal synchronous activity, the PLV was computed for the unfiltered EEG signal and for seven band-pass filtered EEG signals. PCA analysis showed that using these seven filtered versions allowed one to make this distinction. Different types of SVMs (linear/RBF and OVO/OVA) were tested. Also different subsets of the 150-dimensional (10 measures and 15 channel combinations) feature vector were tested. The subset of features that gave the best accuracy results was the 40-dimensional vector with all the ten measures for four specific channel combinations (Ch1+Ch2, Ch2+Ch3, Ch3+Ch6 and Ch5+Ch6). The RBF OVO SVM is chosen, because it offered the best trade-off between accuracy and speed. The obtained classification accuracy, averaged over ten different test sets, is approximately 98%.

This is a very promising result. The next step for this prediction method is to test it on real life signals. It is expected that this method will generalize much better towards real life signals than the thresholding method would do. If applying this prediction framework on real life signals gives promising results, one could compare its performance with existing prediction algorithms. This can be done with the seizure prediction characteristic (SPC) framework. This works in the same way as the receiver operating characteristic (ROC) framework, but is specifically designed for the prediction of epileptic seizures. When the preictal periods can be accurately found in EEG signals, there is still one step to be done. A preictal period can last from a couple of minutes up to an hour. Determining the actual moment of onset of the seizure (once it is know that the signal is in a preictal period) is therefore the last step. This would finish the framework for predicting epileptic seizures and is a topic for future research.

Appendices

Appendix A

Introduction to neuroscience

This appendix is an overview of the fundamental concepts in (computational) neuroscience and is based on courses taken by the author.

The brain consists of a lot of different regions, all with different functions. The regions of main interest in this study are the cerebral cortex, the thalamus and the hippocampus. The cerebral cortex is the outer part of the cerebrum (the big brain) and can be divided into four lobes: the frontal lobe, the parietal lobe, the occipital lobe and the temporal lobe. All these lobes have different functions. The occipital lobe, for example, is responsible for, among other things, vision and perception. The thalamus lies deeper inside the brain and has a couple of important functions. The thalamus sends incoming sensory signals to the cerebral cortex and regulates the level of consciousness, alertness and sleep. The hippocampus is part of the limbic system, which is located near the thalamus. The hippocampus is important regarding emotions and memory.

In 1887, Santiago Ramón Y Cajal proposed the neuron doctrine by using the staining method of Golgi. This doctrine stated that the nervous system is built from individual building blocks and that these blocks are interconnected somehow. Later, these individual building blocks were named neurons and the interconnections were called synapses. From an engineering point of view, the neurons are the central processing units of the brain. A neuron consists of three parts: the soma, the dendrites and the axon. The soma or cell body contains the nucleous and other organelles. The dendrites are short, branched extensions of the soma that receive signals from other neurons. The axon is a long (sometimes short) extension of the soma that sends signals to other neurons. This topology can be seen in Figure A.1. The big blue circle is the soma, the long extension on the right is the axon and the branched blue extensions on the left are the dendrites. In this way, the neuron can be seen as an input-output device: it gets input from other neurons via the dendrites and it sends output to other neurons via the axon. These connections between neurons result in the formation of synapses, indicated on Figure A.1 as little yellow dots. The red and green neurons are called presynaptic neurons and the blue one is the postsynaptic neuron. This blue neuron is of course also a presynaptic neuron for other neurons (not in this figure), just as the red and green neurons are

postsynaptic neurons to other neurons (not in this figure). There is a big difference between the red and the green neurons. The red neurons are inhibitory neurons and the green ones are excitatory neurons. The terminology is very clear: excitatory presynaptic neurons try to excite the postsynaptic neuron, while inhibitory ones try to inhibit the postsynaptic neuron. How this happens will become clear in a minute, first there has to be said a word about what kind of signals are propagating over these neurons. In Figure A.1 two different kinds of signals can be seen: the black bars and the red/green waves. The black bars are called action potentials and are used to send information over the entire brain. Every action potential has the same shape, amplitude and duration. So this is a digital (1 or 0) signal: there is an action potential (1) or there is not (0). The red/green waves are called postsynaptic potentials (PSPs). These signals are analog. So actually, there is an A/D conversion at the soma. An action potential is fired if the total PSP is above a certain threshold. If the total PSP is below this threshold, the neuron will stay quiet. This shows that a neuron will fire action potentials if it is excited enough. Since there is an A/D conversion, there also needs to be a D/A conversion. This D/A conversion happens at the synaps. It is important to note that the axons and dendrites do not touch each other at the synaps. There is a little space between them, called the synaptic cleft. When an action potential of the presynaptic neuron arrives at the synaps, neurotransmitters are released into the synaptic cleft. There are a lot of different neurotransmitters. Glutamate is the major excitatory neurotransmitter and γ-aminobutyric acid (GABA) is the major inhibitory neurotransmitter of the brain. When these neurotransmitters bind to receptors in the postsynaptic neuron, ion-channels open and the potential changes. The major excitatory receptors are the α-amino-3-hydroxy-5-methyl-4-isoxazolepropionic acid (AMPA) receptor and the N-methyl-D-aspartate (NMDA) receptor. The major inhibitory receptor has the same name as the neurotransmitter, namely the GABA receptor. When the neurotransmitters are excitatory, the ion-channels will allow the flow of sodium ions (Na^+) into the cell (because of diffusion) and an excitatory PSP (EPSP) is generated locally. This makes the cell more positive than its resting potential and is called depolarization. When the neurotransmitters are inhibitory, the ion-channels will allow the flow of potassium ions (K^+) out of the cell and generate a local inhibitory PSP (IPSP). This makes the cell more negative and is called hyperpolarization. These mechanisms are not the important part to remember from this appendix. The important concepts are the distinction between excitatory vs. inhibitory, presynaptic vs. postsynaptic, depolarizations vs. hyperpolarization and the notion of a PSP and neurotransmitters.

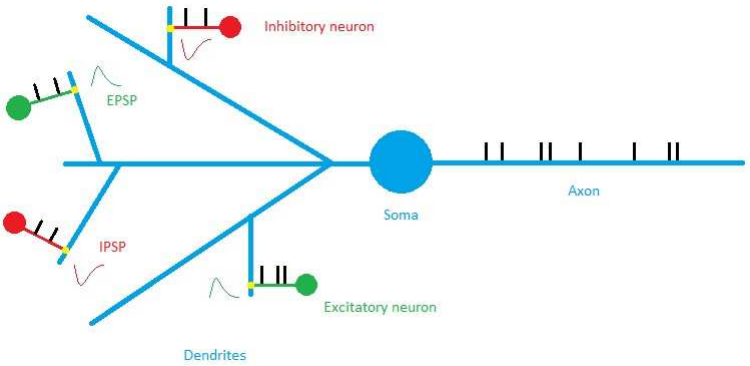

Figure A.1: A neuron as an input-output device. A neuron consists of three parts: dendrites (for input), the soma and an axon (for output). A neuron gets its input from presynaptic neurons and sends its output to postsynaptic neurons. Excitatory presynaptic neurons (green in the figure) will generate an excitatory postsynaptic potential (EPSP) and will depolarize the neuron. Inhibitory presynaptic neurons (red in the figure) will generate an inhibitory postsynaptic potential (IPSP) and will hyperpolarize the neuron. A summation of all these PSPs happens at the soma. If the neuron is depolarized above a threshold, it will fire an action potential (the black bars in the figure).

In computational neuroscience, it is often not so convenient to talk about sequences of action potentials. It is very hard to model the exact spiking pattern of a neuron. For that reason, often a switch is made to the firing rate of a neuron. In this case the model can show how often a neuron is firing action potentials, without having to worry about the exact moments of these spikes. When talking about neuronal populations instead of a single neuron, the concept of a firing rate is extended to the average firing rate of the population.

Appendix B

Mathematical details of the model for absence seizures

This appendix gives a mathematical description of the model of Suffczynski et al. [76]. Specific parameter values are not included in this appendix for the next reason. The interested reader who wants to use this model is encouraged to have a look at the original paper of Suffczynski and his colleagues.

B.1 The model

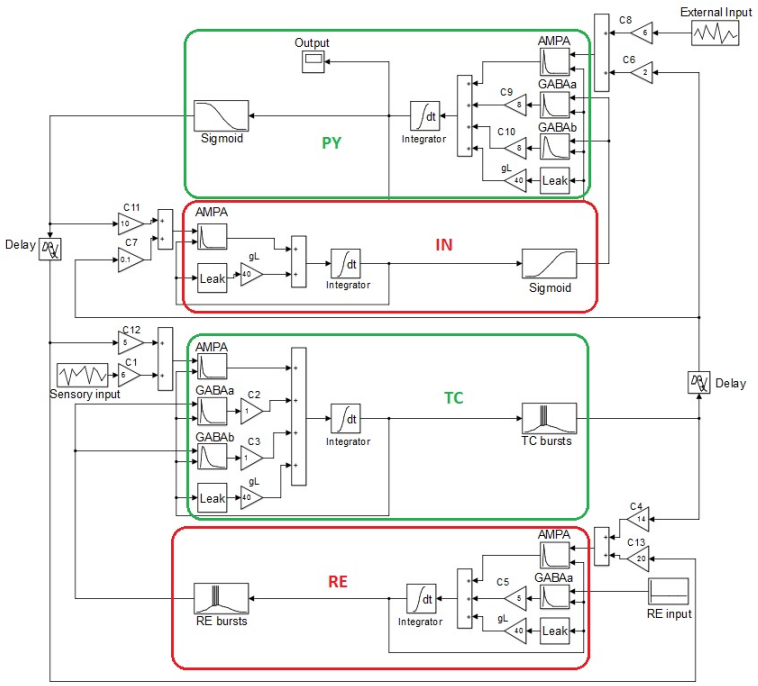

Figure B.1: The thalamocortical model of Suffczynski et al. [76]

The model is shown in Figure B.1 and consists of four neuronal populations which are interconnected with each other. The excitatory pyramidal neurons of the cortex (PY) excite all the other three populations. The inhibitory population of interneurons of the cortex (IN) inhibits this PY population. The excitatory thalamocortical relay cells of the thalamus (TC) excite all the three other populations. The inhibitory population of reticular thalamic neurons (RE) inhibits the TC cells. In every population, the conversion from average presynaptic firing rate into average postsynaptic firing rate follows the next steps. First the presynaptic firing rates are converted into postsynaptic currents. These currents are integrated to form the mean membrane potential of the population. This membrane potential is then finally transformed into the average postsynaptic firing rate. The first two steps will be described in Section B.2 and the third step in Section B.3.

B.2 From presynaptic firing rate to membrane potential

The evolution of the average membrane potential of a population over time is modeled by the next general equation:

$$\begin{aligned} C_m \cdot \frac{dV^{(i)}}{dt} &= -\sum_{syn} I_{syn}^{(i)} - g_{leak} \cdot (V^{(i)} - V_{leak}^{(i)}) \\ i &= \{PY, IN, TC, RE\}, \quad syn = \{AMPA, GABA_A, GABA_B\}. \end{aligned} \tag{B.1}$$

The synaptic currents in this equation are given by:

$$I_{syn}^{(i)} = g_{syn}^{(i)} \cdot (V^{(i)} - V_{syn}^{(i)}). \tag{B.2}$$

In Equations B.1 and B.2, C_m represents the membrane capacitance, V is the average membrane potential of the population, g_{leak} is the conductance of the leak current, V_{leak} is the reversal potential of the leak current, g_{syn} is the conductance of the synaptic current and V_{syn} is the reversal potential of the synaptic current. The membrane potential for which there is no net flow of an ion across the membrane is called the reversal potential of that ion.

The conductances of the synaptic currents are modeled by taking the convolution of the presynaptic firing rate ($r_{syn}(t)$) with a synaptic impulse response function ($h_{syn}(t)$):

$$g_{syn}^{(i)}(t) = \int_{-\infty}^{t} h_{syn}(t-\tau) \cdot r_{syn}^{(i)}(\tau) \cdot d\tau. \tag{B.3}$$

The synaptic impulse response function is given by:

$$\begin{aligned} h_{syn}(t) &= A_{syn} \cdot [exp(-a_{1,syn} \cdot t) - exp(-a_{2,syn} \cdot t)], \\ a_{2,syn} &> a_{1,syn}, \quad syn = \{AMPA, GABA_A, GABA_B\}. \end{aligned} \tag{B.4}$$

In this equation the parameters A_{syn}, $a_{1,syn}$ and $a_{2,syn}$ are respectively the amplitude, decay and rise time of the considered synaptic conductance. The synaptic

conductance, defined by Equations B.3 and B.4, can be obtained by solving a second order ordinary differential equation:

$$\frac{d^2g(t)}{dt^2} + (a_1 + a_2) \cdot \frac{dg(t)}{dt} + a_1 \cdot a_2 \cdot g(t) = A \cdot (a_2 - a_1) \cdot r(t). \tag{B.5}$$

The subscript *syn* should be placed with $g(t)$, a_1, a_2, A and $r(t)$, but this was not done to avoid to overload the equation. The transfer function that corresponds to this equation can be found by taking the Laplace transformation:

$$\frac{G(s)}{R(s)} = \frac{A \cdot (a_2 - a_1)}{s^2 + (a_1 + a_2) \cdot s + a_1 \cdot a_2}. \tag{B.6}$$

It can easily be checked that this is the Laplace transformation of $h_{syn}(t)$, which is defined by Equation B.4.

In Section 2.1.2 is was stated that $GABA_B$ receptors have nonlinear activation properties. This means that the amplitude of the postsynaptic $GABA_B$-mediated currents increases nonlinearly with the incoming firing rate. This nonlinear activation function is given by:

$$N(r) = \frac{1}{1 + exp((r - \theta_a)/\sigma_a)}. \tag{B.7}$$

This is a logistic function where r is the incoming firing rate and N is the nonlinear activation (always between 0 and 1). This nonlinear activation will act as a gatekeeper for giving the incoming firing rate as an input to the transfer function defined in Equation B.6. The passed firing rate can range continuously from 0 to 100% of the incoming firing rate. The parameter θ_a acts as a threshold for the activation and σ_a determines the slope of the function.

B.3 From membrane potential to postsynaptic firing rate

In the cortical populations, the conversion from mean membrane potential into average postsynaptic firing rate can be done with a sigmoidal function (also see Section 1.2):

$$S(v^{(j)}) = \frac{G_s}{1 + exp((v^{(j)} - \theta_s)/\sigma_s)}, \quad j = \{PY, IN\}. \tag{B.8}$$

In this logistic function, $v^{(j)}$ is the mean membrane potential of the population and $S(v^{(j)})$ is the resulting average postsynaptic firing rate. The parameter G_s determines the maximal firing rate, the parameter θ_s acts as a threshold for firing and the parameter σ_s determines the slope of the function.

The situation is not that simple for the thalamic populations. That is because the burst firing of thalamic cells is taken into account in this model. A burst is the result of the combination of a low threshold spike (LTS), which is mediated by I_T calcium currents, and fast sodium-mediated spikes. The fast sodium spikes seem

to ride on top of the LTS. These types of burst occur at hyperpolarized membrane potentials. A neuron can fire a LTS when the I_T current is de-inactivated and, at the same time, the neuron is depolarized above the threshold for generating a LTS. To be able to model this behavior, two new functions are introduced: $n_{\text{inf}}(v)$ and $m_{\text{inf}}(v)$. These express the proportion of cells (in steady-state) in which I_T current is de-inactivated and activated respectively, as a function of the voltage. Both functions have a logistic form:

$$m_{\text{inf}}(v^{(k)}) = \frac{1}{1 + exp((v^{(k)} - \theta_m)/\sigma_m)}, \quad k = \{TC, RE\}, \tag{B.9}$$

$$n_{\text{inf}}(v^{(k)}) = \frac{1}{1 + exp((v^{(k)} - \theta_n)/\sigma_n)}, \quad k = \{TC, RE\}. \tag{B.10}$$

The parameter θ_m will have a positive value and the parameter σ_m will be negative. This means that $m_{\text{inf}}(v)$ will start at 0 for $v = -\infty$ and will be equal to 1 for $v = +\infty$. The rise from 0 to 1 happens in the region around θ_m, so there are positive voltages needed for activation. This situation is opposite to the case of de-inactivation. The parameter θ_n will have a negative value and the parameter σ_n will be positive. This means that $n_{inf}(v)$ will start at 1 for $v = -\infty$ and will be equal to 0 at $v = +\infty$. The fall from 1 to 0 happens around θ_n, so the voltages can not be to large or the I_T current will be inactivated.

It is assumed that the activation of the I_T current happens instantaneously. This means that $m_{\text{inf}}(v(t))$ gives the proportion of cells in which I_T current is activated at a certain time t. Furthermore it is assumed that I_T current de-inactivation reaches its steady-state with a delay with respect to the change in membrane potential. To account for this delay, the steady state function for de-inactivation ($n_{\text{inf}}(v)$) is convolved with a delay function (h_n). A final assumption is that each TLS will trigger a burst of fast spikes with a certain frequency G. This all taken together gives that the average postsynaptic firing rate for thalamic populations in function of the mean membrane potential is given by:

$$S(v^{(k)}) = G \cdot m_{\text{inf}}(v^{(k)}) \cdot n(v^{(k)}), \quad k = \{TC, RE\}. \tag{B.11}$$

The delayed de-inactivation function is given by:

$$n(v) = \int_{-\infty}^{t} h_n(t - \tau) \cdot n_{\text{inf}}(v) \cdot d\tau \tag{B.12}$$

in which the delay function has the next form:

$$h_n(t) = N \cdot (exp(-n_1 \cdot t) - exp(-n_2 \cdot t)), \quad n_2 > n_1 \quad N = \frac{n_1 \cdot n_2}{n_2 - n_1}. \tag{B.13}$$

In this equation the parameters n_1 and n_2 are the decay and rise time of the I_T de-inactivation delay function for the TC and RE cells.

Appendix C

Mathematical details of the model for TLE

This appendix gives a mathematical description of the model of Wendling et al. [42]. Also in this appendix, no specific parameter values are given. This is because the author encourages the interested reader who wants to make use of this model to take a look at the paper of Wendling and his colleagues.

C.1 The model

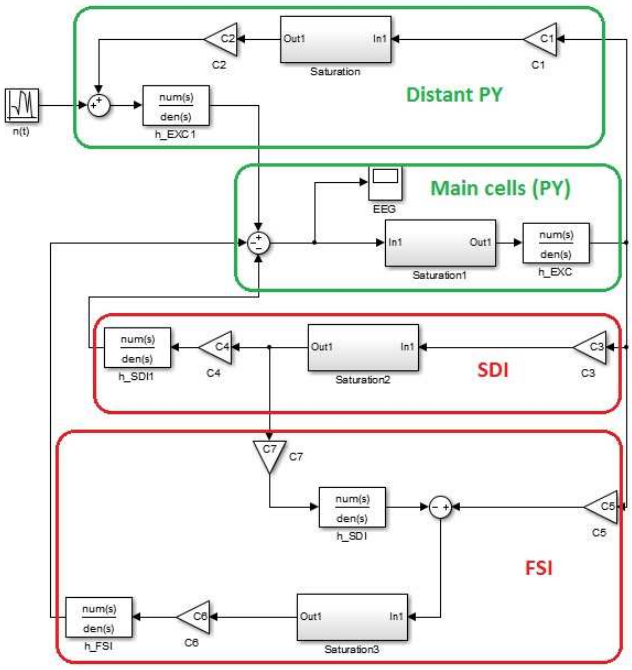

Figure C.1: The model of the hippocampus of Wendling et al. [42]

The model of the hippocampus is show in Figure C.1. It is built from four interconnected neuronal populations. The main cells (excitatory pyramidal neurons) excite the three other populations. The distant excitatory pyramidal neurons excite these main cells. Next to these two excitatory populations, there are also two inhibitory populations included in the model. One of these represents inhibitory interneurons that project to the soma of the main cells. The other one represents inhibitory interneurons that project to the dendrites of the main cells. This means that both inhibitory populations inhibit the main cells. The dendritic projecting interneurons furthermore also inhibit the somatic projecting interneurons. These two types of interneurons are included because there are two types of $GABA_A$ synaptic responses in the pyramidal neurons of the hippocampus. The interneurons projecting to the soma have faster dynamics than the interneurons projecting to the dendrites of the main cells. In all four the populations, the average presynaptic firing rate is converted into an average postsynaptic firing rate in two steps. First, the average presynaptic firing rate is transformed into the mean membrane potential of the population. Next, this mean membrane potential is converted into the average postsynaptic firing rate of the population. This first step is described in Section C.2 and the second step is described in Section C.3.

C.2 From presynaptic firing rate to membrane potential

The conversion from the average presynaptic firing rate of a population into its mean membrane potential is done like explained in Section 1.2. A second order linear transfer function is used. The impulse response function for this transfer function depends on the type of synaptic interaction. There is one type of excitatory interaction and there are two types of inhibitory interactions. All the three types of interaction have an impulse response function of the same form. The differences lie in the values of the parameters, which are different for each impulse response function:

- $h_{EXC}(t) = A \cdot a \cdot t \cdot e^{-at}$ for the excitatory synaptic interactions,
- $h_{SDI}(t) = B \cdot b \cdot t \cdot e^{-bt}$ for the slow dendritic inhibition (SDI) and
- $h_{FSI}(t) = G \cdot g \cdot t \cdot e^{-gt}$ for the fast somatic inhibition (FSI).

The parameters A, B and G are the synaptic gains for each type of synaptic interaction. These three parameters are the ones that define which type of EEG behavior is simulated by the model. The parameters a, b and g are the inverses of the synaptic time constants for each type of interaction. As already shown in Figure 2.5, the FSI has the fastest dynamics and the SDI has the slowest dynamics.

The transfer function for each of these impulse response functions can be found by taking the Laplace transform of the impulse response function. This gives the following second order linear transfer functions:

- $H_{EXC}(t) = (A \cdot a)/((s^2 + 2 \cdot a \cdot s + a^2)$ for the excitatory synaptic interactions,
- $H_{SDI}(t) = (B \cdot b)/((s^2 + 2 \cdot b \cdot s + b^2)$ for the slow dendritic inhibition (SDI) and
- $H_{FSI}(t) = (G \cdot g)/((s^2 + 2 \cdot g \cdot s + g^2)$ for the fast somatic inhibition (FSI).

C.3 From membrane potential to postsynaptic firing rate

Once the mean membrane potential of a population is know, this has to be transformed into the postsynaptic firing rate of this population. This is done by a static nonlinear function, namely an asymmetric sigmoid of the following form:

$$S(v) = \frac{2 \cdot e_0}{1 + exp(p \cdot (v_0 - v))}. \tag{C.1}$$

The input to this function, v, is the mean membrane potential and the output $S(v)$ is the average postsynaptic firing rate. The parameter e_0 determines the maximal firing rate of the population. The parameter v_0 acts as a threshold for firing and the parameter p determines the slope of the sigmoid function.

Appendix D

Paper

Modelleren, voorspellen en controleren van epileptische aanvallen.

Henckaerts Roel

***Samenvatting*—De huidige behandelingen voor epilepsie zijn nog steeds ineffectief voor vele patiënten. De nood aan alternatieve behandelingen is dus zeer groot. Hersenstimulatie technieken krijgen veel aandacht tegenwoordig dankzij de successen van deze technieken in de strijd tegen de ziekte van Parkinson. In deze studie zal een controlesysteem voor absences worden ontwikkeld op basis van een computationeel model. Controle zal gebeuren door stimuli in het model te sturen nadat een aanval wordt gedetecteerd. Het blijkt dat externe stimuli in staat zijn om een begonnen aanval te beëindigen. Dit is enkel zo voor goed afgestelde parameters van het controlesysteem. Deze zijn de drempelwaarde voor detectie en de amplitude en tijdsduur van het controlesignaal. Voor sommige soorten aanvallen is er meer dan detectie mogelijk, namelijk de voorspelling van de aanval. Een computationeel model van de hippocampus wordt gebruikt om typische elektro-encefalografische (EEG) signalen van temporale kwab epilepsie te genereren. Uit deze signalen worden maten voor synchronie tussen verschillende EEG kanalen berekend. De gebruikte maten zijn de maximale kruiscorrelatie, de coherentie, de niet-lineaire interdependentie en de *phase locking value* (PLV). Deze worden gebruikt om de aanval te voorspellen, aangezien er voor de aanvang veel synchronie ontstaat in de hersenen. Support vector machines (SVMs) worden gebruikt om deze periodes in de signalen te vinden. Er wordt een classificatie nauwkeurigheid van 98% bekomen op ongeziene test signalen.**

I. Introductie

EPILEPSIE is een zeer diverse neurologische aandoening, gekarakteriseerd door terugkerende aanvallen. Ongeveer 50 miljoen mensen over de hele wereld lijden aan een soort van epilepsie [1]. Aangezien er zoveel verschillende soorten zijn, is er een onderverdeling in verschillende types van epilepsie nodig. Eerst en vooral wordt er een onderscheid gemaakt tussen focale en gegeneraliseerde aanvallen [2]. De aanvang van een gegeneraliseerde aanval vindt plaats in beide hersenhelften. Een patiënt verliest altijd het bewustzijn tijdens zo een aanval. Bij een partiële aanval is de aanvang gelokaliseerd in een bepaald deel van de hersenen. Het effect van zo'n aanval op de patiënt hangt af van de betrokken hersendelen. Een typisch kenmerk voor elke soort van epilepsie is het uitvoerig en synchroon vuren van neuronen in bepaalde hersendelen.

Tegenwoordig zijn er verschillende behandelingen voor epilepsie [3]. De meest voorkomende zijn medicatie en chirurgie. Ongeveer 30% van de patiënten lijdt aan refractaire epilepsie. Bij deze groep kunnen de aanvallen niet onder controle worden gehouden door anti-epileptica. Voor een patiënt met refractaire epilepsie is er een zorgvuldige analyse nodig, waarin de mogelijkheden van een operatie worden nagegaan. Deze moet namelijk een grote kans hebben op slagen zonder schade aan andere hersenfuncties te berokkenen. Aangezien de plaats van aanvang gelokaliseerd is voor focale aanvallen, is hier de kans groter dat een operatie effectief zal zijn. Een chirurgische ingreep is dus niet altijd mogelijk en levert ook niet in alle gevallen het gewenste resultaat [4]. Het is dus zeer belangrijk dat er alternatieve behandelingen worden ontwikkeld. Een voorbeeld hiervan is het ketogeen dieet, wat vooral bij kinderen wordt voorgeschreven [5]. De successen van hersenstimulatie, als behandeling voor de ziekte van Parkinson, hebben de zoektocht naar hersenstimulatie technieken voor epilepsie gestimuleerd [6]. Ondertussen zijn er verschillende methodes voor hersenstimulatie ontwikkeld (nervus vagus stimulatie) of onder ontwikkeling (diepe hersenstimulatie en responsieve neurostimulator) [7], [8].

Absences zijn gegeneraliseerde aanvallen die abrupt beginnen en eindigen. Zo een aanval kan tot honderd keren op een dag voorkomen. Een patiënt verliest tijdens een aanval altijd het bewustzijn, maar heeft normaal geen last van convulsies. Absences hebben een zeer karakteristiek EEG-patroon, namelijk piek en golf ontladingen [9]. Intracellulaire opnames hebben aangetoond dat de 'piek' en golf' component respectievelijk overeenkomen met neuraal vuren en neurale stilte [10]. Experimentele modellen van de laatste decennia hebben aangetoond dat zowel de thalamus [10], [11] als de cortex [12], [13] een belangrijke rol spelen in het ontstaan van absences. In deze studie wordt het thalamocorticale model van Suffczynski et al. [14] gebruikt om een controlesysteem voor absences te ontwikkelen. Dit model kan zowel interictale (tussen de aanvallen) als ictale (tijdens een aanval) activiteit simuleren.

Temporale kwab epilepsie (TLE) is de meest voorkomende vorm van focale epilepsie. Er zijn twee vormen van TLE, namelijk mesiale (MTLE) en laterale TLE (LTLE). De aanvang van MTLE is gelokaliseerd in het binnenste gedeelte van de temporale kwab, namelijk de hippocampus of amygdala. De aanvang van LTLE is gelokaliseerd in de neocortex (de buitenste laag van de temporale kwab). MTLE heeft een karakteristiek EEG-patroon net voor en tijdens de aanvang van een aanval [15], [16]. Er is typisch de ontwikkeling van pieken met een hoge amplitude en een lage frequentie. Deze activiteit wordt vaak gevolgd door oscillaties met een lage amplitude en hoge frequentie. Een model van de hippocampus van Wendling et al. [17] wordt gebruikt om dat soort typische signalen te genereren. Naast een interictale en ictale fase, bestaat er bij TLE ook een pre-ictale (net voor de aanvang van een aanval) fase. Het model kan deze drie types van activiteit simuleren. Deze signalen zullen in deze studie gebruikt worden om een voorspellingsmethode voor TLE te ontwikkelen. Een overzicht van de geschiedenis van het voorspellen van epileptische aanvallen kan worden gevonden in [18].

II. Materiaal en methoden

A. Modellen van epileptische aanvallen

Beide modellen die worden gebruikt in deze studie zijn macroschaal modellen. Bij deze soort van modellen wordt er typisch gesproken over populaties van neuronen in plaats van individuele neuronen. De output van zo een model zal de gemiddelde potentiaal van een populatie zijn. Deze kan worden geïnterpreteerd als een EEG-meting.

1) Absences: Suffczynski et al. [14] hebben een computationeel model ontwikkeld voor absences bij ratten van de WAG/Rij stam [19]. Het model bestaan uit een corticale en thalamische module, elk opgebouwd uit een exciterende en inhiberende populatie van neuronen. Deze populaties interageren met elkaar via synaptische transmissie. De exciterende interacties worden gemodelleerd door de neurotransmitter glutamaat en de α-amino-3-hydroxy-5-methyl-4-isoxazole-propionzuur (AMPA) receptoren. De inhiberende interacties worden gemodelleerd door de neurotransmitter γ-aminoboterzuur (GABA) en de $GABA_A$ en $GABA_B$ receptoren. Het model kan twee kwalitatief verschillende soorten signalen simuleren (interictaal en ictaal) met spontane overgangen tussen deze twee. De interictale signalen zijn oscillaties met een frequentie van ongeveer 11 Hz en een typisch toenemend en afnemend verloop van de amplitude. De ictale signalen zijn quasi sinusoïdaal met een frequentie van ongeveer 9 Hz. De typische piek en golf ontladingen van absences zijn echter niet zichtbaar. De twee soorten signalen zijn getoond in Figuur 1. Het belangrijkste aan dit model is dat de overgangen van interictaal naar ictaal en omgekeerd op een biologisch plausibele manier worden gemodelleerd.

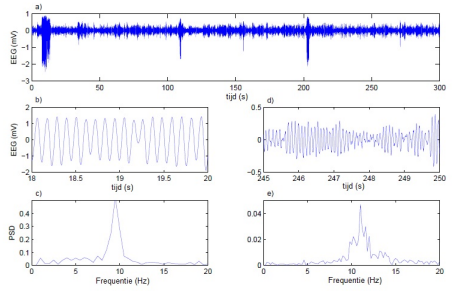

Figuur 1. De signalen gegenereerd door het thalamocorticale model voor absences. a) De tijdsevolutie van de output van het model (EEG). b) Een close-up van het ictale deel. c) Het frequentiespectrum voor het ictale deel. d) Een close-up van het interictale deel. e) Het frequentiespectrum van het interictale deel.

2) TLE: Wendling et al. hebben een model van de hippocampus ontwikkeld dat typische signalen van TLE kan simuleren. Het model bestaat uit twee exciterende en inhiberende populaties, die met elkaar interageren. Exciterende transmissie wordt ook hier gemodelleerd door glutamaat AMPA receptoren. Inhiberende transmissie wordt gemodelleerd door de neurotransmitter GABA en twee verschillende $GABA_A$ receptoren. Er is een groot verschil in dynamiek tussen de twee inhiberende populaties. De ene populatie stelt neuronen voor die synapsen vormen op de dendrieten van andere neuronen, terwijl de andere populatie neuronen voorstelt die synapsen vormen op het cellichaam van andere neuronen. De eerste groep heeft daardoor invloed op de $GABA_{A,traag}$ receptoren en de tweede groep op de $GABA_{A,snel}$ receptoren. Het model kan zes kwalitatief verschillende soorten van activiteit simuleren. Drie hiervan zijn interictale signalen, één is een pre-ictaal signaal en de andere twee zijn ictale signalen. De verschillende types van activiteit zijn weergegeven in Figuur 2. In deze studie werd dit model uitgebreid om een meerkanaal-EEG te kunnen simuleren. Zes verschillende modellen werden als modules aan elkaar gekoppeld. De output van elk model dient als extra input voor de andere modellen. De output van elke module wordt nu geïnterpreteerd als één van de zes kanalen van het EEG.

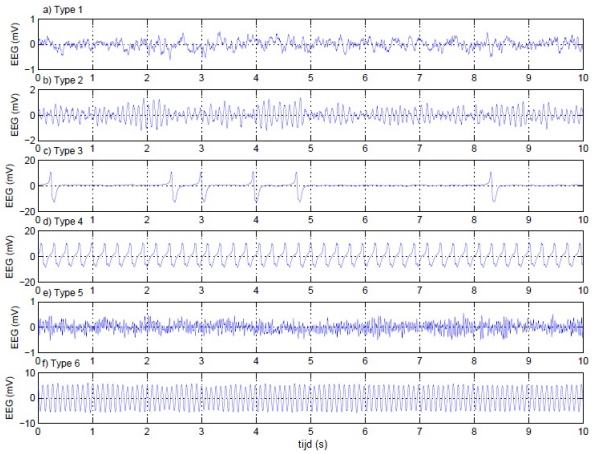

Figuur 2. De signalen gegenereerd door het hippocampale model voor TLE. a) Normale achtergrondactiviteit (interictaal). b) Trage ritmische activiteit (interictaal). c) Sporadische pieken (interictaal). d) Aanhoudende pieken (pre-ictaal). e) Hoogfrequente oscillaties met lage amplitude (ictaal). f) Quasi sinusoïdale oscillaties (ictaal).

B. Controle van epileptische aanvallen

In deze studie wordt een controlesysteem ontwikkeld voor het model van absences. Deze aanvallen hebben een abrupte aanvang en kunnen daardoor niet voorspeld worden. Het is mogelijk om met het model te interageren dankzij de biologisch plausibele manier waarmee de overgangen tussen interictaal en ictaal (en visa versa) zijn gemodelleerd. Het controlesysteem zal bestaan uit een detectiegedeelte en een stimulatiegedeelte. Het gaat hier dus om een gesloten lus systeem.

1) Detectie: Het model simuleert twee soorten van activiteit: interictale signalen met een lage amplitude en ictale signalen met een hoge amplitude. De detectie van een aanval kan daarom gebeuren op basis van de amplitude van het EEG. Wanneer deze groter wordt dan een bepaalde drempelwaarde, dan wordt de detectie van een aanval gesignaleerd. Deze methode van detectie is jammer genoeg niet zomaar uitbreidbaar naar signalen uit het dagelijkse leven. Niet-ictale activiteit met een hoge amplitude zou namelijk een valse detectie veroorzaken. Voor dit model is deze methode echter voldoende. Het grote voordeel van de voorgestelde methode is een snelle detectie.

Deze laat dus toe om na te gaan of absences kunnen worden onderbroken na een snelle detectie. Een goede keuze van de drempelwaarde voor detectie is zeer belangrijk. Deze moet daarom zorgvuldig worden afgesteld.

2) Stimulatie: Na een detectie zal het model gestimuleerd worden, met als doel de begonnen aanval te onderbreken. De voorgestelde controlemethode sluit dus nauw aan bij de hersenstimulatie technieken die tegenwoordig zeer populair zijn. De corticale module zal worden gestimuleerd, aangezien het minder invasief is om de cortex te stimuleren dan de thalamus. Het type signaal is een blokpuls met een bepaalde amplitude en tijdsduur. Dit zijn twee belangrijke parameters en deze moeten nauwkeurig worden afgesteld. De amplitude kan een positieve of negatieve waarde aannemen. Indien de detectie gebeurt tijdens een stijgend EEG signaal, dan zal er een negatieve puls worden gegenereerd. Gebeurt de detectie tijdens een afnemend EEG signaal, dan wordt er een positieve puls gegenereerd. Aangezien er met een macroschaal model wordt gewerkt, zal de eenheid van de amplitude 'pulsen per seconde' (pps) zijn. Een positief aantal pps kan worden geïnterpreteerd als een groep depolariserende pulsen, terwijl een negatief aantal pps een groep hyperpolariserende pulsen voorsteld. De positieve en negatieve pulsen worden elk door een apart detectiesysteem opgewekt. Het volledige controlesysteem samen met het model is weergegeven in Figuur 3.

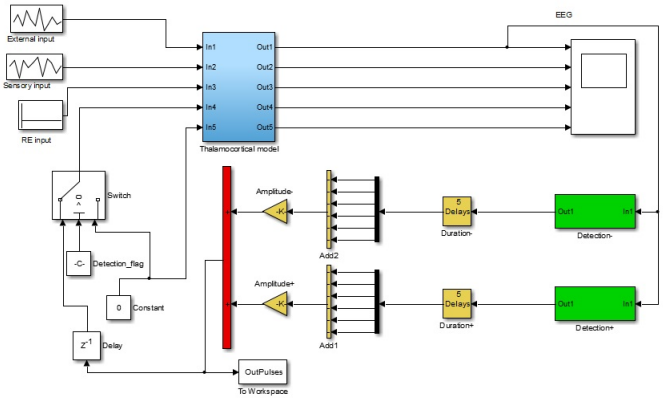

Figuur 3. Het controlesysteem samen met het model voor absences. Het model is inbegrepen in het lichtblauwe subsysteem. De twee detectie- en stimulatiesystemen zijn respectievelijk weergegeven in het groen en geel. Het rode additie-element zorgt voor de combinatie van beide controlesignalen. De schakelaar beslist op basis van een externe parameter of de pulsen in het model worden gestuurd of niet.

C. Voorspellen van epileptische aanvallen

In deze studie zal ook een voorspellingsmethode voor TLE worden ontwikkeld. Deze kunnen, in tegenstelling tot absences, wel worden opgemerkt in het EEG voor de eigenlijke aanvang van de aanval. De nodige data voor de ontwikkeling van de voorspellingsmethode worden gegenereerd met het computationele model voor TLE. Deze data stellen een 6-kanaal EEG voor aan een samplefrequentie van 256 Hz. Het voorspellen van een aanval komt neer op het vinden van de pre-ictale periodes in de EEG en is dus eigenlijk een classificatieprobleem. Er is veel synchrone activiteit in de hersenen net voor en tijdens een epileptische aanval. Daarom zullen er bivariate maten voor synchronie worden gebruikt in het classificatieprobleem [18]. Al deze maten worden via een bewegend venster berekend uit het EEG.

1) Maximale lineaire kruiscorrelatie: De similariteit tussen twee signalen $\{x_i\}$ en $\{y_i\}$ kan worden geëvalueerd door het maximum te nemen van de genormaliseerde kruiscorrelatie:

$$C_{max} = \max_{\tau} \left\{ \left| \frac{C_{xy}(\tau)}{\sqrt{C_{xx}(0) \cdot C_{yy}(0)}} \right| \right\}. \tag{1}$$

De lineaire kruiscorrelatie wordt in deze formule gegeven door:

$$C_{xy}(\tau) = \begin{cases} \frac{1}{N-\tau} \sum_{i=1}^{N-\tau} x_{i+\tau} y_i & \tau \geq 0 \\ C_{yx}(-\tau) & \tau < 0 \end{cases} \tag{2}$$

met N de lengte van beide signalen. C_{max} is gelegen in het interval $[0, 1]$. Lage waarden tonen aan dat de signalen niet op elkaar lijken, terwijl hoge waarden impliceren dat de signalen een gelijkaardig verloop in de tijd vertonen. Het maximum wordt genomen over een klein bereik van τ om wat vertraging tussen de signalen toe te laten.

2) Lineaire coherentie: De hoeveelheid lineaire synchronisatie tussen twee signalen $\{x_i\}$ en $\{y_i\}$ kan worden berekend aan de hand van de coherentie:

$$\Gamma(f) = \left| \frac{G_{xy}(f)}{\sqrt{G_{xx}(f) \cdot G_{yy}(f)}} \right|. \tag{3}$$

$G_{xy}(f)$ is de kruisspectrale densiteit en word gegeven door:

$$G_{xy}(f) = X(f) \cdot Y(f)^* \tag{4}$$

waarin $X(f)$ en $Y(f)$ de Fouriertransformaties voorstellen van respectievelijk $\{x_i\}$ en $\{y_i\}$ en het sterretje de complexe conjugatie aanduidt. De coherentie neemt altijd een waarde aan in het interval $[0, 1]$ en kan worden berekend voor specifieke frequenties. Kleine waarden wijzen op weinig synchronisatie tussen de signalen, terwijl grote waarden veel synchronisatie impliceren.

3) Niet-lineaire interdependentie: De hoeveelheid gegeneraliseerde synchronie tussen twee signalen $\{x_i\}$ en $\{y_i\}$ voor $i = 1, \ldots, N$ kan worden berekend aan de hand van de niet-lineaire interdependentie. Hiervoor moeten beide tijdsignalen eerst worden omgezet in toestandsruimte trajecten $\{\vec{\boldsymbol{x}}_i\}$ en $\{\vec{\boldsymbol{y}}_i\}$. Een punt in de toestandsruimte wordt berekend als: $\vec{\boldsymbol{x}}_i = (x_i, x_{i-\tau}, \ldots, x_{i-(m-1)\cdot\tau})$ en gelijkaardig voor $\vec{\boldsymbol{y}}_i$. De parameter m is de dimensie van de toestandsruimte en de parameter τ is de vertraging in de tijd. De niet-lineaire interdependentie gaat na hoe omgevingen in de ene *attractor* projecteren in de andere *attractor* en is gedefinieerd als:

$$N^{(k)}(x|y) = \frac{1}{N} \sum_{i=1}^{N} \frac{R_i^{(N-1)}(x) - R_i^{(k)}(x|y)}{R_i^{(N-1)}(x)}. \tag{5}$$

Hierin worden $R_i^{(k)}(x)$ en $R_i^{(k)}(x|y)$ gegeven door:

$$R_i^{(k)}(x) = \frac{1}{k}\sum_{j=1}^{k} \left\| \vec{\boldsymbol{x}}_i - \vec{\boldsymbol{x}}_{r_{ij}} \right\|_2^2$$
$$R_i^{(k)}(x|y) = \frac{1}{k}\sum_{j=1}^{k} \left\| \vec{\boldsymbol{x}}_i - \vec{\boldsymbol{x}}_{s_{ij}} \right\|_2^2 \quad (6)$$

met r_{ij} en s_{ij} de tijdsindices van de k dichtstbijzijnde buren van respectievelijk $\vec{\boldsymbol{x}}_i$ en $\vec{\boldsymbol{y}}_i$ voor $j = 1, \ldots, k$. De niet-lineaire interdependentie uit Formule 5 heeft een bovengrens van 1 en kan licht negatieve waarden aannemen. Lage waarden wijzen op onafhankelijkheid van de signalen, terwijl grote waarden veel synchronie impliceren.

4) Phase locking value (PLV): De hoeveelheid synchronisatie tussen de fases van twee signalen $x(t)$ en $y(t)$ wordt gedefinieerd als:

$$PLV = \left| \frac{1}{N} \sum_{j=0}^{N-1} e^{i(\phi_x(j\cdot\Delta t) - \phi_y(j\cdot\Delta t))} \right| \quad (7)$$

met N het aantal samples in beide signalen, Δt de sampleperiode en $\phi_x(t)$ en $\phi_y(t)$ respectievelijk de fase van $x(t)$ en $y(t)$. De PLV ligt in het interval $[0, 1]$. Lage waarden impliceren geen synchronie, terwijl hoge waarden wijzen op veel synchronie. De fase van ieder signaal is nodig om de PLV te berekenen. Hiervoor wordt de Hilberttransformatie gebruikt. De fase van een signaal $s(t)$ is gedefinieerd als:

$$\phi(t) = \arctan \frac{\tilde{s}(t)}{s(t)} \quad (8)$$

waarin $\tilde{s}(t)$ de Hilberttransformatie voorstelt van $s(t)$:

$$\tilde{s}(t) = \frac{1}{\pi} p.v. \int_{-\infty}^{+\infty} \frac{s(\tau)}{t-\tau} d\tau. \quad (9)$$

In deze formule staat $p.v.$ voor Cauchy's principale waarde, een methode om een waarde toe te kennen aan een anders ongedefinieerde integraal.

Deze maten voor synchronie worden in het classificatieprobleem gebruikt om het onderscheid te maken tussen de interictale, pre-ictale en ictale periodes van het EEG. Classificatie zal gebeuren door gebruik te maken van support vector machines (SVMs) [20]. De verschillende maten voor synchronie worden gecombineerd (eventueel ook over verschillende kanaalcombinaties van het EEG) in een vector voor input aan de SVM. Zowel lineaire als Gaussische *kernels* (RBF *kernels*) zullen worden gebruikt. Een SVM is een binaire *classifier*. Meerdere SVMs moeten worden gecombineerd om het onderscheid tussen meer dan twee klassen te maken. Twee verschillende meerklassen-strategiën zullen worden gebruikt: één-versus-één (OVO) en één-versus-allen (OVA). Het zoeken van de optimale parameters van de SVM zal gebeuren via 5-voudige kruisvalidatie. Enkel de regularisatieconstante C is nodig voor de lineaire *kernel*. Deze zal worden gezocht aan de hand van een *line search* Voor de RBF *kernel* is zowel C nodig als een parameter voor de Gaussische functie, namelijk γ. Deze worden gezocht via een *grid search*. De implementatie van de SVMs gebeurde met behulp van LIBSVM [21].

III. Resultaten

A. Controleren van absences

In Figuur 4 zijn de resultaten weergegeven wanneer het controlesysteem niet is verbonden met het model. In Figuur 4a is er duidelijk interictale (lage amplitudes) en ictale activiteit (hoge amplitudes) zichtbaar. De drempelwaarden van het detectiesysteem zijn weergegeven als rode horizontale lijnen. Deze zijn handmatig afgesteld op $2.4 \cdot \sigma$, met σ de standaarddeviatie van een interictaal EEG-segment. Alle activiteit die buiten deze band treedt, wordt beschouwd als een aanval. In Figuur 4b is de activatie van de $GABA_B$ receptor getoond. Activatie van deze receptor is noodzakelijk voor het ontstaan van absences [22]. De waardes in deze figuur zijn negatief omdat het om een inhiberende receptor gaat. In Figuur 4c zijn tenslotte de gegenereerde controlepulsen getoond. De amplitude en tijdsduur van deze zijn ingesteld op 15 pps en 6 ms respectievelijk. Deze pulsen worden echter nog niet in het model gestuurd.

In Figuur 5 zijn de resultaten weergegeven wanneer het controlesysteem wel wordt verbonden met het model. In Figuur 5a is er in dit geval geen merkbare ictale activiteit meer. Er is enkel de interictale activiteit met het typische toenemend en afnemend karakter van de amplitude. In Figuur 5b is er ook nog amper $GABA_B$ activatie te zien. De ordegrootte is gereduceerd van 10^2 tot 10^{-3}. Dit wijst ook op de afwezigheid van absences. In Figuur 5c kan er tenslotte worden gezien dat maar een klein deel van de gegenereerde pulsen uit Figuur 4c nodig zijn om alle aanvallen te onderbreken.

De goede resultaten uit Figuur 5 worden enkel bekomen voor nauwkeurig afgestelde parameters. Indien de drempelwaarde voor detectie te laag wordt gekozen, of de amplitude of tijdsduur van het controlesignaal te hoog, dan zal het EEG vervormen door te veel onnodige stimulaties. Omgekeerd worden aanvallen te laat gedetecteerd of is het controlesignaal zijn invloed niet groot genoeg. Dan is er wel nog ictale activiteit zichtbaar. Een nauwkeurige afstelling is dus noodzakelijk.

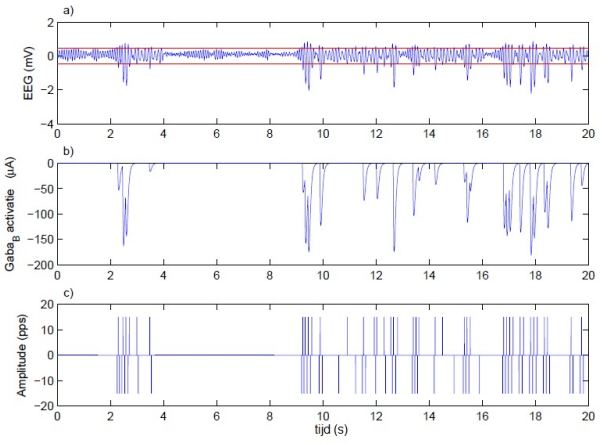

Figuur 4. De resultaten wanneer het controlesysteem niet verbonden is met het model. a) Het EEG bevat zowel interictale als ictale activiteit. De ictale activiteit heeft een hogere amplitude dan de interictale activiteit. De drempelwaarden van het detectiesysteem zijn aangeduid als rode horizontale lijnen. b) De hoeveelheid $GABA_B$ activatie (stroom opgewekt door de $GABA_B$ receptor). c) De pulsen gegenereerd door het controlesysteem.

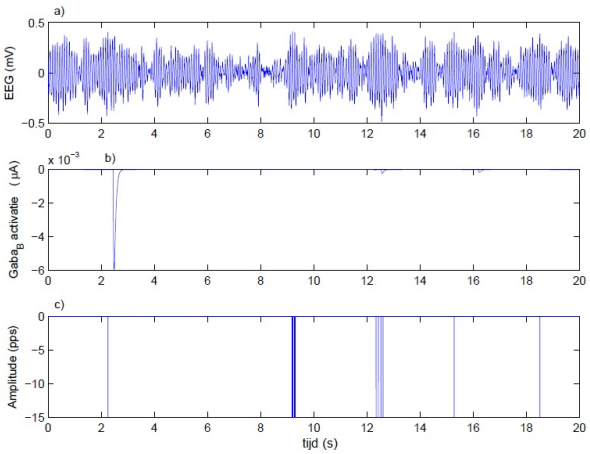

Figuur 5. De resultaten wanneer het controlesysteem wel verbonden is met het model. a) Het EEG bevat nu geen merkbare ictale activiteit meer. Enkel interictale activiteit kan worden gezien. b) Er is zo goed als geen $GABA_B$ activatie meer. c) De controlepulsen die effectief in het model worden gestuurd.

B. Voorspellen van TLE

In Figuur 6 is de tijdsevolutie van de vier maten voor synchronie weergegeven. Deze zijn berekend op een signaal dat 200 seconden bevat van elk type van activiteit dat het model kan simuleren. Dit komt neer op eerst 600 seconden interictale activiteit, dan 200 seconden pre-ictale en daarna 400 seconden ictale activiteit. De maten werden berekend uit niet-overlappende tijdsvensters van 5 seconden. Voor de niet-lineaire interdependentie werden de volgende parameters gekozen: $m = 10$, $\tau = 2$ en $k = 10$. Er kan duidelijk worden gezien dat er veel synchronie is tijdens de pre-ictale periode en tijdens één van de twee types van ictale activiteit.

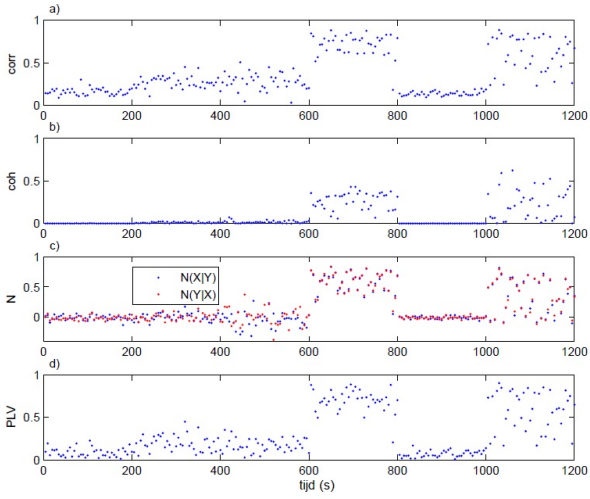

Figuur 6. Het verloop van de vier maten voor synchronie, berekend voor een EEG die 200 seconden van elk type van activiteit simuleert. Hoge waarden duiden op synchronie en kunnen gevonden worden voor twee intervallen: $600 - 800$ s (pre-ictaal) en $1000 - 1200$ s (ictaal). a) De maximale kruiscorrelatie. b) De coherentie. c) De niet-lineaire interdependentie (blauw voor N(X|Y), rood voor N(Y|X)). d) De PLV.

De pre-ictale en ictale synchrone activiteit is van een verschillende frequentie. Om het onderscheid tussen deze te kunnen maken zal de PLV worden berekend op een ongefilterd EEG, maar ook op zeven gefilterde EEG-signalen. De frequentiebanden die worden gekozen zijn de volgende: delta (0.1-4 Hz), theta (4-7 Hz), alpha (7-13 Hz), lage beta (13-15 Hz), hoge beta (14-30 Hz), lage gamma (30-45 Hz) en hoge gamma (45-100 Hz). Deze frequentiebanden worden vaak gebruikt voor de analyse van een EEG. Principale componenten analyse (PCA) heeft aangetoond dat het gebruiken van de gefilterde versies van de PLV ertoe leidt dat de pre-ictale en ictale synchrone activiteit kunnen worden gescheiden.

De niet-lineaire interdependentie wordt verder niet gebruikt omdat het lang duurt om deze te berekenen. Voor een signaal van 5 seconden duurt het langer dan een seconde om deze te berekenen (Intel Core i5 processor, kloksnelheid 2.40 GHz, 4 GB RAM). Aangezien de voorspelling in real-time moet gebeuren op een klein apparaat is dit te traag. De andere maten kunnen in enkele tientallen milliseconden worden berekend. Er zijn dus tien maten: de kruiscorrelatie, de coherentie, de (niet-gefilterde) PLV en zeven gefilterde versies van de PLV.

In totaal zijn er 15 kanaalcombinaties, aangezien er zes EEG-kanalen zijn. Niet elk van deze combinaties is echter een nuttige combinate. Afhankelijk van de locaties van de meetelectrodes kan er wel of geen synchronie tussen kanalen optreden. De beste kanaalcombinaties worden gezocht en de maten van deze combinaties worden in een vector samengenomen. De beste kanaalcombinaties zijn: Ka1+Ka2, Ka2+Ka3, Ka3+Ka6 en Ka5+Ka6. De uiteindelijke vector is dus 40-dimensionaal (4 combinaties van 10 maten).

De resultaten voor verschillende soorten SVMs zijn weergegeven in Tabel I. Dit is de gemiddelde nauwkeurigheid over 10 ongeziene datasets. De RBF SVMs zijn iets nauwkeuriger dan de lineaire SVMs. De nauwkeurigheid is echter niet het enige aspect dat belangrijk is. Ook de snelheid van een SVM is belangrijk. De trainings- en voorspellingstijden zijn weergegeven in Tabel II. De data voor training was 2 uur lang, die voor het testen een half uur. De lineaire SVMs zijn sneller dan de RBF SVMs. De OVO strategie is sneller dan de OVA strategie. Training zal normaal off-line gebeuren, dus vooral de voorspellingstijd is belangrijk. Om een optimale mix tussen nauwkeurigheid en snelheid te bekomen, wordt er gekozen voor de RBF OVO SVM. Resultaten zijn weergegeven in Figuur 7 voor 10 verschillende test signalen.

	Nauwkeurigheid
Lin OVO	96.06%
RBF OVO	98.06%
Lin OVA	96.86%
RBF OVA	98.31%

Tabel I. NAUWKEURIGHEID VOOR VERSCHILLENDE SOORTEN SVMS.

	Trainingstijd (in s)	Voorspellingstijd (in ms)
Lin OVO	2.6	4.2
RBF OVO	154.6	11.6
Lin OVA	15.2	6.9
RBF OVA	334.8	21.9

Tabel II. DE TRAININGSTIJD (IN S) EN VOORSPELLINGSTIJD (IN MS) VOOR VERSCHILLENDE SOORTEN SVMS.

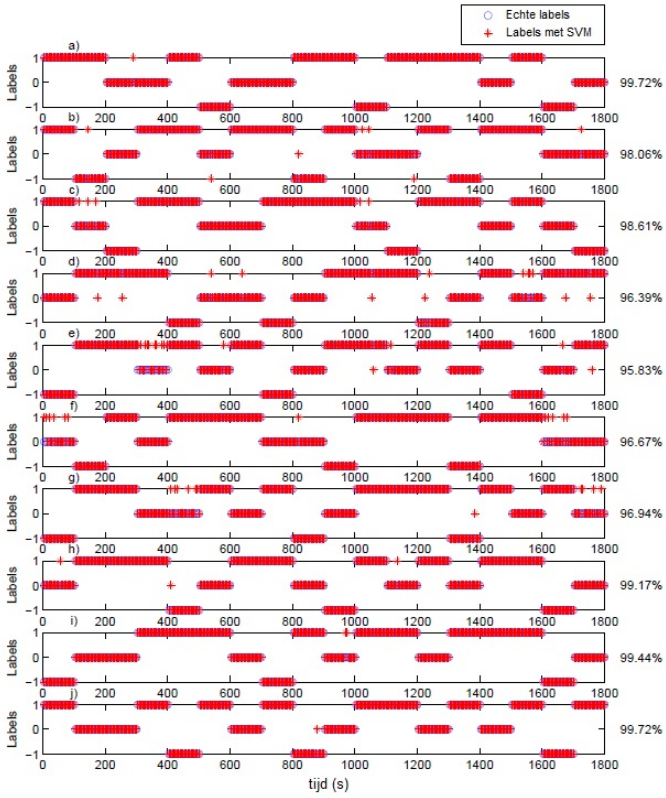

Figuur 7. De resultaten voor 10 ongeziene test datasets. Blauwe cirkels zijn de echte labels (1 interictaal, -1 pre-ictaal en 0 ictaal) en de rode sterren de voorspelde labels. De nauwkeurigheid op elke dataset staat rechts van de figuren.

IV. Discussie

Het controlesysteem voor absences is in staat om alle aanvallen te onderbreken. Om dit uit te breiden naar signalen uit het echte leven is er wel een meer algemeen detectiesysteem nodig. Enkel op basis van amplitude detecteren zal vaak een vals alarm teweeg brengen. Met behulp van het model is het wel duidelijk geworden dat een aanval gecontroleerd kan worden na een snelle detectie.

De voorspellingsmethode slaagt er in om de pre-ictale periodes van de EEG te vinden. De laatste nodige stap is het voorspellen van de aanvangstijd van de aanval. Een pre-ictale periode kan namelijk enkele minuten duren, maar ook een uur. Eens een pre-ictale periode gevonden is, zal er dus een andere methode moeten worden gebruikt om de aanvangstijd te schatten. Dit is een mogelijkheid voor verder onderzoek in dit gebied.

Referenties

[1] Wendling F. Computational models of epileptic activity: a bridge between observation and pathophysiological interpretation. *Expert Review of Neurotherapeutics* 2008; **8**(6):889-896.

[2] Berg AT, Berkovic SF, Brodie MJ, Buchhalter J, Cross JH, Van Emde Boas W, Engel J, French J, Glauser TA, Mathern GW, Moshé SL, Nordli D, Plouin P, Scheffer IE. Revised terminology and concepts for organization of seizures and epilepsies: Report of the ILAE Commission on Classification and Terminology, 2005-2009. *Epilepsia* 2010; **51**(4):676-685.

[3] Shorvon S. *Hanbook of epilepsy treatment.* Wiley-Blackwell; 2010.

[4] Téllez-Zenteno JF, Dhar R, Wiebe S. Long-term seizure outcomes following epilepsy surgery: a systematic review and meta-analysis. *Brain* 2005; **128**(5):1188-1198.

[5] Stafstrom CE, Bough KJ. The ketogenic diet for the treatment of epilepsy: a challenge for nutritional neuroscientists. *Nutritional Neuroscience* 2003; **6**(2):67-79.

[6] Weaver FM, Follet K, Stern M, Hur K, Harris C, Marks WJ, Rothlind J, Sagher O, Reda D, Moy CS, Pahwa R, Burchiel K, Hogarth P, Lai EC, Dude JE, Holloway K, Samii A, Horn S, Bronstein J, Stoner G, Heemskerk J, Huang GD. Bilateral deep brain stimulation vs best medical therapy for patients with advanced Parkinson disease. *The Journal of the American Medical Association* 2009; **301**(1):63-73.

[7] Theodore WH, Fisher RS. Brain stimulation for epilepsy. *The Lancet Neurology* 2004; **3**(2):111-118.

[8] Morell M. Brain stimulation for epilepsy: can scheduled or responsive neurostimulation stop seizures?. *Current Opinion in Neurology* 2006; **19**(2):164-168.

[9] Destexhe A. Spike-and-wave oscillations. *Scholarpedia* 2007; **2**(2):1402.

[10] Pollen DA. Intracellular studies of cortical neurons during thalamic induced wave and spike. *Electroencephalography and Clinical Neurophysiology* 1964; **17**(4):398-404.

[11] Pellegrini A, Musgrave J, Gloor P. Role of afferent input of subcortical origin in the genesis of bilaterally synchronous epileptic discharges of feline generalized penicillin epilepsy. *Experimental Neurology* 1979; **64**(1):155-173.

[12] Steriade M, Contreras D. Spike-wave complexes and fast components of cortically generated seizures. I. Role of neocortex and thalamus. *Journal of Neurophysiology* 1998; **80**(3):1439-1455.

[13] Lytton WW, Contreras D, Destexhe A, Steriade M. Dynamic interactions determine partial thalamic quiescence in a computer network model of spike-and-wave seizures. *Journal of Neurophysiology* 1997; **77**(4):1679-1696.

[14] Suffczynski P, Kalitzin S, Lopes da Silva F. Dynamics of non-convulsive epileptic phenomena modeled by a bistable neuronal network. *Neuroscience* 2004; **126**(2):467-484.

[15] Engel J (Jr), Babb TL, Crandall PH. Surgical treatments of epilepsy: opportunities for research into basic mechanisms of human brain function. *Acta Neurochirurgica Supplementum (Wien)* 1989; **46**:3-8.

[16] Spencer SS, Guimaraes P, Katz A, Kim J, Spencer D. Morphological patterns of seizures recorded intracranially. *Epilepsia* 1992; **33**(3):537-545.

[17] Wendling F, Bellanger JJ, Bartolomei F, Chauvel P. Epileptic fast activity can be explained by a model of impaired GABAergic dendritic inhibition. *European Journal of Neuroscience* 2002; **15**(9):1499-1508.

[18] Mormann F, Andrzejak RG, Elger CE, Lehnertz K. Seizure prediction: the long and winding road. *Brain* 2007; **130**(2):314-333.

[19] Coenen AML, Van Luijtelaar ELJM. Genetic animal models for absence epilepsy: a review of the WAG/Rij strain of rats. *Behavior Genetics* 2003; **33**(6):635-655.

[20] Vapnik V, Cortes C. Support-vector networks. *Machine Learning* 1995; **20**(3):273-297.

[21] Chang CC, Lin CJ. LIBSVM: a library for support vector machines. *ACM Transactions on Intelligent Systems and Technology* 2011; **2**(3):1-27. Software available at http://www.csie.ntu.edu.tw/ cjlin/libsvm

[22] Snead OC. Evidence for $GABA_B$-mediated mechanisms in experimental generalized absence seizures. *European Journal of Pharmacology* 1992; **213**(3):343-349.

Appendix E

Poster

Modeling, predicting and controlling epileptic seizures

KATHOLIEKE UNIVERSITEIT LEUVEN

FACULTEIT INGENIEURSWETENSCHAPPEN

Master Wiskundige ingenieurstechnieken

Masterproef *Roel Henckaerts*

Promotor *Prof. Bart De Moor*

Academiejaar 2013-2014

Epilepsy

- Neurological disorder
- Characterized by recurrent seizures
- 50 million people affected
- Lots of different types of epilepsy
- Excessive firing and synchrony of neurons
- Classification: focal/generalized seizures (ILAE)
- Treatments: medication, surgery and brain stimulation
- Why? Improve quality of life for patients

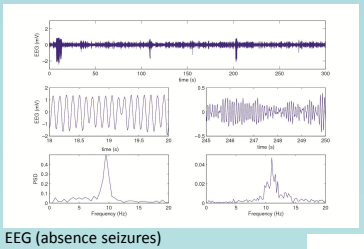

EEG (absence seizures)

Responsive Neurostimulation System (In development by NeuroPace, Inc.)

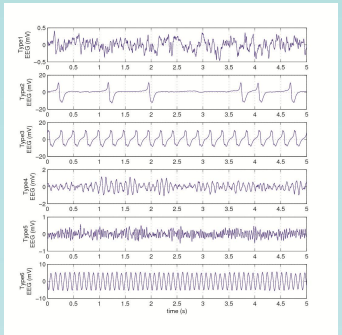

EEG types (temporal lobe epilepsy)

Modeling

- Build a mathematical model of an epileptic brain
- Simplification! → micro/macro-scale
- Presynaptic firing rate

  ⬇

  Postsynaptic potential

  ⬇

  Postsynaptic firing rate
- Generalized seizures
  - Eg., absence seizure (thalamocortical)
  - Model of Suffczynski et. al.

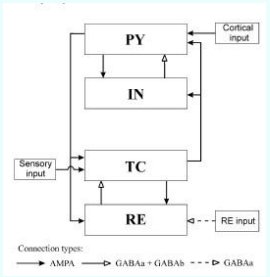

- Focal seizures
  - Eg., temporal lobe epilepsy (hippocampus)
  - Model of Wendling et. al.

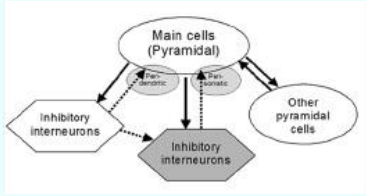

Predicting

- Focal Seizures
  - Interictal-preictal-ictal
- Predict?
  - → find preictal periods
- Extract bivariate features from multi-channel EEG
- Search synchrony
  - Cross-corr, coherence, phase sync,…
- Classification with SVM
  - Linear/RBF-kernel, OVO/OVA

Controlling

- Generalized seizures
  - Interictal-ictal
- No preictal periods
  - → prediction impossible
- Early detection
- Control by brain stimulation after detection

Implantable device

- Ultimate goal for research community
- Extra care for computational complexity

Bibliography

[1] Wendling F. Computational models of epileptic activity: a bridge between observation and pathophysiological interpretation. *Expert Review of Neurotherapeutics* 2008; **8**(6):889-896.

[2] Berg AT, Berkovic SF, Brodie MJ, Buchhalter J, Cross JH, Van Emde Boas W, Engel J, French J, Glauser TA, Mathern GW, Moshé SL, Nordli D, Plouin P, Scheffer IE. Revised terminology and concepts for organization of seizures and epilepsies: Report of the ILAE Commission on Classification and Terminology, 2005-2009. *Epilepsia* 2010; **51**(4):676-685.

[3] Bancaud J, Henriksen O, Rubio-Donnadieu F, Seino M, Dreifuss FE, Penry JK. Proposal for revised clinical and electroencephalographic classification of epileptic seizures. *Epilepsia* 1981; **22**(4):489-501.

[4] Shorvon S. *Hanbook of epilepsy treatment.* Wiley-Blackwell; 2010.

[5] Stefanescu RA, et al. Computational models of epilepsy. *Seizure: European Journal of Epilepsy*(2012), http://dx.doi.org/10.1016/j.seizure.2012.08.012

[6] Bazhenov M, Timofeev I, Fröhlich F, Sejnowksi TJ. Cellular and network mechanisms of electrographic seizures. *Drug Discovery Today Disease Models* 2008; **5**(1):45-57.

[7] O'Sullivan-Greene E, Mareels I, Freestone D, Kulhmann L, Burkitt A. A paradigm for epileptic seizure prediction using a coupled oscillator model of the brain. *Conference Proceedings - IEEE Engineering in Medicine and Biology Society 2009* 2009:6428-6431.

[8] Iasemidis LD. Epileptic seizure prediction and control. *IEEE Transactions on Biomedical Engineering* 2003; **50**(5):549-558.

[9] Lopes da Silva F, Blanes W, Kalitzin SN, Parra J, Suffczynski P, Velis DN. Epilepsies as dynamical diseases of brain systems: basic models of the transition between normal and epileptic activity. *Epilepsia* 2003; **44**(Supplementum s12):72-83.

[10] Destexhe A. Spike-and-wave oscillations. *Scholarpedia* 2007; **2**(2):1402.

[11] Pollen DA. Intracellular studies of cortical neurons during thalamic induced wave and spike. *Electroencephalography and Clinical Neurophysiology* 1964; **17**(4):398-404.

[12] Pellegrini A, Musgrave J, Gloor P. Role of afferent input of subcortical origin in the genesis of bilaterally synchronous epileptic discharges of feline generalized penicillin epilepsy. *Experimental Neurology* 1979; **64**(1):155-173.

[13] Avoli M, Gloor P. Role of the thalamus in generalized penicillin epilepsy: Observations on decorticated cats. *Experimental Neurology* 1982; **77**(2):386-402.

[14] Vergnes M, Marescaux C. Cortical and thalamic lesions in rats with genetic absence epilepsy. *Journal of Neural Transmission* 1992; **35**(Supplementum):71-83.

[15] Kostopoulos G, Gloor P, Pellegrini A, Gotman J. A study of the transition from spindles to spike and wave discharge in feline generalized penicillin epilepsy: microphysiological features. *Experimental Neurology* 1981; **73**(1):55-77.

[16] McLachlan RS, Avoli M, Gloor P. Transition from spindles to generalized spike and wave discharges in the cat: simultaneous single-cell recordings in the cortex and thalamus. *Experimental Neurology* 1984; **85**(2):413-425.

[17] Steriade M, McCormick DA, Sejnowski TJ. Thalamocortical oscillations in the sleeping and aroused brain. *Science* 1993; **262**(5143):679-685.

[18] Steriade M. *Neuronal Substrates of Sleep and Epilepsy* Cambridge University Press; 1983.

[19] Steriade M. Interneuronal epileptic discharges related to spike-and-wave cortical seizures in behaving monkeys. *Electroencephalography and Clinical Neurophysiology* 1974; **37**(3):247-263.

[20] Avoli M, Gloor P, Kostopoulos G, Gotman J. An analysis of penicillin-induced generalized spike and wave discharges using simultaneous recordings of cortical and thalamic single neurons. *Journal of Neurophysiology* 1983; **50**(4):819-837.

[21] Kim D, Song U, Keum S, Lee T, Jeong MJ, Kim SS, McEnery MW and Shin HS. Lack of the burst firing of thalamocortical relay neurons and resistance to absence seizures in mice lacking the alpha-1G T-type Ca2+ channels. *Neuron* 2001; **31**(1):35-45.

[22] Gloor P, Quesney LF, Zumstein H. Pathophysiology of generalized penicillin epilepsy in the cat: the role of cortical and subcortical structures. II. Topical application of penicillin to the cerebral cortex and subcortical structures. *Electroencephalography and Clinical Neurophysiology* 1977; **43**:79-94.

[23] Steriade M, Contreras D. Spike-wave complexes and fast components of cortically generated seizures. I. Role of neocortex and thalamus. *Journal of Neurophysiology* 1998; **80**(3):1439-1455.

[24] Lytton WW, Contreras D, Destexhe A, Steriade M. Dynamic interactions determine partial thalamic quiescence in a computer network model of spike-and-wave seizures. *Journal of Neurophysiology* 1997; **77**(4):1679-1696.

[25] Pinault D, Leresche N, Charpier S, Deniau JM, Marescaux C, Vergnes M, Crunelli V. Intracellular recordings in thalamic neurons during spontaneous spike and wave discharges in rats with absence epilepsy. *The Journal of Physiology* 1998; **509**(2):449-456.

[26] Avoli M, Rogawski MA, Avanzini G. Generalized epileptic disorders: an update. *Epilepsia* 2001; **42**(4):445-457.

[27] McCormick DA, Contreras D. On the cellular and network bases of epileptic seizures. *Annual Review of Physiology* 2001; **63**:815-846.

[28] Wang XJ, Golomb D, Rinzel J. Emergent spindle oscillations and intermittent burst firing in a thalamic model: specific neuronal mechanisms. *Proceedings of the National Academy of Sciences of the United States of America* 1995; **92**(12):5577-5581.

[29] Destexhe A. Spike-and-wave oscillations based on the properties of $GABA_B$ receptors. *The Journal of Neuroscience* 1998; **18**(21):9099-9111.

[30] Destexhe A. Can $GABA_A$ conductances explain the fast oscillation frequency of absence seizures in rodents? *European Journal of Neuroscience* 1999; **11**(6):2175-2181.

[31] Wiebe S, Blume WT, Girvin JP, Eliasziw M. A randomized, controlled trial of surgery for temporal-lobe epilepsy. *The New England Journal of Medicine* 2001; **345**(5):311-318.

[32] de Tisi J, Bell GS, Peacock JL, McEvoy AW, Harkness WFJ, Sander JW, Duncan JS. The long-term outcome of adult epilepsy surgery, patterns of seizure remission, and relapse: a cohort study. *The Lancet* 2011; **378**(9800):1388-1395.

[33] Engel J (Jr), Babb TL, Crandall PH. Surgical treatments of epilepsy: opportunities for research into basic mechanisms of human brain function. *Acta Neurochirurgica Supplementum (Wien)* 1989; **46**:3-8.

[34] Spencer SS, Guimaraes P, Katz A, Kim J, Spencer D. Morphological patterns of seizures recorded intracranially. *Epilepsia* 1992; **33**(3):537-545.

[35] Velasco AL, Wilson CL, Babb TL, Engel J (Jr). Functional and anatomic correlates of two frequently observed temporal lobe seizure-onset patterns. *Neural plasticity* 2000; **7**(1-2):49-63.

[36] Bartolomei F, Wandling F, Régis J, Gavaret M, Guye M, Chauvel P. Pre-ictal synchronicity in limbic networks of mesial temporal lobe epilepsy. *Epilepsy Research* 2004; **61**(1-3):89-104.

[37] Jefferys JGR, Traub RD, Whittington MA. Neuronal networks for induced '40 Hz' rhythms. *Trends in Neurosciences* 1996; **19**(5):202-208.

[38] Whittington MA, Traub RD, Kopell N, Ermentrout B, Buhl EH. Inhibition-based rhythms: experimental and mathematical observations on network dynamics. *International Journal of Psychophysiology* 2000; **38**(3):315-336.

[39] White JA, Banks MI, Pearce RA, Kopell NJ. Networks of interneurons with fast and slow γ-aminobutyric acid type A ($GABA_A$) kinetics provide substrate for mixed gamma-theta rhythm. *Proceedings of the National Academy of Sciences of the United States of America* 2000; **97**(14):8128-8133.

[40] Wendling F, Bellanger JJ, Bartolomei F, Chauvel P. Relevance of nonlinear lumped-parameter models in the analysis of depth-EEG epileptic signals. *Biological Cybernetics* 2000; **83**(4):367-378.

[41] Thomson AM, Radpour S. Excitatory connections between CA1 pyramidal cells revealed by spike triggered averaging in slices of rat hippocampus are partially NMDA receptor mediated. *The European Journal of Neuroscience* 1991; **3**(6):587-601.

[42] Wendling F, Bellanger JJ, Bartolomei F, Chauvel P. Epileptic fast activity can be explained by a model of impaired GABAergic dendritic inhibition. *European Journal of Neuroscience* 2002; **15**(9):1499-1508.

[43] Hodgkin A, Huxley A. A quantitative description of membrane current and its application to conduction and excitation in nerve. *Journal of Physiology* 1952; **117**(4):500-544.

[44] Morris C, Lecar H. Voltage oscillations in the barnacle giant muscle fiber. *Biophysical Journal* 1981; **35**(1):193-213.

[45] Hindmarsh JL, Rose RM. A model of neuronal bursting using three coupled first order differential equations. *Proceedings B* 1984; **221**(1222):87-102 .

[46] FitzHugh R. Impulses and physiological states in theoretical models of nerve membrane. *Biophysical Journal* 1961; **1**(6):445-466.

[47] Nagumo J, Arimoto S, Yoshizawa S. An active pulse transmission line simulating nerve axon. *Proceedings of the IRE* 1962; **50**(10):2061-2070.

[48] Wilson HR, Cowan JD. Excitatory and inhibitory interactions in localized populations of model neurons. *Biophysical Journal* 1972; **12**(1):1-24.

[49] Wilson HR, Cowan JD. A mathematical theory of the functional dynamics of cortical and thalamic nervous tissue. *Kybernetic* 1973; **13**(2):55-80.

[50] Deco G, Jirsa VK, Robinson PA, Breakspear M, Friston K. The Dynamic Brain: From Spiking Neurons to Neural Masses and Cortical Fields. *PLos Computational Biology* 2008; **4**(8): e1000092.

[51] Freeman W. *Mass action in the nervous system* Academic press; 1975.

[52] Jansen BH, Rit VG. Electroencephalogram and visual evoked potential generation in a mathematical model of coupled cortical columns. *Biological Cybernetics* 1995; **73**(4):357-366.

[53] David O, Harrison L, Friston KJ. Modeling event-related responses in the brain. *Neuroimage* 2005; **25**(3):756-770.

[54] David O, Friston KJ. A neural mass model for MEG/EEG: coupling ad neuronal dynamics. *Neuroimage* 2003; **20**(3):1743-1755.

[55] Téllez-Zenteno JF, Dhar R, Wiebe S. Long-term seizure outcomes following epilepsy surgery: a systematic review and meta-analysis. *Brain* 2005; **128**(5):1188-1198.

[56] Stafstrom CE, Bough KJ. The ketogenic diet for the treatment of epilepsy: a challenge for nutritional neuroscientists. *Nutritional Neuroscience* 2003; **6**(2):67-79.

[57] Freeman JM, Vining EPG, Pillas DJ, Pyzik PL, Casey JC, Kelly MT. The efficacy of the ketogenic diet: a prospective evaluation of intervention in 150 children. *Pediatrics* 1998; **102**(6):1358-1363.

[58] Weaver FM, Follet K, Stern M, Hur K, Harris C, Marks WJ, Rothlind J, Sagher O, Reda D, Moy CS, Pahwa R, Burchiel K, Hogarth P, Lai EC, Dude JE, Holloway K, Samii A, Horn S, Bronstein J, Stoner G, Heemskerk J, Huang GD. Bilateral deep brain stimulation vs best medical therapy for patients with advanced Parkinson disease. *The Journal of the American Medical Association* 2009; **301**(1):63-73.

[59] Theodore WH, Fisher RS. Brain stimulation for epilepsy. *The Lancet Neurology* 2004; **3**(2):111-118.

[60] Morell M. Brain stimulation for epilepsy: can scheduled or responsive neurostimulation stop seizures?. *Current Opinion in Neurology* 2006; **19**(2):164-168.

[61] Xiao Z, Tian X. A simulation study of controlling epileptic seizures on simulink. *Bioinformatics and Biomedical Engineering, 2008. ICBBE 2008. The 2nd International Conference on* 2008; 857-860.

[62] Good LB, Sabesan S, Marsh ST, Tsakalis K, Treiman D, Iasemidis L. Control of synchronization of brain dynamics leads to control of epileptic seizures in rodents. *International Journal of Neural Systems* 2009; **19**(3):173-196.

[63] Stigen T, Danzl P, Moehlis J, Netoff T. Controlling spike timing and synchrony in oscillatory neurons. *Journal of Neurophysiology* 2011; **105**(5):2074-2082.

[64] Deisseroth K. Optogenetics. *Nature Methods* 2011; **8**(1):26-29.

[65] Kokaia M, Andersson M, Ledri M. An optogenetic approach in epilepsy. *Neuropharmacology* 2013; **69**:89-95.

[66] Tønnesen J, Sørensen AT, Deisseroth K, Lundberg C, Kokaia M. Optogenetic control of epileptiform activity. *Proceedings of the National Academy of Sciences of the United States of America* 2009; **106**(29):12162-12167.

[67] Krook-Magnuson E, Armstrong C, Oijala M, Soltesz I. On-demand optogenetic control of spontaneous seizures in temporal lobe epilepsy. *Nature Communications* 2012; **4**:1376.

[68] Mormann F, Andrzejak RG, Elger CE, Lehnertz K. Seizure prediction: the long and winding road. *Brain* 2007; **130**(2):314-333.

[69] Viglione SS, Walsh GO. Proceedings: Epileptic seizure prediction. *Electroencephalography and Clinical Neurophysiology* 1975; **39**(4):435-436.

[70] Salant Y, Gath I, Henriksen O. Prediction of epileptic seizures from two-channel EEG. *Medical and Biological Engineering and Computing* 1998; **36**(5):549-556.

[71] Chisci L, Mavino A, Perferi G, Sciandrone M. Real-time epileptic seizure prediction using AR models and support vector machines. *Biomedical Engineering, IEEE. Transactions on* 2010; **57**(5):1124-1132.

[72] Litt B, Echauz J. Prediction of epileptic seizures. *The Lancet Neurology* 2002; **1**(1):22-30.

[73] Iasemidis LD, Sackellares JC, Zaveri HP, Williams WJ. Phase space topography and the Lyapunov exponent of electrocorticograms in partial seizures. *Brain Topography* 1990; **2**(3):187-201.

[74] Martinerie J, Adam C, Le Van Quyen M, Baulac M, Clemenceau S, Renault B, Varela FJ. Epileptic seizures can be anticipated by non-linear analysis. *Nature Medicine* 1998; **4**(10):1173-1176.

[75] Winterhalder M, Maiwald T, Voss HU, Aschenbrenner-Scheibe R, Timmer J, Schulze-Bonhage A. The seizure prediction characteristic: a general framework to assess and compare seizure prediction methods. *Epilepsy & Behavior* 2003; **4**(3):318-325.

[76] Suffczynski P, Kalitzin S, Lopes da Silva F. Dynamics of non-convulsive epileptic phenomena modeled by a bistable neuronal network. *Neuroscience* 2004; **126**(2):467-484.

[77] Coenen AML, Van Luijtelaar ELJM. Genetic animal models for absence epilepsy: a review of the WAG/Rij strain of rats. *Behavior Genetics* 2003; **33**(6):635-655.

[78] Marescaux C, Vergnes M, Depaulis A. Genetic absence epilepsy in rats from Strasbourg: a review. *Journal of Neural Transmission* 1992; **35**(Supplementum):37-69.

[79] Lopes da Silva FH, Hoeks A, Smits H, Zetterberg LH. Model of brain rhythmic activity. *Kybernetik* 1974; **15**(1):27-37.

[80] Bouwman BM, Suffczynski P, Lopes da Silva FH, Maris E, van Rijn CM. GABAergic mechanisms in absence epilepsy: a computational model of absence epilepsy simulating spike and wave discharges after vigabatrin in WAG/Rij rats. *European Journal of Neuroscience* 2007; **25**(9):2783-2790.

[81] Coenen AML, Drinkenburg WHIM, Peeters BWMM, Vossen JMH, van Luijtelaar ELJM. Absence epilepsy and the level of vigilance in rats of the WAG/Rij strain. *Neuroscience and Biobehavioral Reviews* 1991; **15**(2):259-263.

[82] Drinkenburg WHIM, Coenen AML, Vossen JMH, van Luijtelaar ELJM. Spike-wave discharges and sleep-wake states in rats with absence epilepsy. *Epilepsy Research* 1991; **9**(3):218-224.

[83] Vergnes M, Boehrer A, Simler S, Bernasconi R, Marescaux C. Opposite effects of $GABA_B$ receptor antagonists on absences and convulsive seizures. *European Journal of Pharmacology* 1997; **332**(3):245-255.

[84] Snead OC. Evidence for $GABA_B$-mediated mechanisms in experimental generalized absence seizures. *European Journal of Pharmacology* 1992; **213**(3):343-349.

[85] Futatsugi Y, Riviello JJ (Jr). Mechanisms of generalized absence epilepsy. *Brain & Development* 1998; **20**(2):75-79.

[86] Avanzini G, de Curtis M, Franceschetti S, Sancini G, Spreafico R. Cortical versus thalamic mechanisms underlying spike and wave discharges in GAERS. *Epilepsy Research* 1996; **26**(1):37-44.

[87] Danober L, Deransart C, Depaulis A, Vergnes M, Marescaux C. Pathophysiological mechanisms of genetic absence epilepsy in the rat. *Progress in Neurobiology* 1998; **55**(1):27-57.

[88] Sitnikova E. Thalamocortical mechanisms of sleep spindles and spike-wave discharges in rat model of absence epilepsy. *Epilepsy Research* 2009; **89**(1):17-26.

[89] Luhmann HJ, Mittmann T, van Luijtelaar G, Heinemann U. Impairment of intracortical GABAergic inhibition in a rat model of absence epilepsy. *Epilepsy Research* 1995; **22**(1):43-51.

[90] Liu Z, Vergnes M, Depaulis A, Marescaux C. Evidence for a critical role of GABAergic transmission within the thalamus in the genesis and control of absence seizures in the rat. *Brain Research* 1991; **545**(1-2):1-7.

[91] Tsakiridou E, Bertollini L, de Curtis M, Avanzini G, Pape HC. Selective increase in T-type calcium conductance of reticular thalamic neurons in a rat model of absence epilepsy. *The Journal of Neuroscience* 1995; **15**(4):3110-3117.

[92] Wendling F, Hernandez A, Bellanger JJ, Chauvel P, Bartolomei F. Interictal to ictal transition in human TLE: insights from a computational model of intracerebral EEG. *Journal of Clinical Neurophysiology* 2005; **22**(5):343-356.

[93] Cossart R, Dinocourt C, Hirsch JC, Merchan-Perez A, De Felipe J, Ben-Ari Y, Esclapez M, Bernard C. Dendritic but not somatic GABAergic inhibition is decreased in experimental epilepsy. *Nature Neuroscience* 2001; **4**(1):52-62.

[94] Quiroga RQ, Kraskov A, Kreuz T, Grassberger P. Performance of different synchronization measures in real data: A case study on electroencephalographic signals. *Physical Review E* 2002; **65**(4 Pt 1):041903.

[95] Le Van Quyen M, Foucher J, Lachaux JP, Rodriguez E, Lutz A, Martinerie J, Varela FJ. Comparison of Hilbert transform and wavelet methods for the analysis of neuronal synchrony. *Journal of Neuroscience Methods* 2001; **111**(2):83-98.

[96] Vapnik V, Cortes C. Support-vector networks. *Machine Learning* 1995; **20**(3):273-297.

[97] Chang CC, Lin CJ. LIBSVM: a library for support vector machines. *ACM Transactions on Intelligent Systems and Technology* 2011; **2**(3):1-27. Software available at http://www.csie.ntu.edu.tw/ cjlin/libsvm

Fiche masterproef

Student: Roel Henckaerts

Titel: Modeling, predicting and controlling epileptic seizures

Nederlandse titel: Modelleren, voorspellen en controleren van epileptische aanvallen

UDC: 51-7

Korte inhoud:

Epilepsy is a very diverse neurological disorder, characterized by recurrent seizures. Two specific types are considered in this study, namely absence seizures and mesial temporal lobe epilepsy (MTLE). The most common treatments for epilepsy are medication and surgery. Since these are not effective for all the patients, there is a lot of current research aimed towards the development of alternative treatments. Computational modeling can play a major role in this development. Two computational models from the literature are therefore implemented in this study. The first model is a thalamocortical model for absence seizures. This model can simulate normal and epileptic activity. It very well mimics the dynamics that are in play during transitions from one type of activity to the other. This allows some interaction with the model. A control system is designed for this model, with the goal of disrupting a started seizure. Absence seizures have a sudden onset and can therefore not be predicted. The control system consists of a detection and a stimulation part. The detection happens purely based on the amplitude of the electroencephalography (EEG). This allows for a fast detection, but unfortunately lacks the possibility for generalization towards real life signals. The stimulation part will send pulses into the model, to interrupt the seizures. This fits perfectly in the framework of brain stimulation techniques as an alternative treatment for epilepsy. The obtained results show that the seizures can be controlled very well, if a fast detection is possible. However, this is only the case for some well tuned, patient-specific, parameters of the control system. The second model is a hippocampal model for MTLE. This model can simulate six different types of behavior. It is used to generate artificial data to build a prediction framework for MTLE. Interictal (between seizures), preictal (right before a seizure) and ictal (during a seizure) periods of the EEG are simulated. The EEG of MTLE, unlike for absence seizures, shows some dynamical changes prior to seizure onset. These changes can be used to find the preictal periods of the EEG. Predicting a seizure thus boils down to a classification problem. There is a lot of neuronal synchrony during the preictal and ictal periods. Therefore, measures that characterize synchrony are computed from the EEG channels. These measures are used to classify the EEG. Classification is first done by thresholding the synchrony measures, with a resulting classification accuracy of 95%. This method is however very likely to fail on real life signals. Classification is therefore also performed with support vector machines (SVMs) after including some filtered versions of the synchrony measures. An accuracy of 98% is obtained on independent test signals.

Thesis voorgedragen tot het behalen van de graad van Master of Science in de ingenieurswetenschappen: wiskundige ingenieurstechnieken

Promotor: Prof. dr. ir. B. De Moor

Assessoren: Prof. dr. ir. K. Meerbergen
Prof. dr. ir. D. Nuyens

Begeleider: Dr. ir. O. M. Agudelo